UNIVERSITÀ DEGLI STUDI DI NAPOLI

"FEDERICO II"

DIPARTIMENTO DI SCIENZE BIOMEDICHE AVANZATE

TESI DI DOTTORATO

IN

SCIENZE BIOMORFOLOGICHE E CHIRURGICHE

DESIGN AND DEVELOPMENT OF AN E-TEXTILE DEVICE AND A METHODOLOGY FOR PERSONALIZED AND NON-INVASIVE ASSESSMENT OF BIOMECHANICAL RISK ASSOCIATED TO MANUAL HANDLING

Tutor

Prof. Mario Cesarelli

Tutor Estero

Prof. Paolo Gargiulo

Tutor Aziendale

Ing. Michele Ramaglia

Dottorando

Dott. Donisi Leandro

COORDINATORE: PROF. ALBERTO CUOCOLO

XXXIV CICLO

To my dad…

Contents

Declaration of Authorship

I, Leandro Donisi, declare that this thesis titled, "***Design and development of an e-textile device and a methodology for personalized and non-invasive assessment of biomechanical risk associated to manual handling***" and the work presented in it are my own.
I confirm that this work was done wholly during my PhD at this university.
Where I have consulted the published work of others, this is always clearly attributed.

Abstract

Recently, wearable sensors, including electronic textiles, have been developed in order to allow the assessment of human motion in several medical fields, ranging from rehabilitation medicine to ergonomics. About the latter, many activities may elicit a biomechanical overload. Among these, lifting loads can cause work-related musculoskeletal disorders. Aspiring to improve risk prevention, the National Institute for Occupational Safety and Health (NIOSH) established a methodology for assessing lifting actions by means of a quantitative method based on intensity, duration, frequency and other geometrical characteristics of lifting. Therefore these approaches are time consuming, operator dependent and costly in terms of resources. To overcome these limits, recent advances in pervasive sensing, mobile, communication technology, wearable and e-textiles have led to the deployment of new smart sensors that can be worn without affecting a person's daily activities. These sensors are able to measure several kinematics quantities, such as acceleration, magnetic field and angular rate and biosignals such as electrocardiography and electromyography.

In this thesis, a new e-textile-based system for the remote monitoring of biomedical signals is presented. The system includes a textile sensing shirt, an electronic unit for data transmission, a custom-made Android application for real-time signal visualization and a software desktop for advanced digital signal processing. The device allows for the acquisition of electrocardiographic, bicep electromyographic and trunk acceleration signals. The sensors, electrodes, and bus structures are all integrated within the textile garment, without any discomfort for users. A wide-ranging set of algorithms for signal processing were also developed for use within the system, allowing to rapidly obtain a complete and schematic overview of a worker's status.

Moreover in this thesis, the machine learning feasibility to classify biomechanical risk according to the revised NIOSH lifting equation was explored. Acceleration and EMG signals from the biceps were collected using the e-textile shirt proposed during lifting tasks performed by five subjects and further segmented to extract time-domain and frequency-domain features. The features were fed to several machine learning algorithms. Interesting results were obtained in terms of evaluation metrics for a binary risk/no risk classification.

In conclusion, this study indicates the proposed combination of features and algorithms represents a valuable approach to automatically classify work activities in two NIOSH risk

groups. These data confirm the potential of this methodology to assess the biomechanical risk to which subjects are exposed during their work activity. Future investigation on enriched study population will be able to confirm the potentiality of this methodology in the biomechanical risk assessment.

Dissertation outline

The dissertation is organized as follows:

Chapter 1 presents an introduction of the themes developed along the thesis underlining the diffusion of the e-textile and wearable sensors in the occupational medicine and ergonomics. Moreover, several work-related musculoskeletal disorders are presented and the state-of-the-art methods and indexes for biomechanical risk assessment are reported. Finally, new potential solution based on wearable sensors and artificial intelligence are proposed.

Chapter 2 presents two e-textile devices developed, namely an e-textile sock and an e-textile shirt able to monitor several physiological signal and parameters useful also in the occupational medicine and ergonomics.

Chapter 3 presents an interesting methodology to assess the biomechanical risk to which workers are exposed during manual handling and lifting based on machine learning algorithms fed with features extracted from acceleration and angular velocity signals acquired by means of an inertial measurement unit placed in the lumbar region. Moreover, the influence of the weight on gait performances and postures was studied.

Chapter 4 presents an e-textile shirt coupled with dedicated software able to discriminate risk classes according to the Revised NIOSH lifting equation presenting a new solution to assess the biomechanical risk in an automatic, non-invasive and quantitative way.

List of Figures

List of Tables

List of Abbreviations

ABT	**A**da**B**oost **T**ree
AP	**Antero-posterior**
AucRoc	**A**rea **u**nder the **c**urve **R**eceiver **o**perator **c**haracteristic
BLE	**B**luetooth **L**ow **E**nergy
CI	**C**onfidence **I**nterval
CoP	**C**enter **o**f **P**ressure
CRS	**C**omfort **R**ating **S**cale
CV	**C**ross **V**alidation
DFA	**D**etrended **F**luctuation **A**nalysis
DT	**D**ecision **T**ree
ECG	**E**lectro**c**ardio**g**raphy
EMG	**E**lectro**m**io**g**raphy
FDA	**F**ractal **D**imension **A**nalysis
GBT	**G**radient **B**oost **T**ree
GCT	**G**ait **C**ycle **T**ime
HF	**H**igh **F**requency
HR	**H**eart **R**ate
HRT	**H**eart **R**ate **T**urbulence
HRV	**H**eart **R**ate **V**ariability
IG	**I**nformation **G**ain
IMU	**I**nertial **M**easurement **U**nit
IoT	**I**nternet **o**f **T**hings
ISICO	**I**stituto **S**cientifico **I**taliano **C**olonna **V**ertebrale
kNN	**k**-**N**earest **N**eighbor
LF	**L**ow **F**requency
LI	**L**ifting **I**ndex
LoA	**L**imit **o**f **A**greement
LR	**L**ogistic **R**egression
MAC	**M**edia **A**ccess **C**ontrol
MAPO	**M**ovimentazione **A**ssistita dei **P**azienti **O**spedalizzati
MAX	**Max**imum

MEMS	**Mi**cro **E**lectro-**m**echanical **S**ensor
MIN	**Min**imum
ML	**M**achine **L**earning
M-L	**M**edio-**l**ateral
MLP	**M**ultilayer **P**erceptron
MSD	**M**usculoskeletal **D**isorder
NB	**N**aïve **B**ayes
NIOSH	**N**ational **I**nstitute for **O**ccupational **S**afety and **H**ealth
NN	**N**ormal-to-**N**ormal
OWAS	**O**wako **W**orking posture **A**nalysing **S**ystem
PATH	**P**osture **A**ctivity **T**ools and **H**andling
PSD	**P**ower **S**pectral **D**ensity
PVC	**P**remature **V**entricular **C**ontraction
r	Correlation coefficient
RBF	**R**adial **B**asis **F**unction
REBA	**R**apid **E**ntire **B**ody **A**ssessment
RF	**R**andom **F**orest
RMS	**R**oot **M**ean **S**quare
RMSE	**R**oot **M**ean **S**quare **E**rror
RMSSD	**R**oot **M**ean **S**quare of **S**uccessive **D**ifferences
RNLE	**R**evised **N**IOSH **L**ifting **E**quation
ROI	**R**egion **o**f **I**nterest
Rot-F	**Rot**ation **F**orest
RULA	**R**apid **U**pper **L**imb **A**ssessment
RWL	**R**ecommended **W**eight **L**imit
SD	**S**tandard **D**eviation
SDANN	**S**tandard **D**eviation **A**veraged **NN**-intervals
SDNN	**S**tandard **D**eviation **NN**-intervals
SDNNi	**SDNN i**ndex
sEMG	**s**urface **E**lectro**m**io**g**raphy
SVM	**S**upport **V**ector **M**achine
Ti	**T**riangular **i**ndex
TO	**T**urbulence **O**nset

TS	**T**urbulence **S**lope
VLF	**V**ery **L**ow **F**requency
WL	**W**earability **L**evel
WLBD	**W**ork-related **L**ow **B**ack **D**isorder
WMSD	**W**ork-related **M**usculo**s**keletal **D**isorder

Chapter 1

1. Introduction

1.1 E-textile in the medical field

The term Electronic-Textiles, or E-Textiles, refers to a wide range of studies and products that extend the usefulness and functionalities of common fabrics. The innovative feature taken by this novel application regards the embedding of digital components, such as batteries, LEDs, and, in general, electronic components, in common fabrics. Thus, through E-Textile technology, every kind of digital application can be potentially developed on a textile substrate. The advances in e-textile technologies have led to the development of comfortable wearable garments directly integrated in internet of things (IoT) networks. Many applications have been developed exploiting this background in the field of remote monitoring, with the aim of ensuring and increasing the patient's comfort, quality of life and safety. This attractive opportunity is bringing a revolution in the market of wearable devices, with the involvement of big companies which are trying to shift from the wearable electronic hardware to the more comfortable electronic textiles. The market of wearable technologies has a compound annual growth rate of 15.5%, with great opportunities of expansion, it is expected to reach 51.6 billion USD by 2022 (IDTechEx).

Nevertheless, almost all the attendant projects remain within the research field and are not intended for entry into the commercial market. Here, the main barriers include the regulatory issues related to patient safety, privacy, and data management [1,2], as well as the need for a certain degree of reliability in terms of device performance.

Despite the above mentioned problems, E-textile is gradually covering the market of wearable devices, offering cheap and comfortable solution in different sectors, such as fashion, entertainment, military and defense, space exploration, health, and wellness.

Healthcare remains one of the most interesting and promising markets: e-textile features are very suitable for the development of innovative medical devices or applications that can potentially establish significant cost reductions for healthcare systems. Wearable devices for health monitoring can be easily used by patient in domestic environment and, when they are integrated in a complete communication chain, they allow smart remote monitoring with great benefits for caregivers and patient himself. E-textile sensitive fabrics can be developed to acquire and react to clinical signals detectable on body, with some interesting advantages: first, the nature of fabrics makes them the best solution to realize sensors in direct contact with the skin; second, fabrics are flexible and well adaptable to human body offering technological possibilities not available with the common electronics; and third, fabrics are cheap, comfortable, washable, and easily customizable [3]. Thus, smart biomedical clothes potentially represent an innovative tool for the continuous monitoring of vital signs, combining the function of sophisticated medical devices with the comfort and ease of use of clothing products.

Moreover, the opportunity to integrate these innovative devices in IoT networks makes possible to establish smart solution for remote health monitoring, exploring the growing field of m-health and supporting cost reduction in healthcare system by facilitating early hospital discharges. Many E-Textile solutions for health monitoring have been proposed in literature, but most of them are blocked in the research field and are not intended to flow to the pragmatic healthcare world. Regulatory issues regarding patient safety, privacy, data management [1,2], and the need of a safe degree of reliability for device performances represent the main obstacles to the large commercial diffusion of such types of devices.

A detailed review of the wearable systems for health monitoring introduced up to 2010 is provided in [4], with a dedicated section on textile-based devices. The field of electrocardiography (ECG) signal monitoring is one of the fields most covered by e-textile applications. Pani et al. (2018) provided a complete survey on textile-electrode technologies for ECG monitoring [5], with all the examined prototypes exclusively used in the scientific research field with the aim of investigating the feasibility of this form of biosignal monitoring. A number of the prototypes are used as stand-alone devices to record ECG signals in a clinical environment, rather than as part of an integrated tele-monitoring system [6,7]. Meanwhile, other works have presented remote tele-monitoring systems focused on collecting ECG signals and other important biosignals, such as those related to electromyography (EMG) [8], breathing [9-11], accelerometry [6,12], and galvanic skin response [7]. The systems presented in [7] also provide tools for off-line digital signal processing, gathering the principal parameters assessed from signals, including heart rate, blood pressure, respiratory rate, and activity classification.

1.2 Work-related musculoskeletal disorders

Musculoskeletal disorders (MSD) are injuries or pain affecting muscles, joints and tendons. MSD result from incorrect postures and manipulation activities such as: energetic efforts in lifting or transporting loads, bending and twisting the back or limbs, exposure to vibrations or repetitive movements (including typing on the keyboard). If these activities are related to work, the resulting injuries and disorders are referred to as Work-related musculoskeletal disorders (WMSD) [13]. Diseases and MSD due to biomechanical overload are widespread among workers and are one of the main causes of illness in many activities. The consequences of MSD are very heavy, from a social and economic point of view, for workers, to whom they cause personal suffering and possible income reduction; for employers, because they reduce the business efficiency; for the country, because they affect health and social security expenditure. The principle problem regard both lower and upper limbs but in particular the back. This issue involves also the healthcare field, with regard to the manual handling of patients.

Several epidemiological studies provided a strong correlation between physical work exposures and the increased risk of WMSD [14-16]. Radwin et al. showed the relationship between MSD and repeated and long durations of external load handling during the workday [17]. With regard to the health sector, Smedley et al. [18] showed that low back pain is highly prevalent among nurses and it is associated with a high level of sickness absence. A review [19] in this sector confirm that tasks such as assisting patients with deficit in ambulation may possibly contribute to low back pain, especially bariatric patients [20].

Biomechanical exposures during physical work are mainly due to three main factors: intensity (load magnitudes and extent of non-neutral postures), repetition (frequency or number of force exertions and motions) and duration (the time of a physical activity) [21].

1.3 Methods and indexes for biomechanical risk assessment

To avoid WMSD, many government agencies, universities and companies have developed techniques and proposed guidelines to evaluate, modify and reduce in number of accidents and occupational diseases [22].

To achieve this goal, three different general approaches have been applied:

1. Self-assessment
2. Observation
3. Direct measurement

In self-assessment, workers are asked to provide risk-related information. Although this approach has a low initial cost and it is simple, researchers have argued that workers' self-assessments of exposure levels are often inaccurate, unreliable and distorted.
The observation-based approach involves a real-time evaluation or analysis of the recorded video. It is mostly impractical because of the substantial cost, time and technical knowledge required for post-analysis of large amounts of non-heterogeneous data.
Differently from the two previous approaches, direct measurement uses tools to collect data on the posture and movement of workers. Examples of this approach include, but are not limited to, the use of mechanical micro electro-mechanical sensors (MEMS), such as Inertial Measurement Unit (IMU) sensors [23].
Several indexes have been proposed to evaluate the biomechanical risk to which the workers are exposed:

- NIOSH. The Revised NIOSH Lifting Equation (RNLE) is a method published by NIOSH (National Institute for Occupational Safety and Health) to assess the risk of work-related low back disorders (WLBDs). The method determines the recommended weight limit during lifting tasks and compute the lifting index that is function of geometric characteristics, frequency, weight lifted and sex [24].
- OWAS. The OWAS (Owako Working Posture Analysing System) was developed by the steel company Owako with the aim of redesigning its production line. It identifies and evaluates bad working postures on the basis of the daily routine of workers [25]. The postures are classified in more than 250 different positions, evaluating the position of the trunk, arms and legs, as well as the weight of the load. Each posture is coded to allow risk assessment of WMSD.
- PATH. The PATH (Posture, Activity, Tools and Handling), proposed by Buchholz et al. [26], codify postures as originally suggested by Karhu et al. [26] in the OWAS method, adding new codes for different activities, loads and equipment. By evaluating the images recorded during work activities, evaluators identify the percentage of time workers spend in coded postures classified as "neutral" or "non-neutral".
- RULA. The RULA (Rapid Upper Limb Assessment) was proposed by McAtamney and Corlett [27] to evaluate some positions related to neck, torso and upper limbs. The ergonomists codify each posture by visually evaluating the angles between the

body parts studied, and obtaining a score that is used to decide whether a movement is considered acceptable or whether some changes need to be made.

- REBA. The REBA (Rapid Entire Body Assessment), proposed by Hignett and McAtamney [28] was developed to improve and extend the RULA. As well as the RULA index, the REBA evaluates the postures of workers, but it takes into account also the visual assessment of the lower limbs. Moreover the REBA index evaluates the uncomfortable positions of the upper limbs such as if the arms are rotated or if the shoulders are raised.
- MAPO. The MAPO (Movimentazione Assistita dei Pazienti Ospedalizzati) is an index developed by the Ergonomic Research Unit of Posture and Movement in Milan for the assessment of the risk of manual patient handling in hospital departments. The index allows a detailed analysis of the main risk determinants for low back pain in healthcare professionals [29].

1.4 Wearable devices for ergonomics

In addition to the more traditional quantitative or semiquantitative observational methods presented in the previous paragraph, occupational ergonomics studies in the field can employ instrumental methods that offer greater agility, precision and duration of measurement. Among the direct measurement methods, wearable inertial systems based on IMU play an important role in the biomechanical risk assessment [30], and they look very promising for occupational medicine and ergonomics applications [31]. In the field of risk assessment, in fact, wearable inertial technology represents a significant advance in comparison to the evaluation tools traditionally used in ergonomics [32], especially regarding the degree of precision and possibility of automatic measurement detection. IMUs are based on triaxial accelerometers and gyroscopes able to measure 3D acceleration and angular velocity of the sensor with respect to gravity [33]. Often, IMUs also include a triaxial magnetometer useful to give information about the orientation of the sensor in the three-dimensional space. In the absence of standards on the positioning of sensors on the human body [34], the dorsal part of the back was recommended for the ergonomic study of trunk position [35], while the waist was suggested for analyzing the overall motion, as representative of center body mass [36]. In occupational ergonomics, body-worn inertial sensor technology and motion tracking system could be combined to noninvasively collect large amounts of body movement data during physical work [31] and explore their association with occupational risk as assessed with standard methods [37]. The portability and wearability of this technology represents an advantageous alternative to camera-based motion tracking systems [38]. Information on worker exposure obtained through wearable sensors could help to pre-evaluate heavy work, match workers' skills with physical activity requirements, verify the sustainability of work shift combinations as well as prioritize work modification interventions based on the type and severity of the level of exposure [32]. The success and diffusion of IMUs systems are linked to their relative low cost, the low complexity of the experimental setup and data processing procedures, the limited time constraints and the feasibility of evaluation outside the research laboratories [39]. Several IMUs positioned on the body were used in studies [40,41], where the purpose was to predict, by the same accelerometric data, the geometric (initial and final height, horizontal distance, asymmetry and inclination of the trunk) and temporal (frequency and duration) variables related to lifting, thereby validating the measures that the systems produced.

Among the wearable technologies, e-textile devices are also spreading in the ergonomics context even if as preliminary prototypes [42-44].

1.5 Machine learning in ergonomics

Machine learning (ML) algorithms are gaining popularity in the ergonomic field for biomechanical risk assessment by means of data acquired by wearable inertial systems. Several publications have appeared in recent years documenting several strategies [45-47]. IMU systems, which incorporate machine learning into their data analysis pathways, have been found effective in automated exercise detection and in classifying movement quality across a range of lower limb exercises, including lifting, despite studies in this field having so far involved few samples [48].

Chapter 2

2 E-textile devices

2.1 E-textile sock

The first e-textile prototype developed during the research activity was a sock named SWEET Sock [49]. The prototype, based on an e-textile sensing sock, is able to collect the angular velocities of lower limbs, using IMUs, and the plantar pressures, by means of textile sensors. The device can be considered a wearable and portable system for the assessment of both postural and gait tasks, exploiting the recent advances in the field of the e-textile, electronic and signal processing. In particular, the system is intended to provide the assessment of spatio-temporal gait parameters by processing the angular velocities signals while the pressure signals are used to assess the Center of Pressure (COP) displacements during static postural tests. The details of the prototype design and development are presented below followed by its validation.

The first version of this device, presented in [50], has been improved with new more efficient textile and electronic components and through the addition of a set of signal processing algorithms.

SWEET Sock is a wearable sensing device which allows the acquisition of accelerometric and pressure signals. It can be integrated in a complete system for remote health monitoring, presented in the schematic diagram in Figure 1.

Figure 1. System Architecture: (1) SWEET Sock: Textile Unit; (2) SWEET Sock: Control Unit; (3) SWEET App; (4) Web Server; (5) SWEET Lab

The wearable sensor unit allows the acquisition of bio-signals when connected to the analogue front-end located in the electronic unit. This unit also contains a microcontroller and allows data transmission through an integrated Bluetooth Low Energy (BLE) module. A custom-made Android mobile application has been developed to receive and visualize real-time signals on a smartphone, and to upload data on a dedicated web server afterwards.

This is a restricted area that is accessible after prior authentication, exclusively by authorized and appointed health professionals, who can download, analyze, and process data using the custom-made MATLAB desktop software.

Below, the functional modules of the system are individually presented.

The wearable sensing unit consists of a commercial sports sock in which three pressure sensors, in e-textile technology, have been integrated as sensing elements in three strategic points of the foot arch. The number and placement of sensors were based on anatomical considerations: in standing position, the main force transmitted onto the foot originates at the bones of the lower leg. At the ankle, this force is divided into three smaller forces in the style of a tripod. Within the foot, one of these three forces is directly transmitted onto the calcaneus, the second one onto the first metatarsal, and the third one is distributed across the second to fifth metatarsal [51]. Therefore, it was decided to use three pressure sensors per foot: one under the heel (HEEL), one under the first metatarsal bone (MTB1) and one under the fifth metatarsal bone (MTB5) as shown in Figure 2c. The use of the minimum number of sensors needed for the analysis reduces the complexity of textile design and can improve the comfort and wearability for users. Sensors have been realized by using 2 by 4 cm sheets of EeonTex fabric, a conductive and nonwoven microfiber with piezo-resistive functionality (surface resistivity 2000 ohm/sq), offering a reduction of the electrical resistance to the application of force. Their characterization was carried out with load tests using a controlled mechanical clamp with decreasing/increasing loads. The three conductive sensors have been covered by non-conductive fabric to prevent degradation by contact with the skin and are thin enough to provide postural monitoring at natural in-shoe conditions, without distortion of plantar pressure. A conductive ribbon (5 mm tick), with a resistance of less than 0.1 ohm per cm, has been used to connect sensors to the output connectors of the wearable unit. Compared to the conductive wires available on the market, the ribbon has a lower resistance (0.1 vs 0.9 ohm per cm) and it is more robust as it does not break due to stretch. The design of conductive pathways provides a placement of all connectors of the data acquisition system, represented by snap buttons, on the lateral part of the sock, which essentially improves the system usability. The textile connections have been sewn on the side of the sock avoiding, when possible, the passage under the sole of the feet, where they could be deteriorated. Connection lengths have also been minimized by studying the shortest path in order to reduce noise and interference. Figure 2 shows the complete device with its sartorial design.

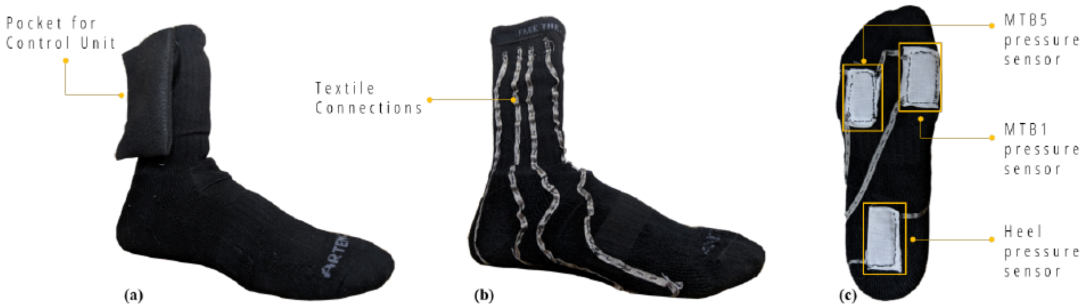

Figure 2. SWEET Sock sensing unit: (a) external view; (b) internal view of textile connections; (c) textile pressure sensors

The electronic unit is a compact module containing all the electric and electronic elements to allow acquisition, digitalization, storage, and wireless transmission of the signals. A conditioning circuit, for each conductive sensor, has been realized in order to read a voltage signal proportional to the applied force. This circuit is realized by means of a voltage divider consisting of two resistors: one of which is of known value and the other represented by the e-textile sensor. The known resistance value is fixed to 18 kohm, around which the conductive sensor resistance ranges, to reach the condition of maximal sensitivity. The IMU FLORA 9-DOF (Adafruit Inc.: New York, NY, USA) has been integrated in the electronic unit to acquire gyroscopic signal. It consists of a small electronic board mounting LSM9DS1 module, a system-in-package featuring a 3D digital linear acceleration sensor, a 3D digital angular rate sensor, and a 3D digital magnetic sensor. A LilyPad SimbleeTM BLE Board (Sparkfun Inc.: Niwot, CO, USA) has been used as microcontroller. It provides the digitalization of pressure signals, and it is connected to Flora IMU through the I2C serial bus interface. LilyPad Simblee also allows to send data via BLE protocol, using SimbleeTM Bluetooth R Smart Module integrated on the shield. BLE technology represents a perfect trade-off between energy consumption, latency, piconet size, and throughput. Its control features are implemented exploiting the ARM RCortexM0 microcontroller that can be programmed using the Arduino IDE. The control unit is programmed to sample pressure analogue signals with a sample period of 15 ms (66.7 Hz), and to receive digital data from the gyroscope with the same rate. Data are collected in 16-bytes-sized packets (2 bytes for each information: Packet, Time, x-y-z axes of the gyroscope, MTB1, MTB5, and HEEL pressure data) and real-time sent, via BLE, to the smartphone using SWEET App. Other signals deriving from IMUs (signals from accelerometer and magnetometer) are not recorded by the device because they do not provide any essential information for the planned assessments. A gyroscope-based algorithm able to evaluate all spatio-temporal parameters was implemented, the choice to use gyroscope signals in the place of the accelerometer signals was due to the fact that accelerometer signals are affected by gravity and are sensitive to sensor location [52]. When using accelerometers, it is important that they are placed in the same location each time as the signal is affected by how far from the center of rotation they are. The advantage of using a shank mounted gyroscope compared to accelerometers is that, as long as the gyroscope is recording data in the correct plane, it does not matter where on the shank the sensor is placed [53,54]. This reduction in the amount of acquired and sent data allows to improve signals sampling and sending rate. All modules making up the electronic unit are powered by a 190 mAh/3.7 V lithium battery, placed on the back of the same unit. The electronic unit is housed in a 3D-printed plastic case (73 mm x 52 mm x 21 mm). On the top part of the case, four snap buttons allow the connection to the wearable sensing unit, in order to provide the input signals for the analogue front ends. In Figure 3 the electronic unit, with its main details, is shown.

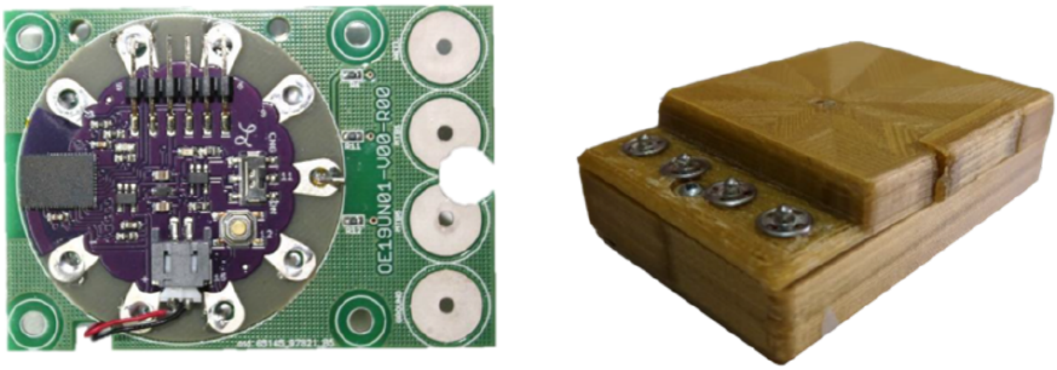

(a) (b)

Figure 3. SWEET Sock Electronic Unit: (a) internal electronic unit; (b) complete unit external view

SWEET App is a custom-made Java language application for mobile devices requiring Android 6.0 or higher operating system and BLE technology. The application allows the smartphone to communicate and receive data coming from the electronic unit, via BLE protocol. When the application is started it is possible to associate and connect the wearable device, using its MAC address. Then, the measurement session can start, data are transferred from the electronic unit to the mobile device, which allows signals real time plotting. At the end of the session data are automatically saved in a ".csv" file, which is stored locally and can be uploaded at any time to a dedicated web server. In Figure 4 the main frames of the app are shown.

(a) (b) (c) (d)

Figure 4. SWEET App main frames: (a) login; (b) unit connection; (c) signal recording; (d) results summary

A custom-made Matlab GUI software, named SWEET Lab, has been developed to allow signal visualization and digital processing. Health professionals have the possibility to download data from the server and analyze them using the tools offered by this software. Pressure and gyroscope signals gathered by the hardware are individually processed to respectively perform posturographic assessment and spatio-temporal gait analysis. The two types of signal were not integrated because they are used in the analysis of two separate phases: pressure signals for static postural assessment while angular velocities in dynamic walking tasks analysis. A gyroscope-based algorithm for gait analysis has been developed. The angular velocity signals on the sagittal plane are selected and low-pass filtered with 5th order Butterworth filter (cut-off frequency 5 Hz) to reduce noise. Mid-swing, heel-strike, and toe-off events are then identified on the filtered signals for both feet, using a threshold-based algorithm [55]. The starting point of the algorithm is the identification of the time events corresponding to the mid-swing, identified as the local maximum peaks of the signal. In the next step, local minimum peaks prior and after the mid-swing point are selected as, respectively, toe-off and heel-strike time events. Starting from these gait events times, all temporal parameters of gait analysis are calculated. In Table 1, the list of temporal parameters is provided with a description clearly outlining the methods used to calculate them. Spatial parameters are assessed using a single pendulum model described in [53], where the distance from the foot to the top vertex of the rotation is modeled as equal to the height of the subject multiplied by a scaling factor. The following equation shows how the stride length is calculated:

$$StrideLength(m) = S\ x\ H\ x\ 2(1 - \cos\theta)$$

S represents the scaling factor chosen equal to 0.52 [53], *H* represents subject height [m] and θ is the angular displacement in the sagittal plane during the stride [rad], assessed by integration of the gyroscope signal. Plantar pressure signals collected by the sensorized socks are used to perform sway analysis, as a systematic assessment of the readiness and stability of the human body to achieve and maintain equilibrium. This analysis starts with the estimation of the COP, whose displacement during stand task is a meaningful parameter for a quantitative evaluation of the ability to maintain equilibrium. At each instant, COP coordinates in the medio-lateral (X_{COP}) and antero-posterior (Y_{COP}) directions have been calculated by processing raw pressure data according to the following equations:

$$X_{COP} = \frac{\sum_{i=1}^{N} X_i P_i}{\sum_{i=1}^{N} P_i}$$

$$Y_{COP} = \frac{\sum_{i=1}^{N} Y_i P_i}{\sum_{i=1}^{N} P_i}$$

where N denotes the total number of sensors, and X and Y are the sensor coordinate inside the whole foot shape area and P the pressure value. The resulting signals express COP displacement along time in the medio-lateral (M-L) and antero-posterior (AP) directions, with respect to a reference point located in the middle between the feet. The mono-dimensional representations of these signals constitute the M-L and AP stabilograms, while the combined bidimensional plot is referred to as statokinesigram, representing the ground projection of the COP during the stand task.

Table 1. Spatio-temporal gait parameters

Temporal Measures	
Variable	**Description**
Gait Cycle Time (GCT) [s]	Defined as the time between two successive heel strikes of the same foot
Stance Time [s]	The amount of time a foot is in contact with the ground within a single gait cycle. It is the time between the heel-strike and the successive toe-off of the same foot
Stance Phase [%]	Stance time expressed in percentage of the GCT
Swing Time [s]	Duration of the swing phase, in which the foot is not in contact with the ground. It is calculated as the time between the toe-off and the successive heel strike of the same foot
Swing Phase [%]	Swing time expressed in percentage of the GCT
Single Support [%]	Part of the GCT in which a single foot is in contact with the ground. It is the time between the toe-off of the opposite foot and the successive heel-strike of the opposite foot, expressed in percentage of the GCT
Double Support [%]	Part of the GCT in which both feet are in contact with the ground. It is the time between the heel-strike of a foot and the successive toe-off of the opposite foot, expressed in percentage of the GCT
Cadence [steps/min]	Number of steps per minute
Spatial Measures	
Variable	**Description**
Stride Length [m]	Distance covered during GCT
Stride Velocity [m/s]	Defined as the ratio between Stride Length and GCT

Signals are filtered with a low-pass 4th-order Butterworth digital filter with a cut-off frequency of 5 Hz [56], and then analyzed in time domain to calculate a set of parameters describing the stability of the subject during the task (Table 2) [57-59].

Stabilometric signals were also analyzed in frequency domain. The Matlab periodogram algorithm is used to estimate power spectral density (PSD), modified using the Hamming window. Frequency assessment is provided by means of a set of measures describing the distribution of PSD, such as peak and centroidal frequencies, band powers, and others. All the parameters assessed are listed in Table 2. The description clarifies the methods used to evaluate both spatial and frequency domain metrics starting from stabilometric signals and ground projection of the COP trajectory.

Table 2. Static postural assessment parameters

Time Domain Measures	
Variable	**Description**
Mean COP coordinates [cm]	M-L and AP mean COP displacements during time
Mean Distance [cm]	Mean distance of COP trajectory from the center of the trajectory itself
COP Trajectory Range [cm]	Maximum distance between 2 points of COP trajectory in M-L and AP directions
Root Mean Square (RMS) [cm]	RMS of COP trajectory. It is provided also for single M-L and AP directions
Angle form AP axis [deg]	Mean angle formed by the segments composing COP trajectory and AP direction
Sway Path [cm]	Total length of COP trajectory, computed as the sum of distances between successivepoints of the trajectory
Mean Velocity [cm/s]	Mean velocity of COP trajectory, computed as the ratio between sway path length and duration of the test
95% Ellipse Area [cm^2]	Area of 95% confidence ellipse encompassing the COP trajectory in transverse plane
95% Ellipse Angle [deg]	95% confidence ellipse inclination with respect to the M-L direction
Frequency Domain Measures	
Variable	**Description**
Peak Frequency [Hz]	Peak frequency for M-L and AP power spectrum
Median Frequency [Hz]	Frequency below which the 50th percentile of total power is present
80% Frequency [Hz]	Frequency below which the 80th percentile of total power is present
Centroidal Frequency [Hz]	Spectral centroid of power spectrum. It indicates where the center of mass of the spectrum is located
Band Power [cm^2]	Power comprised in low [0.1–0.2 Hz], mid [0.2–0.3 Hz], and high [0.3–1 Hz] frequency bands, expressed as absolute and percentage values

The proposed system was validate through a benchmarking study with a reference system. The reference system chosen for the validation analysis is SMART-DX 700 by BTS Bioengineering, an optoelectronic stereophotogrammetric system used in the gait analysis field. Stereophotogrammetry is usually considered a "gold standard" in gait analysis when used appropriately. The system is made of 6 infrared digital cameras, with a sensor resolution of 1.5 megapixel, an acquisition frequency from 250 fps (at maximum resolution) to 1000 fps and an accuracy lower than 0.1mm. The recognition of body segments during movement is achieved through the use of twenty-two retro-reflective passive markers (diameter 14 mm), which are attached to subject's skin at specific landmarks. Video data are processed on a PC workstation running SMART Clinic software, able to store and compute a set of parameters concerning kinematic (spatiotemporal parameters, joint angles) and dynamic (forces exchanged). In [60], a first validation analysis was performed by comparing the raw accelerometric and plantar pressure signals acquired by the prototype with those recorded by reference systems. Following the results obtained, in this work it has been explored the results of gait assessment, in order to carry out any possible unconformity in measurement and/or processing phases managed by the new prototype. Spatio-temporal gait parameters calculated by the proposed device with those found by an optoelectronic stereophotogrammetric system were compared. The comparison was carried out by means of statistical methods.

One-hundred-and-eight records were acquired on three healthy subjects: two males (aged 27 and 26) and one female (aged 25). Participants were free of neurological, muscular, and skeletal comorbidities affecting mobility and gait. The subject wore the sensorized socks connected to the electronic unit and was equipped with the markers of the stereophotogrammetric system, in order to perform simultaneous recording of the walking tasks with the two systems under test (Figure 5). The markers were attached to subject's skin according to the protocol described by Davis et al. [61].

Figure 5. Subject equipped with both systems: SWEET Sock and reflective markers

The trials involved free walking tests on a 11 m walkway. Each subject was instructed to perform eight independent trials respectively at preferred, slow and fast self-selected walking speed. After that, the use of a metronome was introduced to force subjects walking at fixed normal, slow and high speed. Metronome rate was set at 100%, 67%, and 133% of the average cadence previously assessed for each subject over 5 free walking tests using the accelerometers-based gait analysis system Opal by APDM. Subjects performed four walking trials at each speed imposed by metronome. The trials were performed at different walking speed in order to obtain a dataset covering a wider range of values. Doing so, we expect a more specific characterization of the relationship existing between the two methods over all the range of measurement.

In order to validate the proposed e-textile wearable system, the gait analysis parameters obtained from this device have been compared with those obtained by the reference system. Starting from gyroscope signals measured by the Sock, spatio-temporal gait parameters were computed by the custom-made MATLAB algorithms shown previously. The corresponding parameters assessed by the reference system were retrieved from the reports generated by SMART CLINIC software.

The following spatiotemporal parameters were considered for the benchmarking analysis: Gait Cycle Time (s), Cadence (step/min), Stance Time (s), Swing Time (s), and Step Length (m).

The agreement between measurements computed by the two systems - the Sock and SMART-DX 700 - was investigated by means of two-tailed paired t-test, Passing–Bablok regression, and Bland–Altman analysis. The paired t-test has been performed for all the parameters selected for the analysis, in its parametric or nonparametric form (Wilcoxon matched pairs signed-rank test) in according to D'Agostino-Pearson omnibus normality test result. With the paired t-test, the null hypothesis of no difference between the two systems in mean values of each spatio-temporal parameter was tested. A two-tail test was used and the nominal alpha level was set to 0.05 [62]. In combination with the t-test, the linear correlation between each pair of measurements has been assessed, using Pearson's correlation coefficient (r). The agreement was further investigated using Passing-Bablok regression and Bland-Altman plots, with the aim to find out any proportional or constant systematic error between the two methods of measurement. Passing-Bablok regression is a method proposed in 1983 for testing the agreement of two sets of measurement achieved by different systems [63]. The novelties taken by this method, with respect to the standard linear regression are that it is based on nonparametric model, it is not sensitive towards outliers, and it assumes imprecision in both measurement methods and that errors in both methods have the same distribution, not necessarily normal. As quantitative outcomes, this method returns slope (proportional systematic error) and intercept (constant systematic error) of the fitting linear model. The quantitative-based rules to accept the agreement between systems are whether the confidence intervals (CI) of slope and intercept contain respectively 1 and 0 [63]. Bland-Altman analysis is a graphical method based on the plots of the differences between two measurements against their averages, and it is the most popular method used to measure agreement between two measurement systems [64]. If the differences are randomly distributed around the zero-value axis, no proportional nor systematic error is underlined by the analysis. Quantitative assessment is given through the bias, as the mean of the differences, and the limits of agreement (LoA) assessed as the bias minus 1.96 times standard deviation of the differences [65-68]. If the differences between methods do not have a normal and/or symmetric distribution, LoA are considered to be between the 2.5% and 97.5% percentiles. Significant statistical errors are said to be present if the confidence interval does not contain zero value. Bland and Altman propose to accept the agreement between the methods under test if this interval contains zero value [65]. Statistical analyses were performed using R software (ver. 4.0.3).

The analysis of agreement between the two methods of measurement was carried out performing a paired t-test on all the parameters considered for the analysis. For each parameter, the values deriving from all the trials performed were considered, with no separation between subjects or walking speeds adopted. Table 3 shows mean and standard deviation values of each analyzed parameter dataset for each system of measure. The results of the two tailed paired t-test, with a confidence interval of 95%, are reported using a symbol in accordance with the following convention: ns p-value > 0.05, * p-value < 0.05, ** p-value < 0.01, *** p-value < 0.001, **** p-value < 0.0001. The hypothesis of no difference between systems was tested, so lower p-values suggest rejecting the accordance of systems. In the same table (Table 3) Pearson's r values are reported.

The Bland-Altman analysis produces the plots shown in Figures 6a-10a. They provide a qualitative assessment of the distribution of the differences between methods. The descriptive numeric values deriving from the analysis are reported in Table 4. The bias represents the mean of the differences between the measures computed by the systems, it is provided with the limits of its 95% CI. In the plots, biases are reported as continue red lines, while the red dashed lines represent the corresponding confidence intervals. The LoA reported in Table 4 are also shown in the graphical representations as black dashed lines. They are assessed as the 2.5 and 97.5 percentiles of differences, as they do not have a symmetric gaussian distribution.

The last analysis on data was performed using Passing-Bablok regression. In addition to the previous analyses, this analysis can reveal the presence of a trend between the measures of the two systems, thus indicating a proportional error in the tested method according to the slope of the fitting regression line. Figures 6b-10b show the scatter plot of the dataset for each parameter, with the Passing-Bablok regression line in black. The shaded area around the regression line represents its CI, while the red dashed line corresponds to the reference identity line, to which the regression line should be tend in a scenario of perfect agreement. In the Passing-Bablok plots, Pearson's correlation coefficient (r) is also shown because high values of r justify the choice to perform a linear regression analysis. The quantitative outcomes of Passing-Bablok analysis are reported in Table 5: slope and intercept of the regression line are listed for each parameter, along with the corresponding 95% CI limits.

Table 3. Paired t-test between the two devices for each parameter and study of correlation

Variable	Sock (mean ± std)	BTS (mean ± std)	p-value Summary[1]	Pearson's r
Gait Cycle Time [s]	1.15 ± 0.25	1.15 ± 0.26	ns	0.992
Cadence [step/min]	109.30 ± 21.85	109.60 ± 22.25	*	0.996
Stance Time [s]	0.63 ± 0.19	0.70 ± 0.18	****	0.994
Swing Time [s]	0.52 ± 0.07	0.45 ± 0.08	****	0.969
Step Length [m]	0.73 ± 0.08	0.68 ± 0.10	****	0.283

[1] ns $p > 0.05$, * $p < 0.05$, ** $p < 0.01$, *** $p < 0.001$, **** $p < 0.0001$

Table 4. Bland-Altman analysis

Variable	Bias	Lower Bound Bias CI	Upper Bound Bias CI	Lower Bound LoA	Upper Bound LoA
Gait Cycle Time [s]	0.00	-0.01	0.01	-0.06	0.05
Cadence [step/min]	-0.35	-0.74	0.03	-3.83	3.26
Stance Time [s]	-0.07	-0.07	-0.06	-0.11	0.01
Swing Time [s]	0.07	0.07	0.08	0.04	0.10
Step Length [m]	0.06	0.03	0.08	-0.13	0.25

Table 5. Passing-Bablok regression analysis

Variable	Slope	Lower Bound Slope CI	Upper Bound Slope CI	Intercept	Lower Bound Intercept CI	Upper Bound Intercept CI
Gait Cycle Time [s]	1.00	0.99	1.02	0.00	-0.02	0.02
Cadence [step/min]	0.99	0.97	1.00	0.74	-0.95	2.38
Stance Time [s]	1.06	1.03	1.08	-0.11	-0.13	-0.09
Swing Time [s]	0.90	0.87	0.94	0.12	0.10	0.13
Step Length [m]	0.70	0.52	0.95	0.25	0.08	0.36

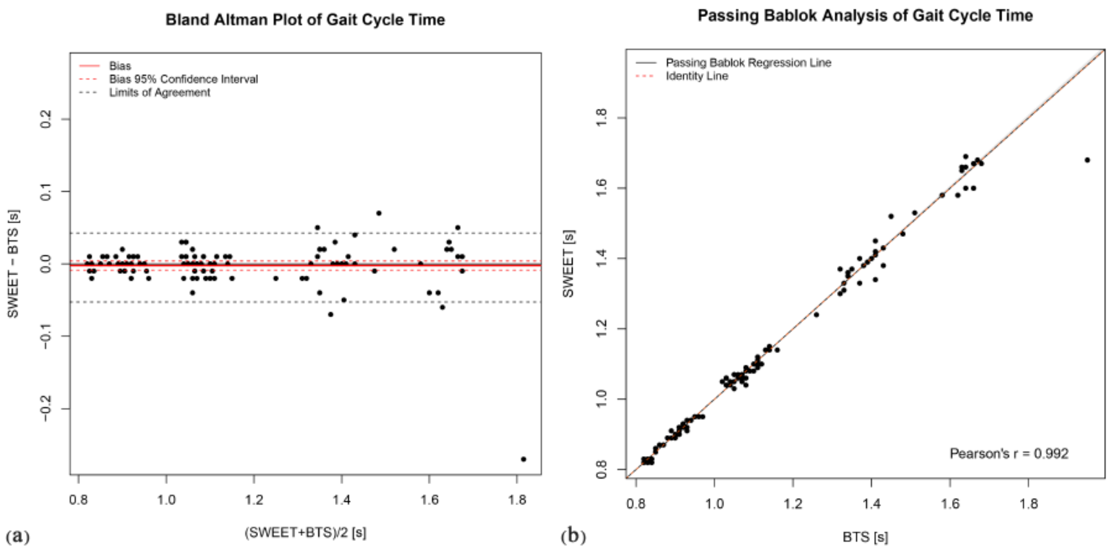

Figure 6. Gait cycle time: (**a**) Bland–Altman plot; (**b**) Passing–Bablok regression analysis

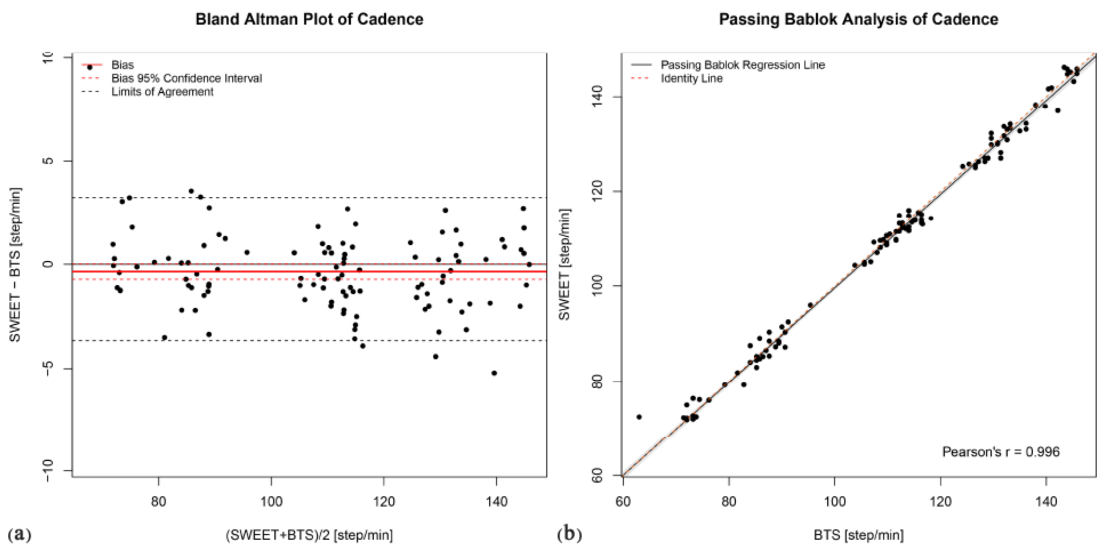

Figure 7. Cadence: (a) Bland–Altman plot; (b) Passing–Bablok regression analysis

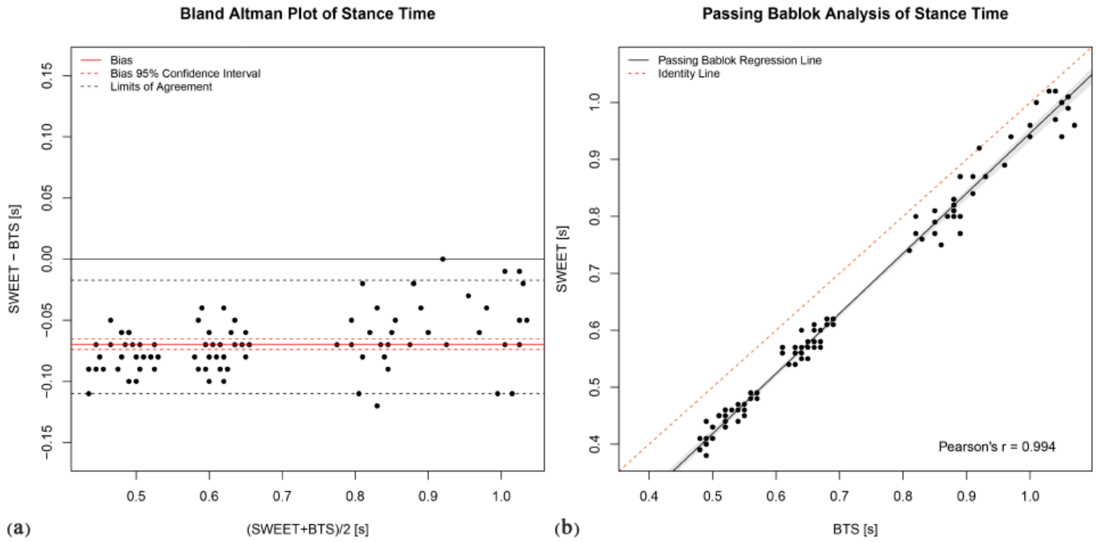

(a) (b)

Figure 8. Stance Time: (a) Bland–Altman plot; (b) Passing–Bablok regression analysis

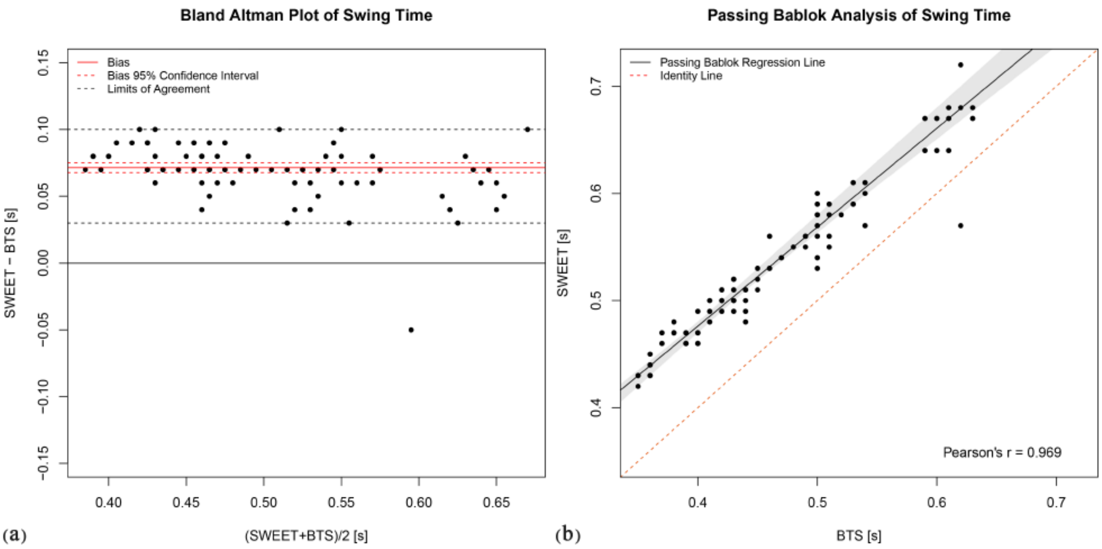

(a) (b)

Figure 9. Swing Time: (a) Bland–Altman plot; (b) Passing–Bablok regression analysis

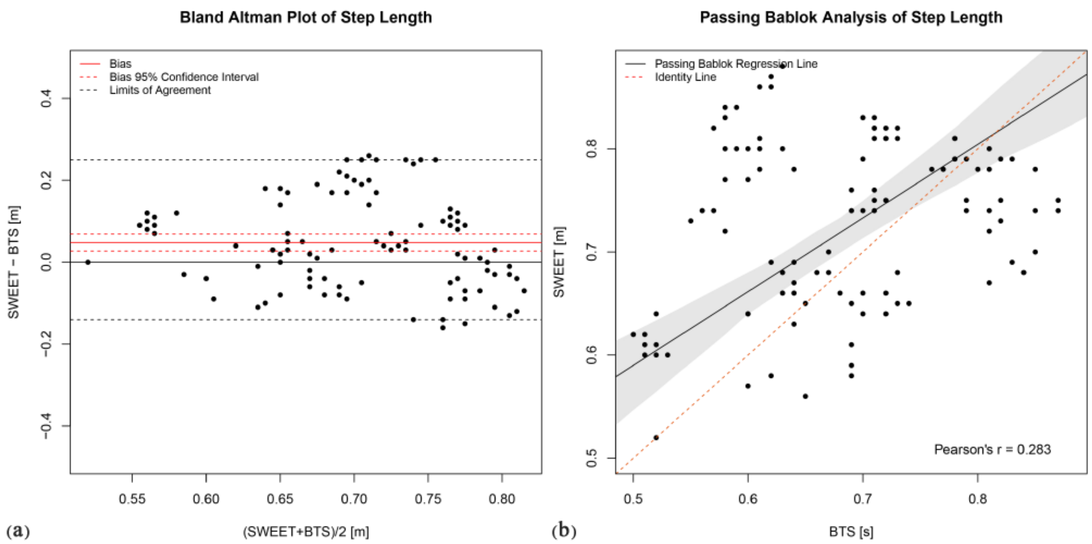

Figure 10. Step length: (a) Bland–Altman plot; (b) Passing–Bablok regression analysis

In the assessment of the mean gait cycle time, significant agreement has been pointed out by the statistical analysis. The paired t-test leads to a non-significant p-value ($p > 0.05$), suggesting to accept the hypothesis of no difference between systems. The bias value in the Bland-Altman analysis is null (0.00 from Table 4) and the LoA are very low (in the order of few hundredths of a second). The Pearson's correlation coefficient is very high (0.992), supporting the concept of a linear dependence between the measures, explored by means of Passing-Bablok analysis. The regression line obtained with this method coincides with the identity line (slope = 1.00, intercept = 0.00), confirming the significant agreement between the two methods in assessing gait cycle time.

Concerning the measure of cadence, a deeper discussion is required. The T-test result suggests to refuse the hypothesis of absence of difference between the methods, but with low significance ($0.05 < \text{p-value} < 0.01$). The bias pointed out by Bland-Altman analysis is very low (-0.35, about 0.3% of the average value of cadence), with its 95% CI containing the zero value and limited to few units of steps per minute (-0.74 to 0.03). Passing–Bablok regression is legitimated by a high value of Pearson's r (0.996): its slope is very close to 1 (0.99 with CI of 0.97–1.00), the intercept is different from 0 (0.74) but its CI contains this value (-0.95 to 2.38). Starting from these results and analyzing the Bland-Altman Plot in Figure 7a, it can be observed that the SWEET system slightly underestimates the value of cadence compared to BTS system. Further exploring data, the cause of the non-perfect agreement was identified in the different range of steps analyzed by the two systems. The reference system SMART-DX 700 by BTS performs gait analysis on a limited range of steps, contained in the central 3 or 4 strides of the walking trial, as they are completely included in the field of view of the cameras. The detected volume cannot be extended because it is limited by the configuration of the system which considers the limited volume of the laboratory. Instead, SWEET Sock system elaborates the entire signal coming from the IMUs, removing only the first and the last steps performed to start and stop walking. The analysis of the punctual values of cadence assessed in each single step of the walking trial by SWEET Sock system clarify that in the first and last part of walking a lower step cadence is adopted. Figure 11 shows, for each step of the walking trial, the average of the differences between the punctual cadence assessed by SWEET and the mean step cadence suggested by BTS system. It can be observed that in the first and last part of walking the difference is higher in absolute value, while in the middle steps it is reduced. Therefore, it can be affirmed that probably a better agreement would have been obtained if the same range of steps were analyzed by the two systems. It has not chosen to do so for two reasons: the first is that in SMART-DX 700 the steps to be considered in the analysis have to be chosen manually, while the signal processing of SWEET Sock is entirely automatic, and second because it has not chosen to modify the methods of analysis of SWEET system, which can provide more accurate results by taking into account the entire walking trial.

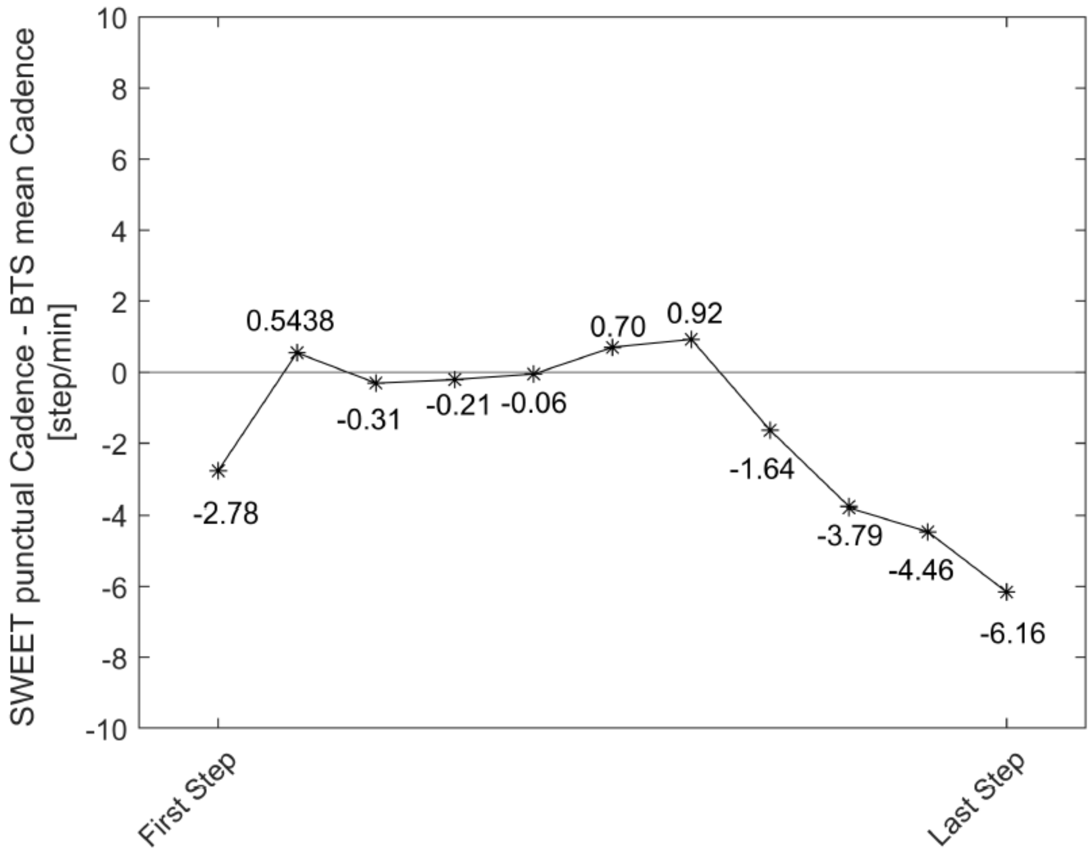

Figure 11. Mean difference between the punctual cadence assessed by SWEET and the mean step cadence suggested by BTS system for each step of the walking trial

Stance and swing phase durations are complementary parameters, because they are the two parts composing the gait cycle time. Gait cycle time is defined as the time between two successive initial contacts of the same foot. Stance phase duration is the time between the initial contact and the successive terminal contact of the same foot, while swing time goes from the terminal contact to the subsequent initial contact. The complementarity of these parameters is perfectly reflected in the results of the statistical analyses. The T-test identified a significative statistical difference between the systems (p-values < 0.0001), even if a linear correlation exists in both stance and swing phase durations as shown by Pearson's r values, respectively 0.994 and 0.969. The Bland-Altman plots clearly show that SWEET system underestimates Stance time compared to BTS system (bias = -0.07), and therefore overestimates of the same quantity the Swing time (bias = 0.07). Passing-Bablok results confirm the presence of a systematic error in the measures: intercepts' CIs are symmetric for the two variables and do not contain zero value (stance CIs = -0.13 to -0.09, swing CIs = 0.10 to 0.13). It also points out a proportional error proven by the fact that the slopes of the two regression lines are different from 1 (the CIs are respectively from 1.03 to 1.08 and, symmetrically, from 0.87 to 0.94). Therefore, the difference between the methods of measures is made of a constant part and a proportional part which grows when the value of the parameter is increased. The error is to be probably addressed to the wrong detection of the initial and terminal contact of the foot with the ground, made by SWEET system through the analysis of the filtered gyroscope signal in accordance to the rules illustrated by Doheny et al. in [69]. Although the gait cycle time shows very good agreement, it does not mean that the initial contacts are well identified in the signal, because they could be all translated in time of the same quantity, still resulting in good output values. To understand the error a further analysis is required on the mutual position of initial and terminal contacts identified on gyroscope signals.

The last parameter is the step length, which has been selected to investigate the performances of SWEET system in the assessment of spatial measures. Results of the statistical analysis are not very encouraging. T-test points out a significative statistical difference between the measures of the systems ($p < 0.0001$), that is confirmed by Bland-Altman analysis. Actually, even if the CI of bias includes the zero, it is quite wide (-0.13 to 0.25 m) for the precision required in this spatial metric. Moreover, the reduced value of Pearson's coefficient shows that no linear correlation exists between the measures ($r = 0.283$), so it does not make sense to perform the Passing-Bablok regression analysis. Actually Passing-Bablok regression line in Figure 10b does not fit accurately the points, which are distributed with no detectable trend. These results allow to affirm that there is not agreement between the systems in the assessment of the step length. Moreover, in this case the cause of the error could be probably found in the processing of the gyroscope signal that lead to the assessment of the spatial parameters. The algorithm proposed in [69] is based on modeling the movement of the shank as a single pendulum, thus deriving the spatial parameters from the calculation of the angle covered by the foot during the swing phase and using geometrical consideration. A further analysis is required to understand if this model is too simplistic to represent leg swing during gait or if other aspects (device positioning, signal filtering, etc.) cause errors in the measure of spatial parameters in SWEET Sock system. The first purpose is to try maintaining a gyroscope-based algorithm for gait assessment, by considering other more specific models proposed in literature regarding the movement of the shank during the swing phase. An example is the double segment gait model involving both shank and thigh proposed by Tong et al. in [70]. Doing so it can be avoid the use of other sensors data, such as linear accelerations, keeping the gyroscope advantages explored in the description of the electronic unit, and avoiding the reconfiguration of the entire system.

A deeply work based on the exploration of the scientific literature was performed to find out and analyze other results from gait analysis systems based on similar measuring principles. Some works exist regarding validation analysis of wearable systems for gait analysis based on processing of kinematic signals. These studies address comparative analyses with clinical instruments, such as instrumented treadmill [71], force platform [72] or pressure sensitive walkway (GAITRite R) [73,74]. No works presenting a comparative analysis with the gold standard (stereophotogrammetry system) has been found. Results from the analyzed works show a common trend: temporal parameters present a better agreement than spatial metrics. Among temporal parameters, step time and GCT show the best agreement, while stance and swing phases measurements are moderately correlated with reference measures. The presented results are in accordance with this trend, confirming the poor performances of IMU-based systems in assessing gait spatial metrics. Only in [52] spatial metrics show a good agreement level, that could be caused by the different placement of IMUs, placed on both feet rather than on shanks. Results from the work in [71] demonstrated that foot placement allow a better measurement of spatial gait parameters. However, it was not chosen this placement because it can worsen the comfort and wearability of the system for users and preclude its in-shoes use.

In addition to the validation of technical performance, the wearability and comfort assessment was carried out in order to evaluate the acceptance of the system by final users and to identify possible areas of improvement in terms of design. To carry out this conformity assessment, an already validated methodology was used, specifically the Comfort Rating Scales (CRSs). The wearability evaluation of a device is a multidimensional analysis: wearable devices affect the wearer in different ways. Among the effects to be taken into consideration, there are those related to comfort. When wearing something, the level of comfort can be affected by several aspects, such as device size and weight, how it affects movement, and pain. The design of the sock has been implemented in order to achieve the greatest comfort for the user. The integrated pressure sensors are made of textile material, therefore are flexible and imperceptible on the skin. The electronic unit has also been designed to be as comfortable as possible for the user: it is light and it can be connected to the textile sock without the need to use bands. In fact, the use of the latter could cause discomfort to the user due to the presence of a narrow element tied to the limb. In addition to physical factors, comfort may be affected by psychological responses such as embarrassment or anxiety. Consequently, Knight and Baber proposed that comfort should be measured across a number of dimensions and for such task they developed the CRSs [75].

The CRSs provide a quick and easy-to-use tool to assess the comfort of wearable devices, which attempt to gain a comprehensive assessment of the comfort status of the wearer of any item of technology by measuring comfort across the six dimensions described in Table 6. In rating perceptions of comfort, the scorer simply marks on the scale his or her level of agreement, from low (0) to high (20), with the statements made in the "description" column of Table 6. According to Knight and Baber, this range was considered large enough to elicit a range of responses that could be used for detailed analysis [75]. The three participants involved in the study were invited to fill in the CRSs to provide a judgment on their comfort. Table 6 shows the scores assigned, for each field, by the subjects involved in the study. Although the evaluation was carried out on only three people, it provides a preliminary measure of the comfort of the prototype device. Knight et al. [76] have proposed five Wearability Levels (WLs), determined by proportioning the scales into equal parts (Table 7). The mean score of Emotion dimension is in the WL2 suggesting that users show little embarrassment in wearing the system. All the other dimensions were rated in the WL1 proving a high wearability and comfort of the device. However, to better identify the wearability level of the device and how to improve it, future analysis will aim to make a significant assessment of comfort, testing the device on a wider cohort of subjects.

Table 6. Comfort rating scales

Title	**Description**	**Subject 1**	**Subject 2**	**Subject 3**	**Mean**
Emotion	I am worried about how I look when I wear this device. I feel tense or on edge because I am wearing the device	7	4	7	6.0
Attachment	I can feel the device on my body. I can feel the device moving	3	3	5	3.7
Harm	The device is causing me some harm. The device is painful to wear	0	0	0	0.0
Perceived change	Wearing the device makes me feel physically different. I feel strange wearing the device	5	0	0	1.7
Movement	The device affects the way I move. The device inhibits or restricts my movement	5	2	1	2.7
Anxiety	I do not feel secure wearing the device	0	0	0	0.0

Table 7. Wearability Levels

Wearability Level	CRS Score	Outcome
WL1	0-4	System is wearable
WL2	5-8	System is wearable, but changes may be necessary, further investigation is needed
WL3	9-12	System is wearable, but changes are advised, uncomfortable
WL4	13-16	System is not wearable, fatiguing, very uncomfortable
WL5	17-20	System is not wearable, extremely stressful, and potentially harmful

Resuming, SWEET Sock is a new wearable and portable device for the measurement and analysis of biosignals, based on textile sensors, able to perform posturographic assessment and gait analysis. The development of the system and the validation analysis of the performances of the novel system in gait assessment was presented.

The sensing unit is a textile sock in which textile sensors and bus structures are integrated, making it possible to use the system during normal daily activities, without any discomfort. The system includes a mobile app for real time visualization of the acquired signals and a software desktop for off-line plotting and digital signal processing.

The analysis of the performances of the system in gait assessment was performed by comparing the results given by the novel system with the corresponding values computed by an optoelectronic stereophotogrammetric system (SMART-DX 700 by BTS Bioengineering) in the analysis of 108 walking trials at different walking speeds. Study results showed that the agreement is not confirmed for all the spatio-temporal gait parameters analyzed. In particular, gait cycle time and cadence are the two parameters presenting the best agreement, even if the latter presents a small systematic difference between the values computed by the two systems. Stance and swing phase durations presented both systematic and proportional errors in the comparison between the methods. Although both errors could be removed by taking into account this misalignment, a further analysis need to be performed to understand and correct the problems directly in the processing phase. Worse results are achieved in the analysis of spatial parameters' agreement. The measures of step length provided by the two systems are not correlated. For this parameter, a further analysis is required to correct the issues in the computational process. Based on these findings, it can affirmed that the novel system can be safely used in the evaluation of gait cycle time while some issues were found in the validation of the other temporal and spatial parameters. Future developments will concern the resolution of the problems encountered in this work and the execution of a similar validation analysis regarding the posturographic assessment provided by the system. The innovative features of the system rely in the multiparametric approach in health monitoring and in its ease of use. The “wearability” of the system and its comfortable use make it very suitable to be used in domestic environment for the continuous remote health monitoring of de-hospitalized patients. The CRSs were used to assess the comfort of the wearable system. The scores provided by the subjects involved in the study, allow to assume a good level of comfort when the socks are used.

Another valid field of interest regards occupational ergonomics, related to the prevention of WSMDs in healthcare workers.

The use of SWEET Sock during working hours by nurses and therapists could help monitor postural and dynamic variables in activities most associated with exposure to biomechanical overload (i.e., frequent patient handling, pushing and pulling, awkward postures, prolonged standing, and significant sideways twisting).

The biomechanical advantage of using patient handling devices and technological aids, including exoskeletons, could be verified through the analysis of postural parameters. Gait analysis could help rethink preventive strategies aimed at work organization (for example by providing for the alternation of dynamic and static phases, and adequate recovery breaks). Last, but not least, balance analysis and COP coordinates could provide insights into the prevention of slips, trips, and falls, which are the second most common cause of injuries leading to lost working days in hospitals. The advantages combined in a minimally invasive device, together with the accuracy and reliability of the measurement, and the future opportunity of integration into IoT networks open new perspectives to increase the effectiveness of prevention and safety strategies in healthcare workers.

2.2 E-textile shirt

The second e-textile prototype developed during the research activity was a shirt named SWEET Shirt [77].

The SWEET Shirt is a wearable sensing device that allows for the acquisition of ECG, bicep EMG and trunk acceleration signals. It can be integrated within a complete system for remote healthcare purposes, as illustrated by the schematic shown in Figure 12.

Figure 12. System architecture: 1) wearable sensing device; 2) electronic unit; 3) SWEET App; 4) cloud; 5) SWEET Lab

The wearable sensor unit allows for bio-signal acquisition when connected to the analogue front-end located in the electronic unit. This unit also contains a microcontroller and allows for data transmission through an integrated BLE module. A custom-made Android mobile application was developed to receive and visualize real-time signals on a smartphone, and to subsequently upload data on a dedicated web server. This server presents a restricted area that is exclusively accessible (following prior authentication) by authorized and appointed healthcare professionals, who can download, analyze and process the data using the custom-made MATLAB desktop software.

Below, the functional modules of the system are individually presented.

The wearable sensing unit is comprised of a commercial elastic t-shirt in which e-textile electrodes are integrated. A knit conductive fabric with a resistance of less than 0.03 ohm per cm in any direction across the textile was used to produce the electrodes. This fabric (Adafruit Inc. www.adafruit.com – product ID: 1167) is plated with real silver, which gives it highly conductive properties. Two 4 x 2 cm electrodes were integrated within the garment as sensing elements for ECG processes, with two 2 x 2 cm electrodes placed on each shirt sleeve for EMG acquisition and a 2 x 2 cm electrode integrated within the upper part of the chest as a ground electrode for all the biosignals. A conductive ribbon (5 mm in width; Adafruit Inc. product ID: 1244) was then used to connect the electrodes to the output connectors of the wearable unit, represented by snap buttons placed in a pocket on the chest of the shirt. The conductive ribbon is made of woven conductive stainless-steel fibers, with a resistance of less than 0.1 ohm per cm. Conductive traces sewn onto the shirt were covered by a non-conductive fabric to avoid contact with the skin. Figure 13 shows a schematic of the wearable sensing unit, with the complete unit and the main details shown.

Figure 13. SWEET shirt sensing unit: a) internal view with textile electrodes and connections; b) external view

The electronic unit is a compact module containing all the electric and electronic elements that allow for the acquisition, digitalization and wireless transmission of the signals. It was decided to develop a custom-made analogue front-end for the ECG and EMG measurement in view of suitably dealing with the higher impedance caused by the fabric electrodes. The analogue front-end for ECG measurement comprises four principal stages: an instrumentational amplifier INA 118 from Texas Instruments, a high-pass passive filter with a cut-off frequency of 0.05 Hz, an isolation stage designed with an OpAmp LM358 in voltage follower configuration, and a low-pass active filter with a cut-off frequency of 40 Hz. The first filter is a first order high-pass CR passive filter, while the last stage is represented by a first-order active filter comprising an OpAmp LM324 in non-inverting configuration with a RC feedback. In terms of the EMG analogue front-end, three principal stages were designed, with the first two similar to those used for the ECG analogue front-end but with the high-pass cut-off frequency set to 15 Hz. The last stage is a precision rectifier circuit with the integration of a low-pass filter. The rectifier circuit comprises an OpAmp LM324, two diodes and a resistor on the feedback connection. This form of configuration is also known as super-diode configuration. Meanwhile, a capacitor was added in parallel to the resistor to ensure this stage acts as a first-order low-pass filter. The various components were chosen to set the filter cut-off frequency at 30 Hz. The introduction of this rectifying stage was important as we are interested in the EMG envelope signal for performing the subsequent processing operations. Generally, an EMG signal is sampled and then rectified in the digital domain; however, it was preferred to rectify it in the analogue domain in order to use a lower sampling frequency. The digitalization of EMG signals requires a high sampling frequency, around 800 - 1.000 Hz, since the highest spectral components are at around 400 - 500 Hz. In contrast, an EMG envelope requires a lower sampling rate since its main spectral information is at low frequencies. The use of a lower sampling rate facilitates the real-time transmission of the signal. Moreover, using this configuration, the mobile application can provide the user with real-time EMG envelope signals, without the use of a processing stage that would increase the complexity of the system and potentially introduce delays. The electronic board, FLORA 9-DOF (Adafruit Inc.), which mounts the triaxial inertial module iNEMO LSM9DS0, was integrated within the electronic unit to acquire accelerometric signals, while a LilyPad Simblee™ BLE board (Sparkfun Inc.), was used as the system control unit. This unit provides the digitalization of the ECG and EMG signals and is connected to the Flora accelerometer through the serial I2C bus. The LilyPad Simblee board also allows for sending data via a BLE protocol, using the Simblee™ Bluetooth® Smart Module integrated on the shield. In fact, BLE technology presents a perfect trade-off between energy consumption, latency, piconet size, and throughput [78]. The choice of using BLE technology can also be regarded as a means of increasing the battery life of the device as much as possible. Battery life is a central issue in the development of portable devices and, in this type of application, it is mostly influenced by the data transmission operations. Indeed, BLE is one of the most data-saving transmission protocols, while other solutions have been proposed based on reducing the amount of data to be sent, using a compression method that does not degrade the signal quality [79,80]. The control unit features were implemented through employing an ARM® Cortex M0 microcontroller that can be programmed using the Arduino IDE. The control unit was programmed to digitalize ECG and EMG analogue signals and to receive digital data from the accelerometer. Here, the ECG signal is digitalized with a sample rate of 200 Hz, while the EMG and accelerometric signals are acquired using a sample period of 15 ms (66.7 Hz). All data are collected in 20-bytes-sized packets and are sent in real time via BLE to the smartphone using the SWEET app. The packet transfer rate was set to 66.7 Hz, which was experimentally identified as the maximum rate supported by BLE transmission without data loss. Hence, each packet contains one sample from EMG and triaxial acceleration signals and three successive ECG samples in accordance with their sampling rates. Despite the fact that the sampling rates chosen for the ECG and EMG signals were lower than those usually used, they were in line with the time resolution required by conventional target applications. In ECG digital processing, since the focus was not in signal morphology but on heart rate analysis, the latter can be accurately performed with a lower sampling rate [81]. With regard to EMG signaling, the envelope signal was extracted in the analogue domain such that it can be safely sampled using the chosen rate. All the modules that make up the electronic unit are powered by a 1,200 mAh/3.7 V lithium battery placed on the back of the unit, which is enclosed in a 3D-printed plastic case (10 x 7.5 x 2 cm^3). On the top part of the case, eight snap buttons were integrated to allow for connection to the wearable sensing unit, thus providing the input signals for the analogue front ends. Figure 14 shows the internal electronic board and the complete unit.

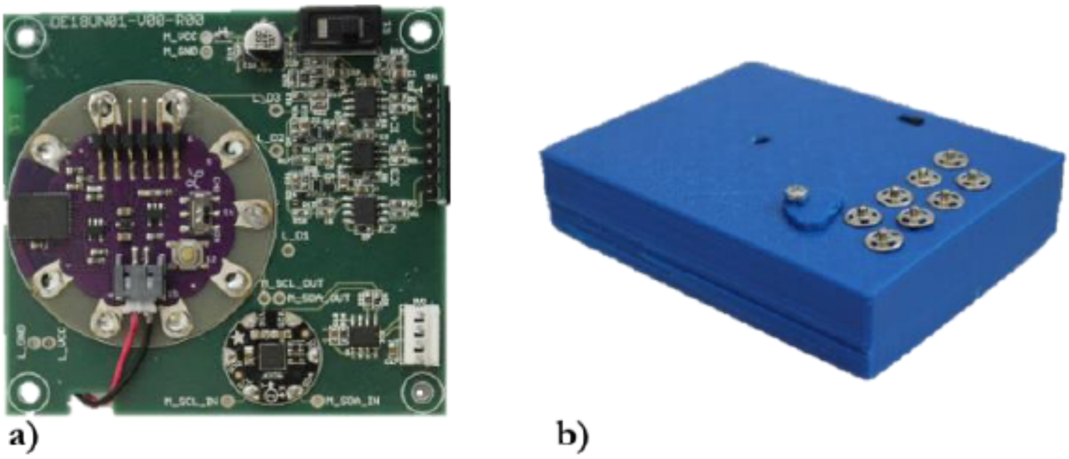

Figure 14. SWEET Shirt electronic unit: a) internal electronic unit, b) complete unit, external view

The SWEET app is a custom-made application for mobile devices requiring an operating system of Android 6.0 or higher and BLE technology. The application allows the smartphone to communicate and receive data coming from the electronic unit, via the BLE protocol. When the application is started, it is possible to associate and connect the wearable device using its MAC (media access control) address. Following this, the measurement session can commence, with the data transferred from the electronic unit to the mobile device, which allows for real-time signal plotting. At the end of the session, the data will be automatically saved in a '.csv' file, which is stored locally and can be uploaded at any time to a dedicated web server. Figure 15 shows the main frames of the app.

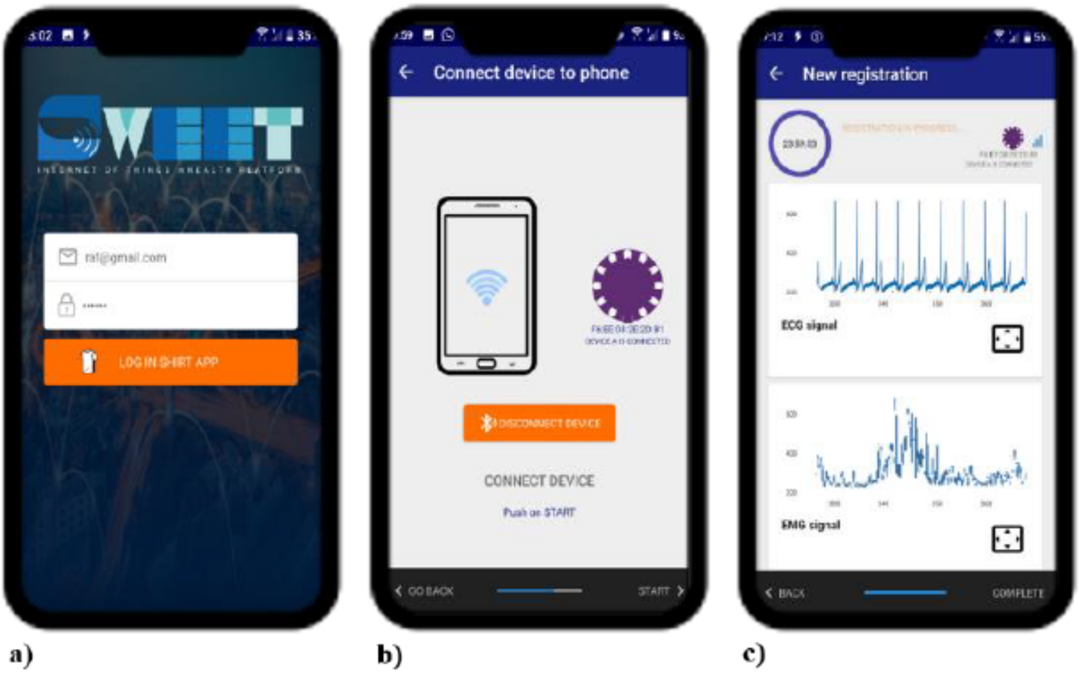

Figure 15. SWEET app main frames: a) login; b) unit connection; c) real-time signal visualization

Data from the web server can be accessed and downloaded only by authorized healthcare professionals. The custom-made MATLAB GUI software, SWEET Lab, can be used to plot and post-process signals in order to achieve a huge set of synthetic parameters of clinical interest.

The first step in ECG signal processing involves the detection of QRS complexes using an Okada algorithm [82] for the assessment of the tachogram and the discrete series of RR intervals. The subsequent analysis is divided into seven frameworks, the first of which relates to the heart rate (HR) analysis, with the instantaneous HR assessed as the mean over four successive beats. From this series, the minimum, the maximum, the medium and the median HRs can be extracted and the tachycardia (HR > 110 bpm) and bradycardia (HR < 60 bpm) events subsequently searched and listed.

The second framework is dedicated to the heart rate variability (HRV) analysis in terms of the time, frequency and time–frequency domains. Here, the beats are first classified in terms of normal, ectopic, premature ventricular contraction (PVC) and artifacts based on their timing before the RR series is edited to exclude any artifacts and any beat-to-beat intervals that are too short or too long. The new RR series is then processed in the time domain to extract the statistical and geometrical measures, as listed in Table 8 [83].

Table 8. HRV time domain variables

STATISTICAL MEASURES	
Variable	**Description**
SDNN [ms] (Standard Deviation NN-intervals)	Standard deviation of normal-to-normal intervals (NN). SDNN reflects all cycles responsible for heart rate variation in time, thus representing the total variability
SDANN [ms] (Standard Deviation Averaged NN-intervals)	Standard deviation of the average NN intervals calculated over 5 min. SDNN is therefore a measure of the changes in heart rate due to cycles longer than 5 min
SDNNi [ms] (SDNN index)	Mean of SDs of NN intervals, calculated over 5 min
RMSSD [ms] (Root Mean Square of Successive Differences)	Square root of the mean of the squares of the successive differences between adjacent NN intervals
NN50	Number of pairs of successive NNs that differ by more than 50 ms
pNN50 in %	Proportion of NN50 divided by total number of NN intervals
GEOMETRICAL MEASURES	
Variable	**Description**
HRV Ti (Triangular index)	Area of the histogram distribution of RR intervals, normalized to the maximum value of the histogram
TINN	Base width of the RR intervals histogram

The HRV is also assessed in the frequency domain by analyzing how the PSD is distributed as a function of frequency. The PSD presents three main components in terms of very low frequency (VLF), low frequency (LF) and high frequency (HF). The frequency peaks and the absolute and relative power values of each component are computed along with the LFHF ratio [84]. Three different methods are provided by the software to compute the PSD, namely, the Welch Periodogram [85], Burg Periodogram [86] and e Lomb-Scargle Periodogram [87] methods. The same analyses are conducted on the windowed periodogram of the RR series to obtain a time-frequency domain analysis of the HRV variability.

The third framework in the ECG processing relates to heart rate turbulence (HRT) analysis. This form of analysis presents a non-invasive method that explains the response of the heart to ventricular arrythmias [88] and is a good predictor of mortality following acute myocardial infarction [89]. Two numerical parameters are assessed by the software to describe HRT: turbulence onset (TO: to describe the initial acceleration in heart rate following PVC), and turbulence slope (TS: to reflect the subsequent deceleration of the sinus rhythm) [88]. Meanwhile, the fourth framework provides a nonlinear analysis of ECG signals using four different approaches: sample entropy, detrended fluctuation analysis

(DFA), Poincaré plots and fractal dimension analysis (FDA). Here, sample entropy presents a nonlinear method for determining the complexity of a RR series, which is computed in terms of various values of k and is used for HRV analysis [90]. Meanwhile, DFA is used to quantify the fractal properties of brief intervals of the tachogram signal [91], while a Poincaré plot is a plot of RR intervals vs. the previous RR intervals used to quantify self-similarity. Two numerical parameters are assessed in Poincaré plot analysis: SD2 (the magnitude of the major axis of the ellipse fitting the data; represents the short-term variability) and SD1 (the magnitude of the minor axis of the ellipse; represents the long-term variability). Finally, FDA provides the measurement of the fractal dimension of the RR series assessed using a Higuchi algorithm [92]. The fractal dimension is a useful indicator in cardiology since it assumes different values for different types of heart disease [93].

The presented shirt prototype was validated through a benchmarking analysis with a gold standard with reference only to the EMG signal. Three different type of analysis were conducted in order to address any possible unconformity in the measurement and/or processing phases managed by the new prototype. Firstly, the RR intervals identified by the SWEET Shirt were compared with those obtained via a reference device. Secondly, the similarity between the ECG signals obtained via the different devices was assessed. Finally, comparative analysis was carried out to validate a specific subset of parameters derived from the SWEET Lab software signal processing.

A three-channel digital Holter recorder (Oxford Medilog FD5) was used as the reference for the ECG signal measurement. The device incorporates seven electrodes and operates with a sampling rate of 8000 Hz and a resolution of 15.5 bits. A healthy subject, aged 25, was equipped with the clinical Holter device along with the prototypal wearable device, SWEET Shirt, for the ECG measurement (Figure 16). Here, the Holter's electrodes were placed on the subject's thorax (Figure 16a, b) in order to avoid any overlapping with the SWEET Shirt e-textile electrodes and to ensure the two ECG waveform were as similar as possible by means of visual analysis. The ECG acquisition time was set to 2 h.

Figure 16. ECG electrode configuration used for signal acquisition

The ECG signals from both measurement units were loaded in the MATLAB environment for pre-processing and analysis operations, with both signals passed through a notch digital filter to remove any 50 Hz interference. The R peaks in the ECG signal from the SWEET Shirt were identified using the Okada algorithm, while those in the Holter ECG were automatically detected via its own software and could be loaded in the MATLAB environment. The first analysis was carried out to compare the RR intervals by means of Passing-Bablok regression. To achieve interval-to-interval correspondence, six RR values from the Holter series were removed since they corresponded to a region of artefacts in the SWEET ECG signal. Following this, comparative analysis was performed using the MATLAB function for Passing-Bablok regression [94].

The waves for each beat were subsequently isolated to allow for a beat-to-beat morphology comparison. The cut-off point was chosen as the midpoint between two subsequent R peaks in order to cover the complete signal. The R peaks was chosen as fiducial points since no significant differences were found among the RR locations in the first analysis. A set of a total of 6968 corresponding beats were obtained for the analysis. The waveforms were then resampled on a normalized axis, with common number of samples in order to allow for correlation analysis among the corresponding beats. The number of samples was chosen to equal the maximum number of samples found in a non-normalized beat. A resampling operation allows for avoiding any signal distortion in the normalizing time axis. It was decided to individually analyze the three principal constituent waves, namely, the P-wave, the QRS complex and the T-wave. Two cut-off points were set in the normalized time axis to divide the three single waves, which were selected to be the two stationary points between the three local maxima representing the single waves, as calculated based on the average beat waveform from the SWEET Shirt recording (Figure 17).

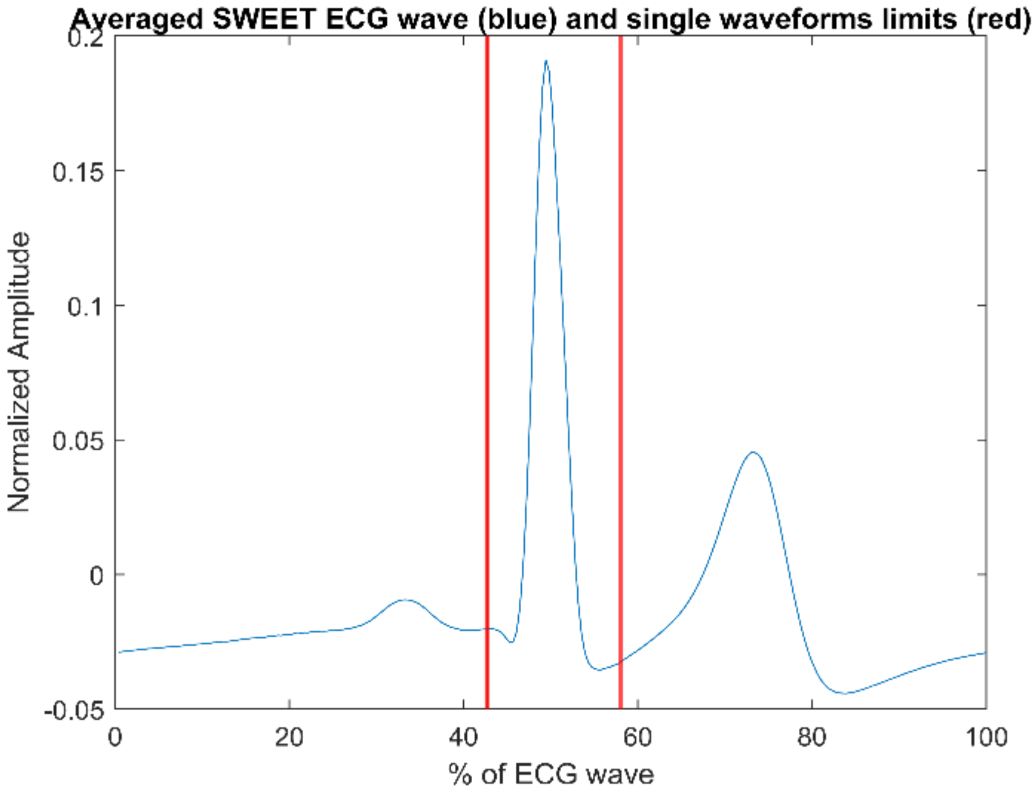

Figure 17. Average beat waveform from the SWEET Shirt and the cut-off points (red vertical lines) used to isolate single waves

The complete beat and the single waveforms were rearranged in eight matrices (four for each device recording), with each column containing the signal corresponding to an occurred beat. Correlation analysis for the waveforms was carried out using the MATLAB function, ‘corr’, which computes the linear correlation between each pair of columns in the input matrices. The diagonal elements of the output matrix hence represent the linear correlations between the corresponding waveforms recorded by the devices under examination. The ‘corr’ function also returns a matrix of p-values for testing the hypothesis of no correlation vs the alternative hypothesis of a non-zero correlation.

Finally, it was compared a subset of parameters derived from our software to those provided by the commercial Holter software in order to validate our signal processing algorithms. To this end, a further 2-h ECG recording was measured using a 68-year-old volunteer experiencing a pathological disorder (cardiopathic), with the same experimental setup as used previously. The two records were then windowed in terms of 24 five-minute segments, which were individually processed, carrying out a set of 24 measures for each record and for each parameter. The ECG signals were also windowed to enlarge the dataset for the comparison, and because five minutes is the recommended duration for short-term ECG analysis [83]. Since Holter software only provides HRV measures in the time and frequency domains, validation analysis was carried out on a subset of two representative parameters, one for each HRV field, which were computed by both systems, that is, the standard deviation of normal-to-normal beats (SDNN) for the time domain, and the ratio between low- and high-frequency spectral power (LF/HF ratio) for the frequency domain. The agreement between the measures was assessed using root mean square error (RMSE), Passing-Bablok regression and Bland-Altman analysis.

The RR series were compared using Passing-Bablok regression. This method was first proposed in 1983 as a method for testing the agreement between two sets of measurements obtained via different systems [95]. Here, the Passing-Bablok regression involved searching for a linear relationship between the measures from the two systems and the returns slope and offset of the fitting linear model. The systems could be considered as equivalent if the confidence intervals of slope and offset contained 1 and 0, respectively. Table 9 shows the results of the PB regression for the RR intervals.

Table 9. Summary statistics and results of the Passing-Bablok regression analysis for the RR interval series

Statistics	**Mean ± standard deviation**	
RR intervals from SWEET Shirt [ms]	1032 ± 77.44	
RR intervals from Holter MEdilog Darwin [ms]	1032 ± 77.41	
PB Regression	**Mean**	**Confidence interval**
Slope	1.00	[1.00 ÷ 1.00]
Offset [ms]	0.00	[0.00 ÷ 0.00]

The ECG waveforms were compared using Pearson's linear correlation analysis. Figure 18 shows the distribution of Pearson's correlation coefficients for the complete ECG waveform, the P-wave, the QRS complex and the T-wave.

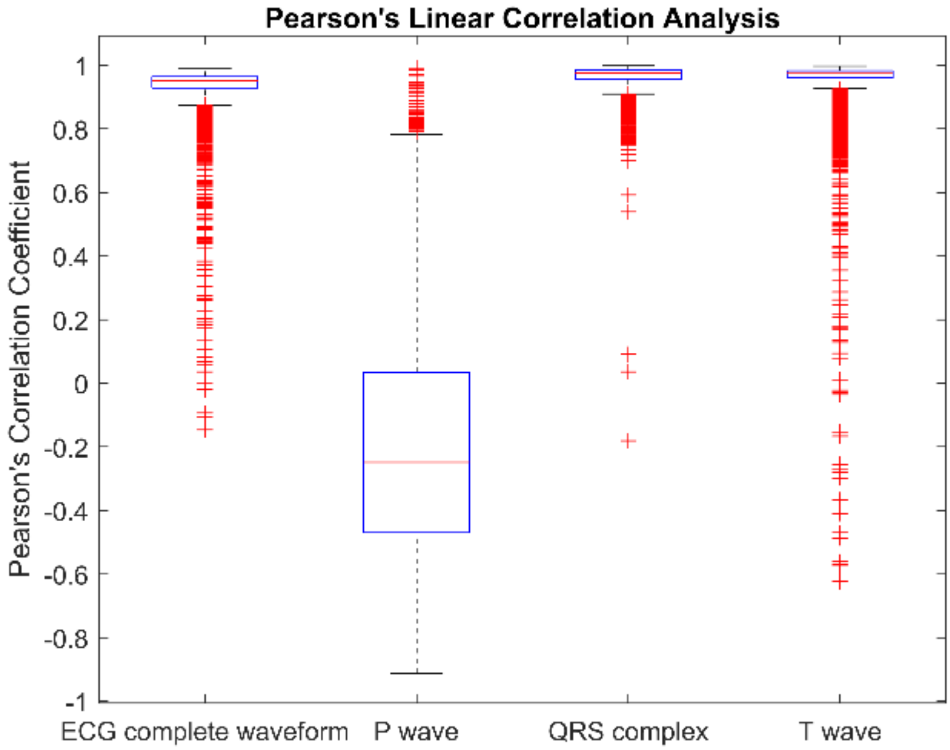

Figure 18. Boxplot of Pearson's correlation coefficient for complete and single ECG waveforms

High values of correlation were found for the ECG waveform (mean value ± standard deviation: 0.94 ± 0.07), QRS complex (0.96 ± 0.04) and T-wave (0.96 ± 0.09), while lower values were returned in the P-wave analysis (- 0.19 ± 0.36).

The quality of the correlation between each couple of beats was assessed using the following rules: (i) high correlation if $|r| \geq 0.7$, (ii) moderate correlation if $0.3 \leq |r| < 0.7$ and (iii) low correlation when $|r| < 0.3$. Table 10 shows a summary of the qualitative assessment of the correlation in terms of the percentage of beats, indicating high, moderate or low correlation.

Table 10. Qualitative assessment of correlation for ECG waveforms

	Quality of correlation		
% of the entire set	**High**	**Moderate**	**Low**
P-wave	5.97***	49.13**	44.90
QRS Complex	99.92***	0.04**	0.04
T-wave	98.87***	0.82**	0.31
ECG waveform	98.82***	0.88**	0.30

**p-value < 0.005; ***p-value < 0.001

Almost all ECG beats recorded by the prototypal device exhibited a high correlation with the corresponding waveforms obtained via the standard instrument, with a p-value excluding the hypothesis of null correlation between them. Specifically, the QRS complex and T-wave were the most comparable components, while the P-waves mainly exhibited moderate or low correlation values.

The first approach to the analysis of the parameters generated by the signal processing algorithms involved assessing the RMSEs among the different sets of measures. Table 4 shows the RMSE values and the principal descriptive statistics of the datasets, which were divided according to subject.

In the first section of Table 11, the results from the non-pathological volunteer session are reported. In this case, the RMSE values were extremely low for both parameters: ~ 0.3 % of the mean value for the SDNN and ~ 3.6 % of the mean value for the LF/HF ratio. However, different results were obtained with the pathological subject, with the RMSE values greater in terms of both parameters: the SDNN presented a RMSE of almost 20 % of the mean value, while the LF/HF ratio RMSE was higher than 50 % of the mean.

Table 11. Main statistics and RMSE assessed for the HRV variables under examination

Non-pathological subject			
	Holter mean ± std	**Sweet Shirt mean ± std**	**RMSE**
SDNN [ms]	63.2 ± 11.2	63.2 ± 11.2	0.184
LF/HF Ratio [adim]	1.54 ± 0.846	1.53 ± 0.850	0.0561
Pathological subject			
	Holter mean ± std	**Sweet Shirt mean ± std**	**RMSE**
SDNN [ms]	20.9 ± 6,15	19.8 ± 5.87	4.41
LF/HF Ratio [adim]	3.64 ± 3,62	2.96 ± 2.92	1.97

The analysis of agreement was then further investigated using Passing-Bablok regression and Bland-Altman analysis, with the attendant results presented in Table 12.

Table 12. Results of Passing-Bablok regression and Bland-Altman analysis for HRV measures

Passing-Bablok Regression			Bland-Altman Analysis	
Non-pathological subject				
	Slope [95 % CI]	**Offset [95 % CI]**	**Bias [95 % CI]**	**LoA**
SDNN	1.00 [0.993÷1.01]	0.00 [-0.454÷0.430]	0.009 [-0.071÷0.089]	[-0.360÷0.377]
LF/HF Ratio	1.00 [0.974÷1.04]	-0.007 [-0.051÷0.027]	0.005 [-0.019÷0.030]	[-0.107÷0.117]
Pathological subject				
	Slope [95 % CI]	**Offset [95 % CI]**	**Bias [95 % CI]**	**LoA**
SDNN	0.932 [0.597÷1.39]	0.692 [-8.86÷7.02]	1.10 [-0.711÷2.92]	[-7.44÷9.65]
LF/HF Ratio	0.919 [0.618÷1.39]	-0.409 [-1.50÷0.358]	0.684 [-0.101÷1.47]	[-3.01÷4.38]

For each of the analyzed parameters, the slope and offset from the PB regression are provided, along with their 95 % CI. Across all the results, the slope values were close to 1 and their CIs always included values of 1. Similarly, the offset values were close to 0 in all analyses, with the CIs always including 0 values. In terms of the pathological subject results, the CIs were larger than the corresponding CIs in the non-pathological subject, confirming a better agreement in the measurements derived from the recording involving the healthy volunteer.

The Bland-Altman analysis results included some bias with the 95 % CI and the LoA. In terms of the results from the non-pathological volunteer, the bias values were very close to 0, while both the bias CIs and LoA exhibited a low width and always included a 0 value. Meanwhile, in terms of the results for the pathological subject, the bias values for the SDNN and the LF/HF ratio were higher, with a wider LoA including 0.

The Bland-Altman plots are presented in Figure 19 and Figure 20. While the differences between the methods were greater in terms of both parameters assessed using the pathological subject, they exhibited a random distribution, meaning no systematic or proportional error could be confirmed from this analysis

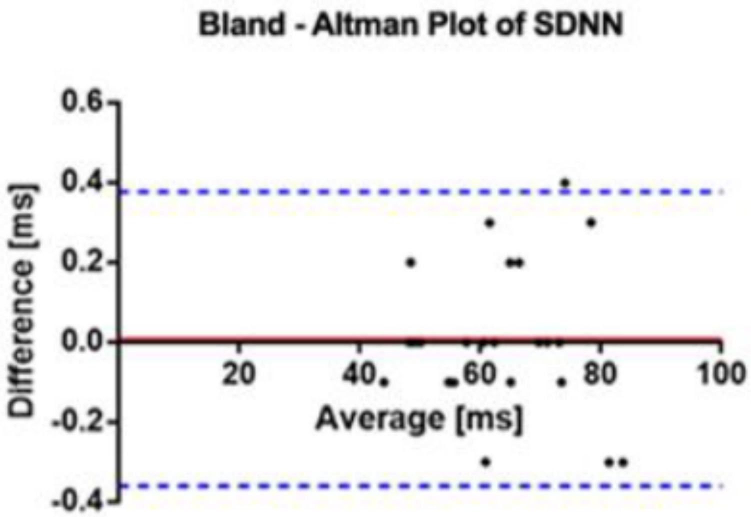

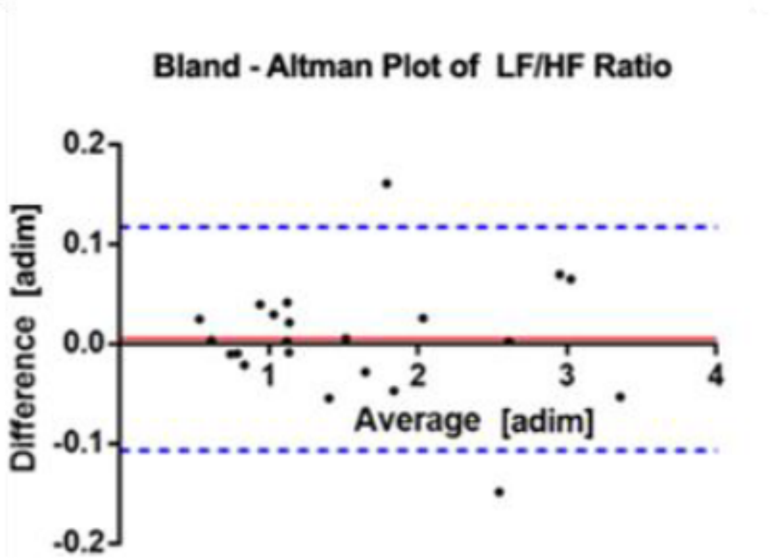

Figure 19. Bland-Altman plots of the parameters for the non-pathological volunteer. The red lines represent the bias, while the blue dashed lines represent the LoA

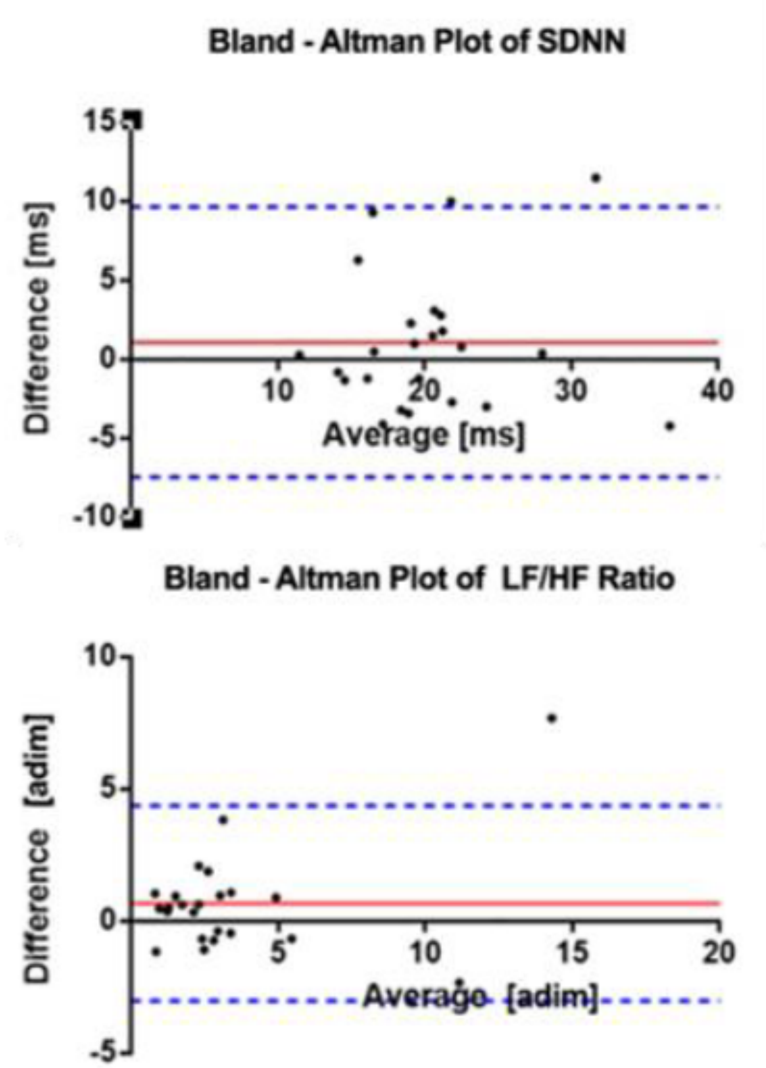

Figure 20. Bland-Altman plots of the parameters for the pathological volunteer. The red lines represent the bias, while the blue dashed lines represent the LoA

In the first analysis, the RR intervals obtained via the two systems under examination were compared by means of Passing-Bablok regression. The results (Table 9) confirmed that the systems can be considered as equivalent in terms of the identification of the R peaks along the ECG signal as beat reference points.

Moreover, the signal waveforms by means of Pearson's correlation analysis were compared. This assessment demonstrated that good agreement existed between the signals, particularly in terms of the QRS complex and T-wave, while less correspondence was found in the comparison of the P-waves (see Figure 18 and Table 10). Figure 21 shows the averaged ECG waveforms recorded by the two systems. Here, the P-waves were less visible in the Holter signal than in the SWEET Shirt recording. This was due to the non-standard electrode placement used for the Holter system (see Figure 16), which was chosen to avoid the overlapping with the textile electrodes enclosed in the shirt. Therefore, the lower agreement level with the P-waves can be attributed to the different electrode placements used, which is all but compulsory in a simultaneous recording. Therefore, it can be affirmed that the prototypal shirt has the capacity to clearly record an ECG signal that is comparable with those acquired by commonly used clinical portable devices.

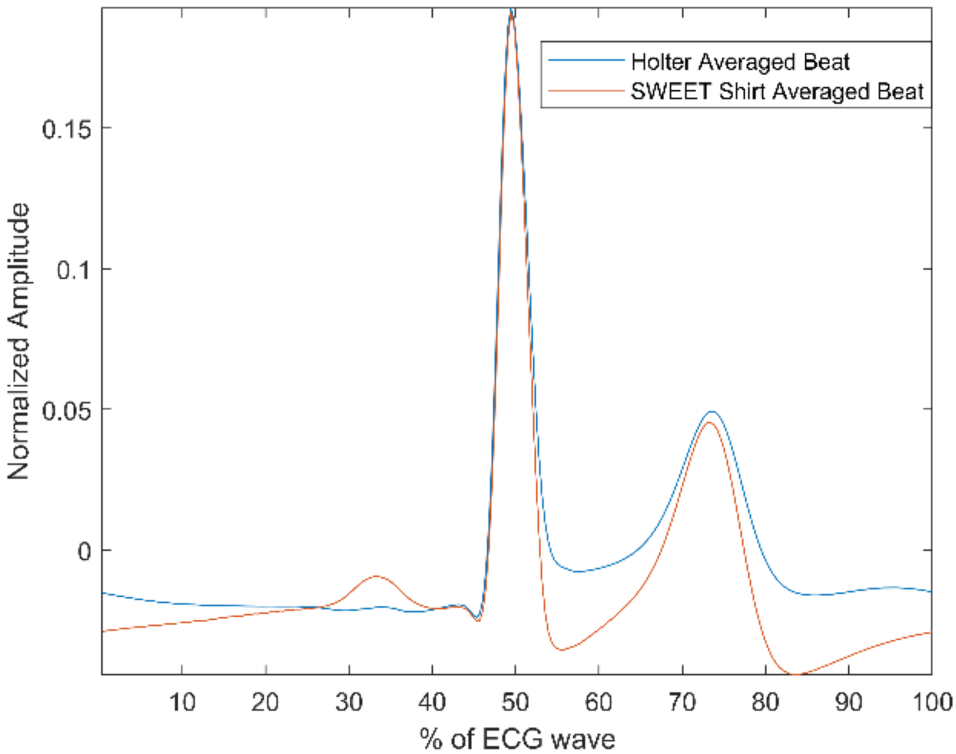

Figure 21. Comparison of averaged ECG beat waveforms from the Holter device (blue) and the sensorized shirt (red)

Finally, the performances of the developed software in terms of signal processing was investigated. As shown in Figure 19, Table 11 and Table 12, excellent results were achieved in the analysis of the parameters assessed using the non-pathological subject. The RMSE for both parameters under examination was extremely low, as were the biases assessed via the Bland-Altman analysis. Meanwhile, the Passing-Bablok analysis revealed that there was a regression line very close to the identity line, underlining a strict correspondence between the measurements from the two devices. However, lower agreement was found in the analysis involving the pathological subject. Here, the RMSE and bias values were higher (Table 11) and the Passing-Bablok CIs were wider (Table 12), albeit that they still involved values that allowed for concluding that there was some agreement between the two methods. However, the Bland-Altman plots (see Figure 20) did not exhibit any prevalent trend in the distribution of the differences, thus suggesting that no systematic or proportional differences existed between the measurement systems.

Based on these results, the lower agreement level in the parameters related to the pathological subject can be attributed to the greater presence of artefacts in the SWEET Shirt record, which was likely due to the weak adherence of the textile electrodes on the patient's skin or the higher number of movements made by the subject during the recording session. The ECG signal from the SWEET Shirt was clearly visible in 94.66 % of the registration time, while the signal from the Holter recorder did not present any artefacts. The presence of artefact regions will affect any signal processing results since the artefacts must be replaced by a specific number of normative RR intervals to ensure the continuity of the RR series. In this case, the results were further affected by the fact that they were averaged using a reduced window of 5 min.

Chapter 3

3 Wearable for ergonomics

3.1 Work-related risk assessment during lifting tasks

Among the activities involving biomechanical overloading, material handling and lifting is one of the most studied in the scientific literature, including its association with the development of work-related MSDs. With a view to prevention, NIOSH established a methodology for assessing lifting actions by means of a quantitative method based on intensity, duration and frequency of the task, and other geometrical characteristics of lifting [24]. The method determines the Recommended Weight Limit (RWL) for the lifting tasks and calculates the risk index namely Lifting Index (LI).

In the scientific literature, among the many applications of wearable technology to ergonomics, and in particular among those which use the NIOSH methodology [96], the association of features extracted directly from raw signals (acceleration and angular velocity) with NIOSH risk classes related to repeated load lifting activities has not yet been explored. The question remains whether it is possible to classify lifting tasks belonging to different risk classes according to the value of LI using a machine learning approach by means of features extracted from raw signals.

A study was carried out with two objectives:

1. Exploring the possibility to use a single IMU placed on the lumbar region to monitor the biomechanical risk
2. Assessing if the time-domain features extracted from acceleration and angular velocity signals acquired by the IMU sensor allowed to classify risk/no-risk tasks according to the NIOSH methodology

To classify lifting tasks belonging to different LI classes according to the RNLE, several ML algorithms were fed with time-domain features extracted from acceleration and angular velocity signals. The signals relating to the lifting activities were acquired through the wearable Opal System. The validation of the methodology was carried out through the tenfold cross-validation and different evaluation metrics in order to make the result more robust [97].

The Opal System by APDM Inc., a commercial IMU-based wearable system, was used (Figure 22).

Figure 22. Opal System: Access Point, Docking Station, Opal Sensor and Mobility Lab software

The system is composed of several Opal sensors worn by the participants kept in position by straps. Each Opal sensor is composed by a 3-axes accelerometer with 14-bit resolution and two alternative ranges of values (± 16 g and ± 200 g, where g is the gravitational constant), a 3-axes gyroscope (16-bit, range ± 2000 deg/s) and a 3-axes magnetometer (12-bit, range ± 8 Gauss). The sampling frequency of the acceleration and angular velocity signals was 20 Hz. Opal sensors communicate with a laptop equipped by the Mobility Lab Software by the Bluetooth 3.0. The Access Point manages the communication between the Opal sensors and the laptop, while the Docking Station allows charging and configuring of Opal sensors. The Opal system has proved to be a repeatable [68], reliable [98,52] and accurate [99], and it was used in several scientific studies, e.g., to compute the main spatiotemporal and kinematic parameters relating to the lower limb, upper limb and spine [100,101]. It also allows users to access raw signals such as acceleration and angular velocity. In this study, we used a single Opal sensor positioned on the lumbar region (Figure 23) [102,103] to acquire raw signals (acceleration and angular velocity) during lifting activities designed to correspond to different risk classes according to the NIOSH methodology.

Figure 23. Placement of the Opal Sensor in lumbosacral region through an elastic belt

Figure 24 shows the Opal sensor with the direction of the axes.

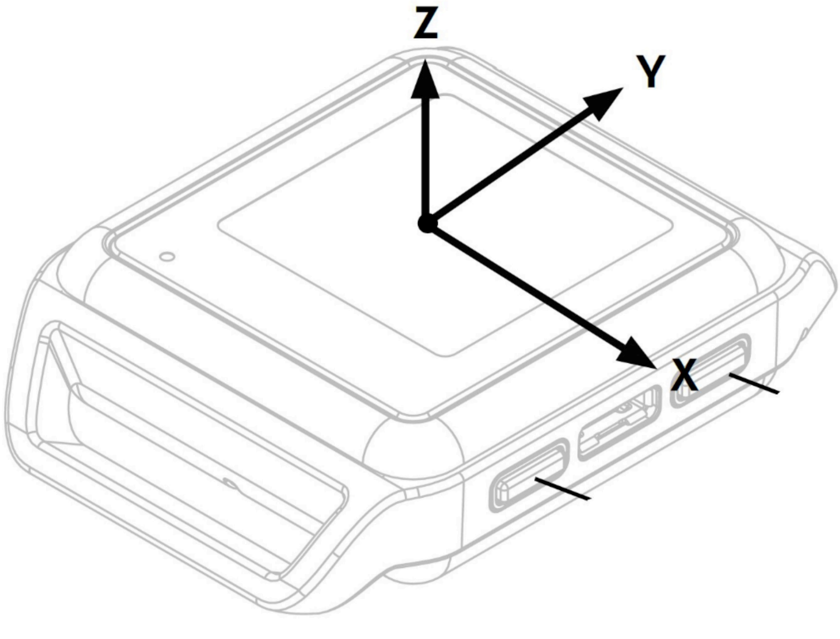

Figure 24. Opal Sensor with the illustration of the x-axis, y-axis and z-axis

The RNLE is a method published by NIOSH to assess the risk of WLBDs [104]. An equation provides the RWL, namely the weight limit for a healthy worker to safely perform lift tasks during a work shift, starting from a load constant (25-15 kg for the Italian legislation) and through a multiplicative model with six variables relating to the lifting task.

LI, namely the ratio of actual weight to RWL for lifting activity, is a good indicator of the risk of WLBDs for manual lifting [105,106].

In the preventive approach, RNLE is useful for verifying that LI is not greater than 1 in lifting activities. Lifting activities with LI values between 1 and 3 are associated with an increased biomechanical risk in the working population, while lifting activities with LI less than 1 indicate acceptable conditions and no risk of WLBDs [24].

The RWL equation is as follows:

$$RWL = LC\ x\ HM\ x\ VM\ x\ DM\ x\ AM\ x\ FM\ x\ CM$$

Where:

- LC: Load Constant = 25/20 kg (males, <45/>45 years old respectively), 20/15 kg (females, <45/>45 years old respectively);
- HM: Horizontal Multiplier;
- VM: Vertical Multiplier;
- DM: Distance Multiplier;
- AM: Asymmetric Multiplier;
- FM: Frequency Multiplier.

Healthy volunteers were recruited. Subjects were included if they were between the ages of 20 and 60, and excluded if they had hypertension (i.e., blood pressure above 100/160 mmHg), or any other heart disease (i.e., congestive heart failure), or a musculoskeletal disorder (i.e., low back pain, herniated disc or trunk surgery). Seven subjects were selected for this preliminary study, whose anthropometric characteristics are shown in Table 13.

Table 13. Anthropometric characteristics of the study population presented as mean ± standard deviation

Age (years)	27.71 ± 1.60
Height (cm)	167.40 ± 4.86
Weight (kg)	68.71 ± 10.17
Body Mass Index (kg/m^2)	24.43 ± 2.60

Each subject performed a task session based on two trials. Each trial consisted of 30 consecutive lifting tasks. Between the two trials, a pause of 1 h was considered. Specifically, the first trial consisted of repeated liftings in a condition of LI less than one (LI = 0.5) named the NO RISK class, while the second one consisted of repeated liftings in a condition of LI greater than one (LI = 1.3) named the RISK class. LI of 0.5 and 1.3 were derived from the RNLE [24] by variously combining height, frequency and weight of lifting tasks. The details of the combinations are displayed in Table 14. Five out of seven subjects performed the task lifting the load from 50 cm to 125 cm, namely, the optimal geometric condition. One subject performed the task lifting the load from 30 cm to 125 cm, namely, non-optimal geometric conditions (start point: height < 50 cm); one subject performed the task lifting the load from 50 cm to 150 cm, namely, non-optimal geometric conditions (end point: height > 125 cm). The choice of different geometric conditions was adopted to assess the proposed data mining system for the prediction of biomechanical risk in a general context in order to have more interesting and generalizable results.

Table 14. Combinations of the height, frequency and weight variables for lifting activities corresponding to LI 0.5 and 1.3

First Trial LI < 1 (0.5)				Second Trial LI > 1 (1.3)				
Displacement [Start-End] (cm)	Frequency (Lifts/min)	Weight Lifted (kg)		Displacement [Start-End] (cm)	Frequency (Lifts/min)		Weight Lifted (kg)	
	m & f	m	f		m	f	m	f
[50 - 125]	2.5	7	5	[50 – 125]	6	4	15	10
[30 – 125]	2.5	5	4	[30 – 125]	5	3	13	8
[50 – 150]	2.5	5	4	[50 – 150]	5	3	13	8

The trial (Figure 25) was performed using a plastic container (56 x 35 x 31 cm^3) with weights equally distributed inside; the size of the plastic container is such that it can be held close to the barycenter of the body during the lifting task. The subjects were instructed to adopt a stable upright posture with the lower limbs slightly apart and to perform the squat technique with a two-handed grip. Each lifting task was performed in a slow, controlled manner without any jerk or sudden acceleration [107]. The researcher was in charge of visually checking the performance, and possibly having the subject repeat the execution to acquire the signal again if the task was carried out in an uncontrolled manner.

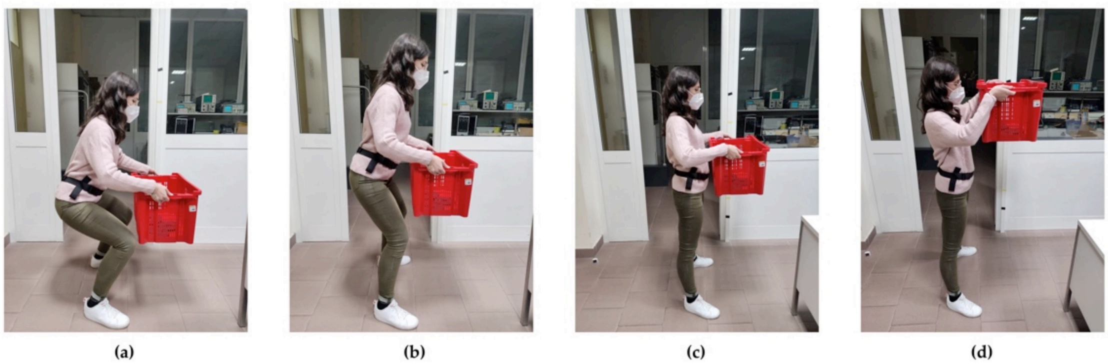

Figure 25. Lifting phases of the lifting task: picking point (a) with squatting technique, intermediate points (b,c) with trunk extension, and destination point (d) up to the final height, and then restart the cycle

Acceleration and angular velocity signals were not filtered (Figure 26). The signals underwent a segmentation process in order to extract the region of interest (ROI) corresponding to the window time in which the subject performed the lifting task. A temporal synchronization was performed to pick up the portion of the signal corresponding to the time point of the start and end of the lifting task. For each ROI, several features were extracted in the time-domain. Four features were extracted from each of the three axes of the accelerometer and from each of the three axes of the gyroscope, giving a total of twenty-four attributes.

The feature extracted were:

- Root mean square (RMS);
- Standard Deviation (SD);
- Minimum (MIN);
- Maximum (MAX).

As during the lifting activity the subject moved in two different directions (from bottom to top, and vice versa), giving rise to positive or negative variants of the signals, it was considered that RMS represented the potential differences in the two different study conditions (LI < 1 and LI > 1) better than the average. SD captured the fact that the range of possible acceleration and values of the angular velocity signals can differ for different LI values, as the SD of the acceleration data was associated with the intensity of motion [108]. Both RMS and SD were predictive features in monitoring physical activities [109]. MIN and MAX values were collected as the task was performed in two opposite directions.

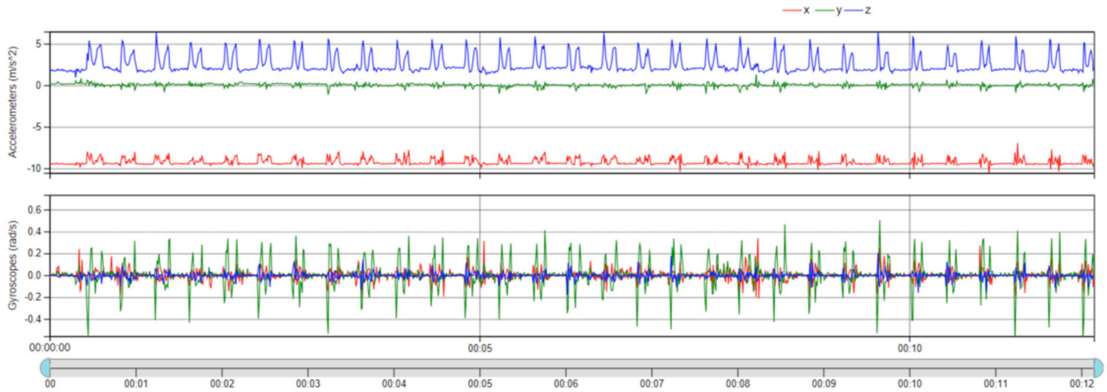

(a)

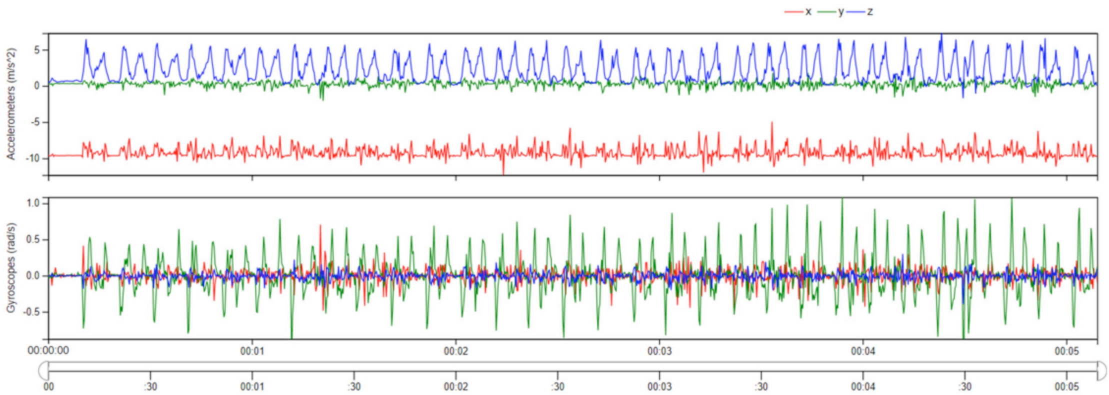

(b)

Figure 26. (a) Acceleration and angular velocity signals along the 3 axes associated to the NO RISK class, lifting task performed with a LI < 1. (b) Acceleration and angular velocity signals along the 3 axes associated to the RISK class, lifting task performed with a LI > 1

Several ML algorithms were trained to evaluate the performance of our predictive model based on features in the time-domain extracted from raw signals (acceleration and angular velocity) to discriminate two risk conditions according to the RNLE.

The following ML algorithms were implemented.

Random Forest (RF) is a ML algorithm based on bagging and randomization. RF uses several decision trees. An instance is assigned to a certain class through a majority vote procedure on the basis of the decision given by the trees that make up the forest. Although this type of ML shows optimal performance on large datasets, it was chosen for its simplicity of parameterization and for its stability to noise and outliers [110].

Decision Tree (DT) is a hierarchical classifier method, as well as representing the simplest and most used logic-based classification technique [111]. The test data are classified by ordering them as trees based on the values of their characteristics.

Gradient Boost Tree (GBT) redefines boosting as a numerical optimization problem with the goal of minimizing model loss of function by adding learning weaknesses and using gradient descent to set the local minimum of the differential function [112]. The GB method implemented is a combination of a decision trees measure and boosting technique.

The AdaBoost Tree (ABT) algorithm [113], short for Adaptive Boosting, is a ML meta algorithm used as an ensemble method. Weights are reassigned to each instance, with higher weights for instances classified incorrectly. Boosting reduces the bias and variance for supervised learning. A set of decision stumps (decision trees with only one node and two leaves) was considered.

k-Nearest Neighbor (kNN) ranks the unlabeled instance vector on the basis of the majority label class between its nearest k neighbors in the training set. Several distance metrics, employed to recognize the nearest neighbors, are present in the literature and can influence the algorithm performance. Without prior knowledge, typically the distance metric implemented is the Euclidean distance [114], as in the case analyzed. The algorithm usually assumes that the training instances are uniformly distributed across classes, an assumption in line with our perfectly balanced dataset with reference to the two classes. The choice of k has a significant impact on the classification performance [115]; a k equal to 3 was considered.

Naive Bayes (NB) is a probabilistic ML algorithm, based on Bayes' Theorem. It calculates the probability of each class for a specified instance and then returns the class with the highest probability. This algorithm, which requires little data for training and little storage space, is suitable for the small size of the datasets that perform the analysis for each subject in our study. It is also fast during training without many parameters to set, based on the assumption of the conditional independence of the characteristics [116].

Multilayer Perceptron (MLP) consists of multiple layers of simple, two-state sigmoid processing elements, i.e., nodes or neurons interacting using weighted connections, only between neurons of adjacent layers [117]. A configuration with a single hidden layer and 10 neurons was considered.

Support Vector Machine (SVM) in a binary classification, as in the case under study, creates a hyperplane that separates data from two different classes. The largest possible distance is established between the separating hyperplane by maximizing the margin, thus creating the separation [118]. The kernel choice determines the separation boundary of the classes. The Radial Basis Function (RBF) or Gaussian Kernels are the most popular kernels used as default for any nonlinear model, but also polynomial kernels are very popular [119]. A SVM with a linear kernel was implemented.

Logistic Regression (LR) is an efficient and powerful way to analyze the effect of several independent variables on a binary outcome, as in the case under study, and allows quantifying the contribution of each feature. LR iteratively identifies the strongest linear combination of variables with the highest probability to detect the observed outcome [120].
K-fold cross-validation is one of the most widely used approaches for estimating classifier error and was employed as tenfold cross-validation (CV) to validate the predictive models described above and provide more robust evidence on the proposed predictive biomechanical risk model, based on features extracted from raw signals. Tenfold CV involves splitting a dataset into ten subsets, with the iterative use of nine to train the model and one to evaluate its performance [121]. A stratified CV was adopted in order to keep the proportions between the two classes unaltered among the folds [122].
Moreover, in order to better generalize the validation of the proposed approach, a leave-one-subject-out cross-validation using six subjects to train the predictive models and one subject to test the algorithms was implemented.
The performance of the predictive models proposed was evaluated through the following evaluation metrics: Accuracy, Sensitivity, Specificity and Area under the curve Receiver operator characteristic (AucRoc). The Accuracy metric is a measure of the ratio of correct predictions over the total number of instances considered. The Sensitivity metric is employed to measure the fraction of positive patterns that are correctly classified, while the Specificity metric is used to measure the fraction of negative patterns that are correctly classified. Finally, the AucRoc reveals the generally ranking performance of a classification algorithm. The Confusion Matrix of the best algorithm in terms of evaluation metrics scores was also reported, with matching between instances in an expected class and an actual class [123].
Finally, the Feature Importance was also reported through the calculation of the Information Gain (IG), an indicator of the amount of information provided by the features [124]. A feature selection on the basis of the IG was implemented as filter method before the classification task. WEKA data mining software was used for the feature importance analysis [125], selecting InfoGainAttributeEval as Attribute Evaluator and Ranker as Search Method.
ML algorithms have been implemented through the artificial intelligence platform Knime Analytics Platform (version 3.7.1), which finds increasing diffusion in the scientific literature [126,127].
First, a ML analysis for each subject to assess the feasibility of the proposed data mining system to assess the biomechanical risk for a single subject was carried out. For each subject, two datasets were considered: the first dataset is composed of 60 instances, 30 for each class

(NO RISK, RISK), and 12 features extracted from the acceleration signals; the second dataset is composed of 60 instances, 30 for each class (NO RISK, RISK), and 12 features extracted from the angular velocity signals. For each dataset, the ML analysis was performed by averaging the results among the seven subjects, and the standard deviation was further showed in order to include prediction uncertainty. The results for each dataset are shown in Tables 15 and 16, respectively, where Sensitivity and Specificity were computed considered as reference for the NO RISK class.

Table 15. Scores from stratified tenfold cross-validation (CV) evaluation metrics averaged over the seven subjects (mean ± standard deviation) using the features extracted from the acceleration signals along the three axes

Algorithms	Accuracy	Sensitivity	Specificity	AucRoc
DT	0.97 ± 0.05	0.97 ± 0.04	0.97 ± 0.05	0.97 ± 0.03
RF	0.98 ± 0.02	0.98 ± 0.03	0.99 ± 0.02	0.99 ± 0.01
GBT	0.97 ± 0.04	0.98 ± 0.03	0.96 ± 0.06	0.98 ± 0.02
ABT	0.98 ± 0.02	0.98 ± 0.02	0.98 ± 0.04	0.97 ± 0.03
kNN	0.90 ± 0.09	0.88 ± 0.10	0.91 ± 0.11	0.94 ± 0.06
NB	0.96 ± 0.03	0.96 ± 0.04	0.96 ± 0.04	0.99 ± 0.01
MLP	0.95 ± 0.06	0.93 ± 0.07	0.96 ± 0.06	0.97 ± 0.03
SVM	0.83 ± 0.20	0.83 ± 0.29	0.82 ± 0.37	0.85 ± 0.22
LR	0.79 ± 0.15	0.79 ± 0.14	0.79 ± 0.19	0.84 ± 0.13

Abbreviations. ABT: AdaBoost Tree; AucRoc: Area under the curve Receiver operator characteristic; DT: Decision Tree; GBT: Gradient Boost Tree; kNN: k-Nearest Neighbor; LR: Logistic Regression; NB: Naïve Bayes; MLP: Multilayer Perceptron; RF: Random Forest; SVM: Support Vector Machine

Table 16. Scores from stratified tenfold CV evaluation metrics averaged over the seven subjects (mean ± standard deviation) using the features extracted from the angular velocity signals along the three axes

Algorithms	Accuracy	Sensitivity	Specificity	AucRoc
DT	0.88 ± 0.11	0.87 ± 0.14	0.88 ± 0.08	0.88 ± 0.12
RF	0.90 ± 0.11	0.90 ± 0.13	0.89 ± 0.09	0.94 ± 0.10
GBT	0.89 ± 0.13	0.90 ± 0.14	0.88 ± 0.13	0.92 ± 0.09
ABT	0.89 ± 0.14	0.89 ± 0.16	0.89 ± 0.12	0.92 ± 0.12
kNN	0.82 ± 0.10	0.81 ± 0.14	0.82 ± 0.09	0.88 ± 0.09
NB	0.86 ± 0.12	0.83 ± 0.17	0.89 ± 0.08	0.92 ± 0.08
MLP	0.90 ± 0.12	0.88 ± 0.16	0.92 ± 0.09	0.94 ± 0.08
SVM	0.68 ± 0.19	0.91 ± 0.13	0.44 ± 0.42	0.82 ± 0.16
LR	0.84 ± 0.08	0.84 ± 0.13	0.84 ± 0.05	0.90 ± 0.07

Abbreviations. ABT: AdaBoost Tree; AucRoc: Area under the curve Receiver operator characteristic; DT: Decision Tree; GBT: Gradient Boost Tree; kNN: k-Nearest Neighbor; LR: Logistic Regression; NB: Naïve Bayes; MLP: Multilayer Perceptron; RF: Random Forest; SVM: Support Vector Machine

Second, a Feature Importance by means of the calculation of the IG was performed, considering the entire study sample and the features extracted from both the acceleration and angular velocity signals along the three axes (Figure 27).

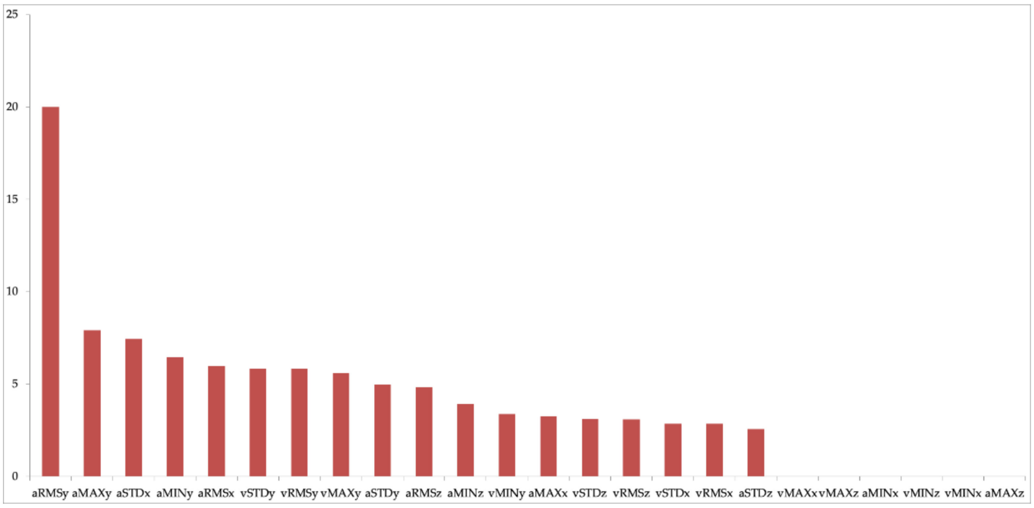

Figure 27. Feature importance based on the Information Gain value. Abbreviations. aRMSx: x-axis acceleration Root Mean Square; aRMSy: y-axis acceleration Root Mean Square; aRMSz: z-axis acceleration Root Mean Square; aSTDx: x-axis acceleration Standard Deviation; aSTDy: y-axis acceleration Standard Deviation; aSTDz: z-axis acceleration Standard Deviation; aMINx: x-axis acceleration Minimum; aMINy: y-axis acceleration Minimum; aMINz: z-axis acceleration Minimum; aMAXx: x-axis acceleration Maximum; aMAXy: y-axis acceleration Maximum; aMAXz: z-axis acceleration Maximum; vRMSx: x-axis angular velocity Root Mean Square; vRMSy: y-axis angular velocity Root Mean Square; vRMSz: z-axis angular velocity Root Mean Square; vSTDx: x-axis angular velocity Standard Deviation; vSTDy: y-axis angular velocity Standard Deviation; vSTDz: z-axis angular velocity Standard Deviation; vMINx: x-axis angular velocity Minimum; vMINy: y-axis angular velocity Minimum; vMINz: z-axis angular velocity Minimum; vMAXx: x-axis angular velocity Maximum; vMAXy: y-axis angular velocity Maximum; vMAXz: z-axis angular velocity Maximum

Third, a ML analysis considering all seven subjects to assess the feasibility of the proposed data mining system for biomechanical risk assessment for a general study population was performed. In this analysis, a unique dataset consisting of 420 (60 x 7) instances, 210 for each class (NO RISK, RISK), and 18 features extracted from both acceleration and angular velocity signals excluding the six features with IG equal to zero (Figure 27) was considered. In this study, the general rule is respected that foresees at least equal to 10 the ratio n/d, between the number n of instances available in the training set and the dimension d of the feature space [128]. This strengthens and makes the result of the analysis shareable.

The results of the ML analysis on the entire dataset are shown in Table 17, where the NO RISK class was considered as the reference class for Sensitivity and Specificity.

Table 17. Scores from stratified tenfold CV evaluation metrics considering the entire study sample and using the features extracted from both acceleration and angular velocity signals along the three axes with a non-zero IG

Algorithms	Accuracy	Sensitivity	Specificity	AucRoc
DT	0.91	0.89	0.92	0.93
RF	0.95	0.94	0.95	0.99
GBT	0.95	0.94	0.96	0.99
ABT	0.80	0.72	0.87	0.90
kNN	0.84	0.83	0.85	0.91
NB	0.67	0.63	0.71	0.75
MLP	0.91	0.91	0.91	0.97
SVM	0.71	0.70	0.71	0.79
LR	0.66	0.67	0.66	0.68

Abbreviations. ABT: AdaBoost Tree; AucRoc: Area under the curve Receiver operator characteristic; DT: Decision Tree; GBT: Gradient Boost Tree; kNN: k-Nearest Neighbor; LR: Logistic Regression; NB: Naïve Bayes; MLP: Multilayer Perceptron; RF: Random Forest; SVM: Support Vector Machine

Table 18 shows the Confusion Matrix of the best algorithm (GB) resulting from the analysis on the entire study sample and according to the scores of the evaluation metrics: Accuracy, Sensitivity, Specificity and AucRoc. The resulting confusion matrix is perfectly balanced with the following values: TP = 197, FP = 13, FN = 8, TN = 202.

Table 18. Confusion matrix of the best algorithm in terms of evaluation metrics scores: the GBT

	NO RISK	YES RISK
NO RISK	197	13
YES RISK	8	202

Finally, a ML analysis on the entire dataset was performed using as validation strategy the leave-one-subject-out, namely, using six subjects for the training set and one subject for the test set. Results are shown in the Table 19.

Table 19. Scores from leave-one-subject-out evaluation metrics considering the entire study sample and using the features extracted from both acceleration and angular velocity signals along the three axes

Algorithms	Accuracy	Sensitivity	Specificity	AucRoc
DT	0.88	0.93	0.83	0.88
RF	0.88	0.97	0.80	0.97
GBT	0.75	0.97	0.53	0.92
ABT	0.88	0.97	0.80	0.96
kNN	0.50	0.00	1.00	0.48
NB	0.82	0.97	0.67	0.97
MLP	0.73	0.97	0.50	0.87
SVM	0.77	0.97	0.57	0.82
LR	0.70	0.97	0.43	0.72

Abbreviations. ABT: AdaBoost Tree; AucRoc: Area under the curve Receiver operator characteristic; DT: Decision Tree; GBT: Gradient Boost Tree; kNN: k-Nearest Neighbor; LR: Logistic Regression; NB: Naïve Bayes; MLP: Multilayer Perceptron; RF: Random Forest; SVM: Support Vector Machine

The goal of this research was to explore the feasibility of several state-of-the-art ML algorithms - fed with specific time-domain features extracted from the acceleration and angular velocities signals during a lifting activity - to classify the lifting risk classes based on the LI values according to the RNLE. The results obtained suggest ML algorithms - operating on the time-domain features (RMS, SD, MIN and MAX) extracted during lifting activities from the acceleration and angular velocity signals along the three dimensions of space - can offer valid help to experts in ergonomics for the precise and automatic classification of the biomechanical risk of workers engaged in load-lifting activities.

The ML analysis performed was aimed at the classification of lifting activities based on the presence or absence of risk, defined by the LI index.

First, having carried out a ML analysis for each subject, we obtained the average scores and the standard deviations of the evaluation metrics of the seven subjects by considering separately the characteristics extracted from the acceleration signal and the angular velocity signal. As shown in Tables 15 and 16, the application of state-of-the-art algorithms on the time-domain features extracted from the acceleration signal provides superior performance (evaluation metric scores) compared to that achieved by using the angular velocity signal, albeit with satisfactory results for the latter as well. The proposed combination of algorithms and features extracted from the acceleration signal achieved an accuracy of between 0.79 and 0.98, a sensitivity between 0.79 and 0.98, a specificity between 0.79 and 0.99, and AucRoc between 0.84 and 0.99. The proposed combination of algorithms and features extracted from the angular velocity signal achieved an accuracy between 0.68 and 0.90, a sensitivity between 0.84 and 0.91, a specificity between 0.44 and 0.92, and an AucRoc score between 0.82 and 0.94.

Second, in this study, eighteen out of twenty-five features showed a non-zero IG (Figure 27), highlighting their predictive power for this specific classification task. Specifically, the most informative features, according to IG, were those associated with the acceleration of the y axis, i.e., the mediolateral direction (Figure 24). This means that the trajectory of the subject's center of gravity along the y axis during the lifting task (Figure 25) tends to have a greater information to separate risk classes, despite the load being moved along the x trajectory. In particular, the aRMSy alone shows an information gain equal to 20%, highlighting its high discriminating power between the two risk conditions.

As for the features relating to the acceleration along the y axis, the most informative ones according to IG (Figure 27) are, once again, those relating to the angular velocity around the y axis. Approximately 60% of the information provided by the features derives from those relating to the angular velocity and acceleration of the y axis, and this result must be taken into account.

Third, as shown in Table 17, a ML analysis was performed considering the whole sample of the study in order to have more generalizable results and to evaluate if the proposed method was applicable not only to the single subject, but also to a whole sample. This property could in fact represent a substantial advantage for using the proposed methodology during preventive interventions for the health and safety of workers in the workplace. This further analysis was carried out using the features extracted from both acceleration and angular velocity signals relating to the three axes (considering the entire study sample, and excluding the features with IG equal to zero). All classifiers (with the exception of the NB, SVM and LR algorithms) showed an accuracy between 0.80 and 0.95, a sensitivity between 0.72 and 0.94, a specificity between 0.85 and 0.96, and AucRoc between 0.90 and 0.99. As shown in Table 5, six out of nine ML algorithms discriminated excellently (AucRoc values > 0.90) the two risk classes. Conventionally, AucRoc values > 0.70 are considered to represent moderate discrimination, value > 0.80 good discrimination and values > 0.90 excellent discrimination; on the basis of the results, as shown in the Table 17, six of nine ML algorithms showed an excellent discrimination of the two risk classes. The poor performance of the NB algorithm was due to the presence of a statistically significant correlation between characteristics [129] (correlation study not shown). The LR algorithm, as the NB one, is based on the concept of probability, and this could explain the limited performances of LR. Instead, the poor performance of the SVM with linear kernel could be explained by the fact data are not linearly separable. The best algorithm was the GBT which reached values of 0.95, 0.94, 0.96 and 0.99 in Accuracy, Sensitivity, Specificity and AucRoc, respectively. As shown in Table 18, the almost symmetric Confusion Matrix of GBT presents only 21 instances wrongly classified out of 240 total instances, confirming the potential of this methodology applied to biomechanical evaluation.

Finally, to better generalize the performance of the proposed models, they were tested using leave-one-subject-out, training the classifiers on six subjects and testing them on one subject. Although the metrics resulted slightly lower, the data shown in Table 19 are comparable with the ones obtained from the stratified tenfold CV. Once again, the tree-based ML algorithms has proven more efficient in terms of evaluation metrics for this purpose.

This is the first study that considers risk discrimination (by ML) according to NIOSH using a single IMU placed on the subject's pelvis to extract four basic time-domain features. The achieved results, when compared with the recent ones described by other research groups, are in line or superior to those based on more complex methodologies.

In the study by Varecchia et al. [130], the combination of an artificial neural network fed with time-domain and frequency-domain features extracted from surface electromyography and optoelectronic systems resulted in classification Accuracy of up to 90% against three NIOSH risk classes (LI = 1, LI = 2, LI = 3). In a subsequent work by the same authors [131], the new feature of Lifting Energy Consumption [132] was used to feed a neural network similar to the previous one, demonstrating an Accuracy up to 100%. The limit of this methodology, as pointed out by the authors themselves, is due to the poor applicability in the workplace, an aspect that is solved using wearable inertial sensors as in the case proposed.

Snyder et al. [133] proposed a modified Convolutional Neural Network model to distinguish three risk levels (low, medium and high) according to the American Conference of Governmental Industrial Hygienist Threshold Limit Values for lifting. Similar to our work, they used IMU sensors, albeit in larger number, to achieve 90% Accuracy.

With a similar goal to ours, Brandt et al. [107] tried to classify lifting activities into low and high-risk categories according to the guidelines of the Danish Working Environment Authority, reaching an Accuracy score equal to 65% using a Linear Discriminant Analysis algorithm. In the study by Conforti et al. [134], which aimed to distinguish between correct and incorrect postures, the extraction of data from an IMU positioned on the pelvis of the subject, and coupled with an IMU placed on the trunk, did not allow obtaining scores higher than 75% using a Support Vector Machines algorithm with four different kernels.

Although the presented methodology is powerful, doubts could be raised about the effective capabilities of a single IMU for the validation of such results. Although a single IMU on the pelvis is not sufficient to fully predict the parameters associated with lifting (e.g., the weight of the object to be handled, the horizontal distance, etc.), this solution estimates the lumbar load fairly well, when the displaced mass is known and is in a consistent position with respect to the body [103]. In addition to significantly increasing the convenience in field trials, the use of a single IMU, positioned on the back, is considered sufficient to provide the data necessary to distinguish lifting classes [133].

Based on these results, the experimented approach - which combines time-domain features and machine learning algorithms - proved to be a valid indicator, although preliminary because of the low number of samples analyzed, of the risk of WLBDs for manual lifting (according to the NIOSH index) to which workers are potentially exposed during their working activity.

In conclusion, the results showed that the proposed combinations of features – extracted from acceleration and angular velocity signals acquired by a single IMU placed at pelvis - and state-of-the-art ML algorithms represents a potential valid approach to automatically classify the biomechanical risk to which subjects may be exposed during lifting activities, for example, at work. The presented methodology could represent a valid integration to the established protocols (e.g., NIOSH lifting equation) to evaluate the biomechanical risk more quickly and easily. Moreover, it could represent a valid alternative when the conditions required for the application of standardized evaluation methods do not exist. These results are of direct practical relevance for occupational ergonomics, as they present the opportunity for automatic, economic and non-invasive detection (by placing an IMU on the pelvis of the subjects), to assess the musculoskeletal and biomechanical risk associated with lifting. Based on the promising results presented in this article, the next phase of the research could consider an extension of the sample under consideration to further validate the methodology, new experiments that consider more than two LI values, and the integration of additional features from the time-domain and possibly the frequency-domain. The main limitation of the study is in fact the low sample size making this a preliminary study. Future work will benefit both from the inclusion of larger groups of participants as well as the use of deep learning techniques for classification such as convolutional neural networks [135]. It is known these are especially advantageous for analyzing time series data, reducing the risk of overfitting and improving system Accuracy.

3.2 Estimating lifted load from features extracted from inertial data

Work-related MSD are among the main occupational health problems. Substantial evidence has shown that work-related physical risk factors are the main source of low back complaints, particularly affecting heavy and repetitive manual lifting activities. The aim of the study published in [136] is, during load lifting tasks, to explore the correlation between the time domain features extracted from the acceleration and angular velocity signals of the performing subject and the load lifted, and to explore the feasibility of a multiple linear regression model to predict the lifted load.

The study was conducted on a sample made up of seven healthy subjects. The anthropometric characteristics of the study sample are shown in Table 20. Exclusion criteria were musculoskeletal disorders (i.e. low back pain, herniated disk, trunk surgery). All the participants signed the informed consent.

Table 20. Anthropometric characteristics of the study sample

Age [years]	27.71 ± 1.60
Body Height [cm]	167.40 ± 4.86
Body Weight [kg]	69.00 ± 10.89
Body Mass Index [kg/m^2]	24.51 ± 2.74

In this study the Opal System, an IMU-based wearable system, was used.

Each subject performed a lifting task session based on three consecutive trials for each load. The load was increased linearly by 1 kg from 0 kg to 18 kg for each session. Each trial consisted in lifting a load from 50 cm to 125 cm (optimal geometric conditions), as shown in Figure 28. Each subject performed 3 x 19 trials. The data obtained from the three trials of each session were averaged and an average of the data among subjects was computed for the specific session based on a specific load.

Figure 28. The lifting task; on the left the start point (50 cm above the floor), on the right the end point (125 cm above the floor)

The trial was performed using a plastic container with weights equally distributed inside (40 x 40 x 10 cm). A two-handed grip and stable support on the feet with the lower limbs slightly apart were the indications given to the subjects to perform the lifting task as a squat. During the lifting task acceleration and angular velocity signals along the three direction of the space were acquired by means of an inertial sensor, namely Opal sensor, placed on the chest. The direction of three axes are shown in Figure 24.

The acquired acceleration and angular velocity signals were not filtered (Figure 29 and Figure 30). The signals were segmented to extract the ROI related to the lifting activity. For each signal, for each ROI and for each axis (x, y, z), the following three features in the time domain were extracted:

- Root Mean Square (RMS), the arithmetic mean of the squares of a group of values;
- Standard Deviation (SD), a measure of the amount of variation or dispersion of a set of values;
- MinMax value (MINMAX), the difference between maximum and minimum for each ROI.

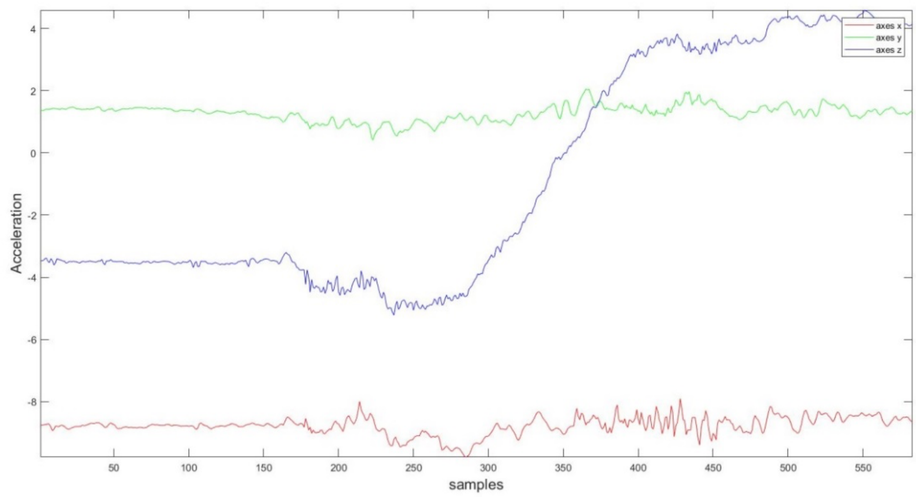

Figure 29. Acceleration signals along the x,y,z axes

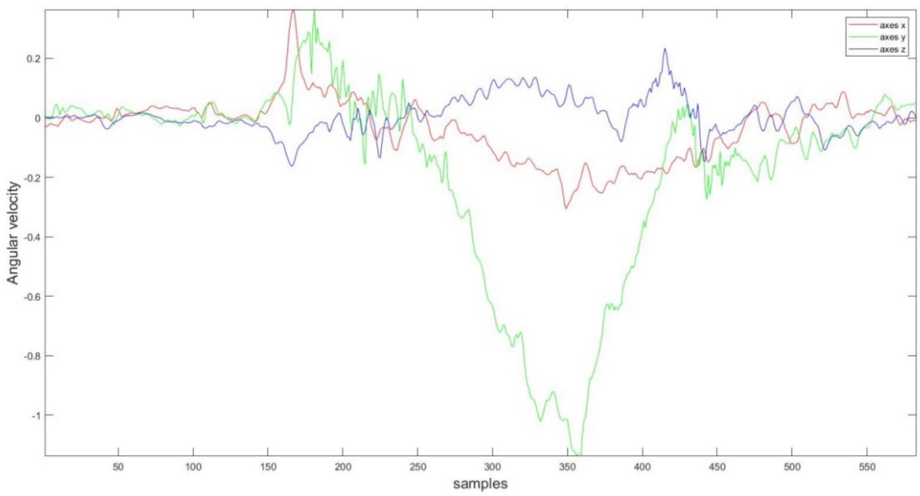

Figure 30. Angular velocity signals around the x,y,z axes

A correlation analysis was performed between each feature extracted from the raw signals (acceleration and angular velocity) and the load. Pearson's correlation coefficient was calculated by first evaluating the Gaussian distribution of the data according to the Shapiro-Wilk test considering a two-tailed 95% confidence interval. Furthermore, on the basis of the most informative signals (variation during lifting) and the most informative features (value of the correlation coefficient) a multiple linear regression was performed to find a predictive linear equation to compute the load lifted (function of the selected features), using MATLAB R2020a. Regress function in MATLAB implements the Multiple linear regression using least squares. B = regress(Y,X) returns the vector B of regression coefficients in the linear model Y = X*B. X is an n-by-p design matrix, with rows corresponding to observations and columns to predictor variables. Y is a n-ny-1 vector of response observations. Regress function also returns a vector STATS containing, in the following order: the R-square statistic, the F-statistic and p-value for the full model, and an estimate of the error variance. X should include a column of ones so that the model contains a constant term. The F statistic and p value are computed under the assumption that the model contains a constant term, and they are not correct for models without a constant. The R-square value is one minus the ratio of the error sum of squares to the total sum of squares. This value can be negative for models without a constant, which indicates that the model is not appropriate for the data.

Table 21 summarizes the results of the correlation analysis, with the p-value (p) and correlation coefficient (r) for each feature and for each signal. Table 22 reports the results of the multiple linear regression analysis.

Tabella 21. Results of the correlation analysis

	RMS		**MINMAX**		**STD**	
WEIGHT	p	r	p	r	p	r
x-axes acceleration	0.0001 s ***	-0.77	0.0033 s ***	0.64	0.0152 s *	-0.55
y-axes acceleration	0.7764 ns	0.07	0.5399 ns	0.15	0.0002 s ***	0.75
z-axes acceleration	<0.0001 s ****	0.83	<0.0001 s ****	0.84	0.0004 s ***	0.73
x-axes angular velocity	0.0005 s ***	0.72	<0.0001 s ****	0.80	<0.0001 s ****	0.78
y-axes angular velocity	<0.0001 s ****	0.87	<0.0001 s ****	0.92	<0.0001 s ****	0.92
z-axes angular velocity	0.0002 s ***	0.76	0.0002 s ***	0.75	<0.0001 s ****	0.83

RMS: Root Mean Square; MINMAX: Min Max value; STD: Standard Deviation; s: significant; p: p-value; r: Pearson correlation coefficient; *p < 0.05, **p < 0.01, ***p < 0.001, ****p < 0.0001

Tabella 22. The multiple linear regression analysis

R	F	p	EV
0.90	18.11	0.0000	4.72

R: R-square; F: F-statistic; p: p-value; EV: Error Variance

The linear equation to calculate the lifted weight (LW) as a function of the features extracted from raw signals, weighted with the coefficient calculated through multiple regression analysis, is as follows:

$$LW = -17.91 + 0.61 * aRMSz + 0.94 * aMINMAXz - 0.03 * aSTDz - 42.07 * vRMSy + 1.63 * vMINMAXy + 48.49 * vSTDy$$

The goal of this research was to explore the correlation between features extracted from raw signals (acceleration and angular velocity) by means of a wearable inertial system and loads lifted, and to find a linear equation to estimate the lifted load using the most informative extracted features according to the correlation analysis. The results suggest that there is a correlation between the time domain features and the load lifted, and a multiple linear regression analysis with an R-squared greater than 0.9 confirms the feasibility of this methodology for predicting the load lifted. Correlation study was carried out through the calculation of the Pearson correlation coefficient while the lifted load was estimated through a multiple linear regression analysis. Our results showed that the z-axes acceleration and y-axes angular velocity were the most informative signals in terms of correlation and variability, therefore the features extracted from these two signals were used to feed the multiple linear regression model obtaining a valuable R-square. This methodology looks promising in the field of ergonomics and prevention of WRMDs. Continuous and quantitative monitoring of the lifting activities performed by workers could be used in applications to automatically detect critical phases during the work shift. This would allow safety operators and ergonomists to plan remediation and preventive interventions, and occupational doctors to verify the compatibility of work requirements with individual conditions.

In conclusion, the results showed that the proposed combination of features extracted from inertial data and the multiple linear regression model represents a valid approach to automatically monitor the load lifted during manual handling activities. Further studies on enriched datasets and new features (both in the time domain and in the frequency domain) will further confirm the potential of this methodology and verify its applicability in the workplace.

3.3 Influence of the weight on gait performances and postures

Studies and reviews show that the vast majority of students around the world use heavy and uncomfortable backpacks, which could negatively affect their musculoskeletal development or at least generate a non-physiological functional overload. In this regard, non-invasive analyses were carried out on a sample of 150 healthy students aged between 14 and 15 years using a wearable inertial device for gait analysis: G-Walk System by BTS Bioengineering. Each student performed a gait analysis session consisting in a walk of 15 meters along a straight path in two different conditions: free walk and walk with backpack. A backpack with a sturdy backrest, wide and padded straps and abdominal belt with buckle was chosen. The weight inside the backpack was fixed at 9.3 kg in accordance with scientific studies conducted by Stefano Negrini of ISICO (Istituto Scientifico Italiano Colonna Vertebrale). Aim of this work is to understand, through an accurate analysis both instrumental and statistical, if we can talk about differential influence of musculoskeletal type generated by a school backpack full load compared to no backpack, trying to find out if and how much this affects walking both in terms of space-time parameters and detachment from normality values, and in terms of kinematic parameters such as pelvic rotations angles. Results showed a statistically significant difference between the space-time parameters computed in the two different study conditions, moreover a qualitative and quantitative difference was found for kinematic parameters too, which could imply potential musculoskeletal disorders associated with prolonged and long-lasting use of heavy and uncomfortable backpacks. This study has the ambition to raise awareness of this issue in order to extend legislative limits to the "working" environment of children, that is the school, as it is done for working environments adults (D. lgs 81/08 related to manual maintenance of loads) [1].

The study was carried out considering a study population composed of 150 healthy students aged between 14 and 15 years (86 males). The anthropometric characteristics of the study population are reported in the Table 23.

Table 23. Anthropometric characteristics of the study population

Weight (kg)	59.64 ± 11.60
Height (cm)	166.82 ± 7.93
Left lower limb length (cm)	86.40 ± 4.60
Rigth lower limb length (cm)	86.32 ± 4.63

All the subjects wore the inertial sensor G-Walk through a belt placed in the lumbosacral region as shown in Figure 31.

Figure 31. Placement of the inertial sensor G-Walk

Each subject performed two sessions. The first session consisted in 4 consecutive trials consisting in a free walk on a 15 meters straight path. The second session consisted in 4 consecutive trial consisting in a walk with backpack on a 15 meters straight path. Several kinematic parameters were recorded:

- Cadence (steps/min)
- Stride length (m)
- Stance Phase (% cycle)
- Swing Phase (% cycle)
- Double Initial Support Phase (% cycle)
- Propulsion (adimensional)

Moreover the following pelvis angles were recorded:

- Pelvic tilt (degrees)
- Pelvic obliquity (degrees)
- Pelvic rotation (degrees)

In the Table 24 are reported the results of the t-test between the two study condition: free walk and walk with backpack for each kinematic parameter.

Table 24. Paired t-test between Free Walk and Walk with backpack for each kinematic parameter

Parameters	Free Walk	Walk with Backpack
Cadence (steps/min)	114.80 ± 8.68	113.70 ± 8.08***
Stride Length (m)	1.48 ± 0.15	1.51 ± 0.14****
Stance Phase (%)	59.09 ± 1.41	61.38 ± 1.33****
Swing Phase (%)	40.91 ± 1.41	38.62 ± 1.33****
Initial Double Support Phase (%)	9.11 ± 1.38	11.40 ± 1.34****
Propulsion (adim)	9.74 ± 1.84	9.12 ± 1.49****

The average component of the weight force along the spine during free walk is:

$$F_{s,1} = P\cos 10° = mg\cos 10° \simeq 573\ N$$

The average component of the weight force along the spine during walk with backpack is:

$$F_{s,2} = (P + P_b)\cos 7° = (P + m_z g)\cos 7° \simeq 670\ N$$

Where m: the mean mass of the reference sample, g: gravitational acceleration, m_z: backpack weight (9.3 kg).

The percentage variation of the force exerted on the spine in the two different walking conditions is:

$$var\% = \frac{(670 - 573)}{573} \simeq 17\%$$

In the Figures 32-34 the variations of the pelvic rotation angles during the two different walking conditions (with and without backpack) are shown.

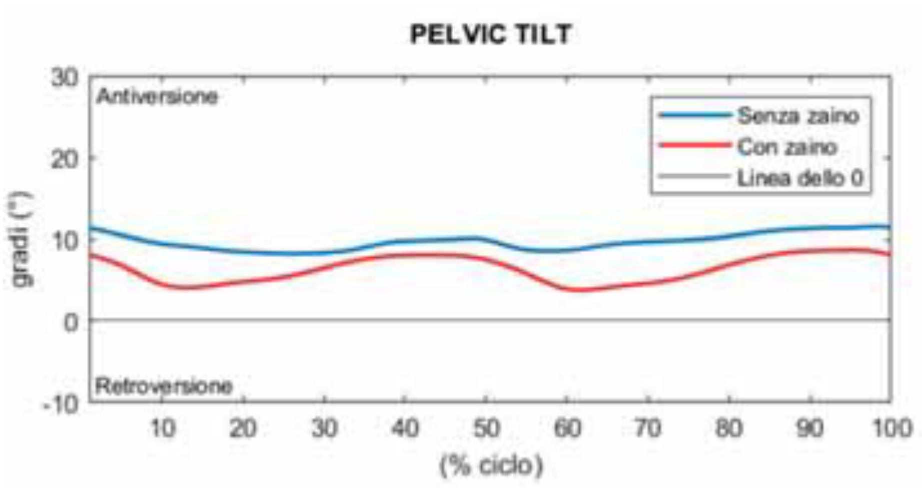

Figure 32. Pelvic tilt with and without backpack

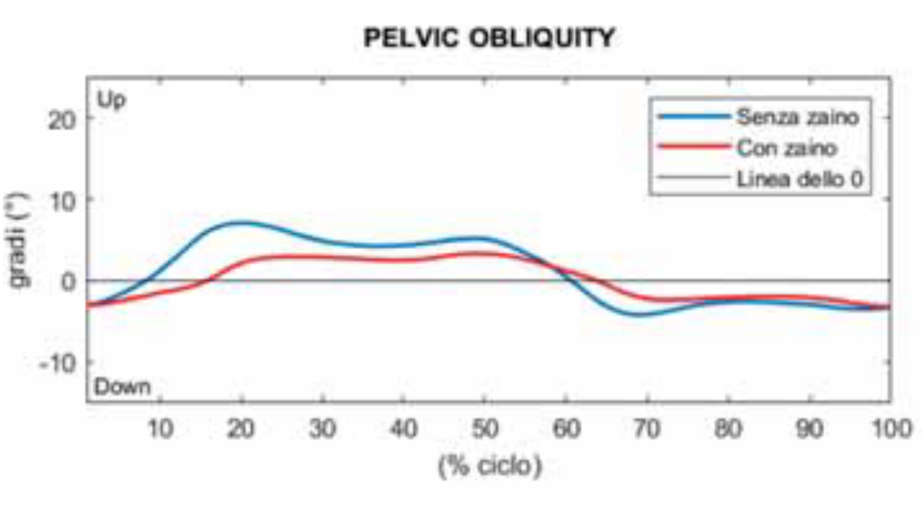

Figure 33. Pelvic obliquity with and without backpack

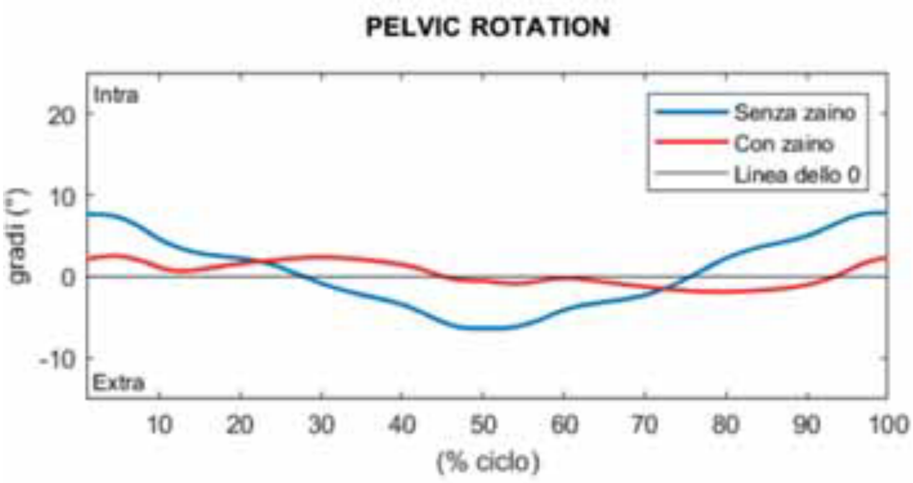

Figure 34. Pelvic rotation with and without backpack

Considering the results obtained, it can be seen that the cadence decrease in a significant statistical way because of the backpack in according with the study of Ahmad et al. [138] while the stride length increase.

About the stance phase and swing phase, these parameters in the free walk are close to the normal values presented in the scientific literature namely 60% for the stance phase and 40% for the swing phase. Because of the backpack, a variation of about 2% is observed. More precisely, in according with the study of Hong et al. [139], the stance phase increases of 2% and consequently the swing phase decrease of 2% because of the backpack; this variation is due to the fact that when subjects wearing the backpack tend to increase durability of the support phase to compensate for the instability that generates in the swing phase.

With regard to the Initial double support phase, it is noted that there is an increase in accordance with the results obtained by Hong et al. [139] of 2.5% in the case of walking with backpack compared to the free walking condition that leaves assume that, because of the backpack, increases the initial double support phase thus remaining for a longer time anchored to the ground so as to provide to the instability that is generated during the single support phase when the weight is supported by only one limb; a detachment is always observed in relation to this parameter from the literature standard value of 10%.

Finally, a statistically significant decrease is observed in the propulsion index during the walk with backpack compared to free walk. The higher value of this parameter in the case of walking without backpack indicates greater capacity during the advancement movement in the supporting phase. This result can be associated with a greater effort that is not able to compensate for the weight of the backpack and thus a potential biomechanical overload of musculoskeletal structures.

As for pelvic tilt (Figure 32), it can be observed that the subject is more antiverse when it makes the walk without the additional load of the backpack. The trend of the curve without backpack has an average value of about 10 degrees, and an excursion not particularly significant during the gait cycle. The curve that identifies the pelvic tilt in case of walking with backpack is, instead, translated downwards of a few degrees, with an average value of about 7 degrees presenting greater variability during the gait cycle. This difference is attributable to the non-negligible weight of the backpack that therefore brings the subject to walk less antiverse; this also suggests a small variation of the center of gravity of the body which, moving posteriorly, involves a reduction in the stability of the subject, which in response tends to remain more anchored to the soil justifying the increase in the support phase and that of double support both initial and final. It can be observed variations also for the other two angles: pelvic obliquity and pelvic rotation.

Finally, A 17% percentage increase in the force exerted on the spine during walking with backpack can determine a biomechanical overload on the spine which could determine potential associated musculoskeletal disorders.

It can therefore be concluded that all spatiotemporal parameters analyzed are negatively affected in statistically significant way because of the backpack, determining a potential biomechanical overload on musculoskeletal structures in students exposed to such prolonged conditions. The angles related to the kinematics also undergo a qualitative and quantitative variation.

Chapter 4

E-textile for Ergonomics

4.1 An E-textile shirt for the biomechanical risk assessment

The e-textile shirt prototype presented in the Chapter 2 coupled with a dedicated software developed has been used as device for the biomechanical risk assessment.
The software has been developed using MATLAB. The software is able to segment the EMG signals and the acceleration signals during the time window corresponding to the lifting task. The proposed methodology has been tested on a study population composed of 5 males and healthy subjects whose anthropometric characteristics are shown in the Table 25.

Table 25. Anthropometric characteristics of the study population

Subject id	Age [years]	Height [cm]	Weight [kg]	BMI [kg/cm^2]
1	27	173	77	25.73
2	27	175	65	21.22
3	30	171	61	20.86
4	27	175	65	21.22
5	30	170	80	27.68

Each subject performed a session based on two trials. Each trial consisted in 20 consecutive lifting. The first trial was performed in a condition with LI < 1 (LI = 0.5) which corresponds to the NO RISK class while the second trial was performed in a condition with LI > 1 (LI = 1.3) which correspond to the RISK class. LI of 0.5 and 1.3 were derived from the RNLE by variously combining height, frequency and weight of lifting tasks. The details of the combinations are displayed in Table 26.

Table 26. Combinations of the height, frequency and weight variables for lifting activities corresponding to LI 0.5 and 1.3 for a study population based on male subjects under the age of 45 according to the RNLE

First Trial LI < 1 (0.5)			Second Trial LI > 1 (1.3)		
Displacement [Start-End] (cm)	Frequency (Lifts/min)	Weight Lifted (kg)	Displacement [Start-End] (cm)	Frequency (Lifts/min)	Weight Lifted (kg)
[50 - 125]	2.5	7	[50 – 125]	6	15

Each trial was performed using a plastic container (56 x 35 x 31 cm^3) with weights equally distributed inside; the size of the plastic container is such that it can be held close to the barycenter of the body during the lifting task. The subjects were instructed to adopt a stable upright posture with the lower limbs slightly apart and to perform the squat technique with a two-handed grip. Each lifting task was performed in a slow, controlled manner without any jerk or sudden acceleration. The researcher was in charge of visually checking the performance, and possibly having the subject repeat the execution to acquire the signal again if the task was carried out in an uncontrolled manner.

In Figure 35 is reported the surface Electromiography (sEMG) biceps signal for the NO RISK and RISK trials while in Figure 36 is reported the z-axis acceleration (component perpendicular to the plane of the body) for the NO RISK AND RISK trials.

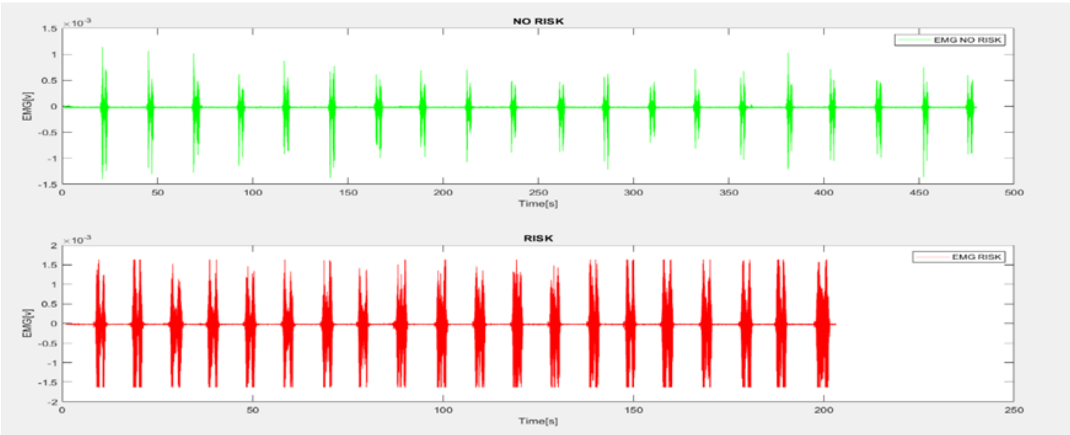

Figure 35. sEMG bicep signal acquired during the NO RISK trial (green) and during the RISK trial (red)

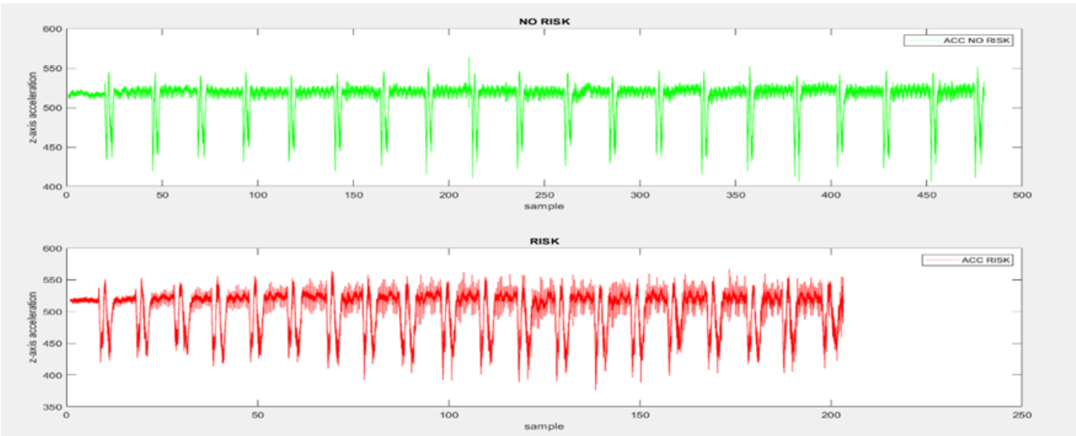

Figure 36. z-axis acceleration acquired during the NO RISK trial (green) and the RISK trial (red)

The sEMG bicep signal and the z-axis acceleration were segmented capturing the lifting activity in order to extract predictive features both in the time and frequency domains able to discriminate the risk classes according to the RNLE.

The following time-domain features were extracted:

- Area
- Root mean square
- Mean
- Standard deviation
- Maximum

The following frequency-domain features were extracted:

- Power
- Peak frequency
- Maximum frequency
- Mean frequency
- Median frequency
- Kurtosis
- Skewness

The segmentation process started from the EMG signal extracting the ROI corresponding to the lifting action and therefore the start and the end points were used to segment the z-axis acceleration signal in order to have the same time window for both signal.

In Figure 37 is shown the sEMG bicep signal and z-axis acceleration signal for one specific lifting corresponding to the trial NO RISK while in Figure 38 is shown the z-axis acceleration for one specific lifting corresponding to the the trial RISK.

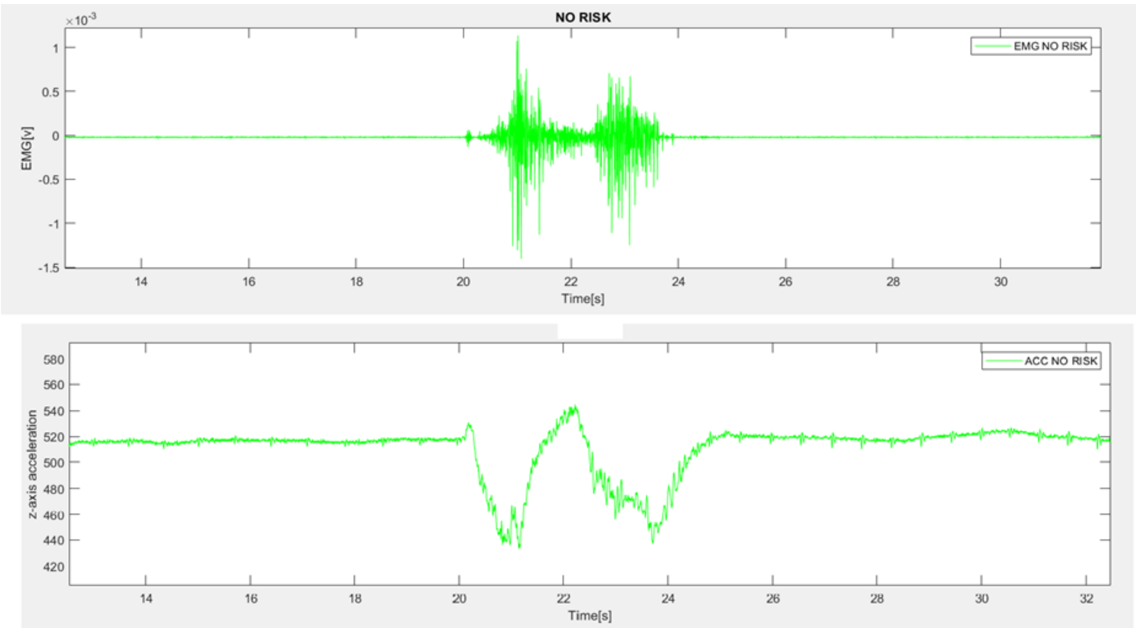

Figure 37. sEMG bicep and z-axis acceleration signals corresponding to a lifting action for the NO RISK trial

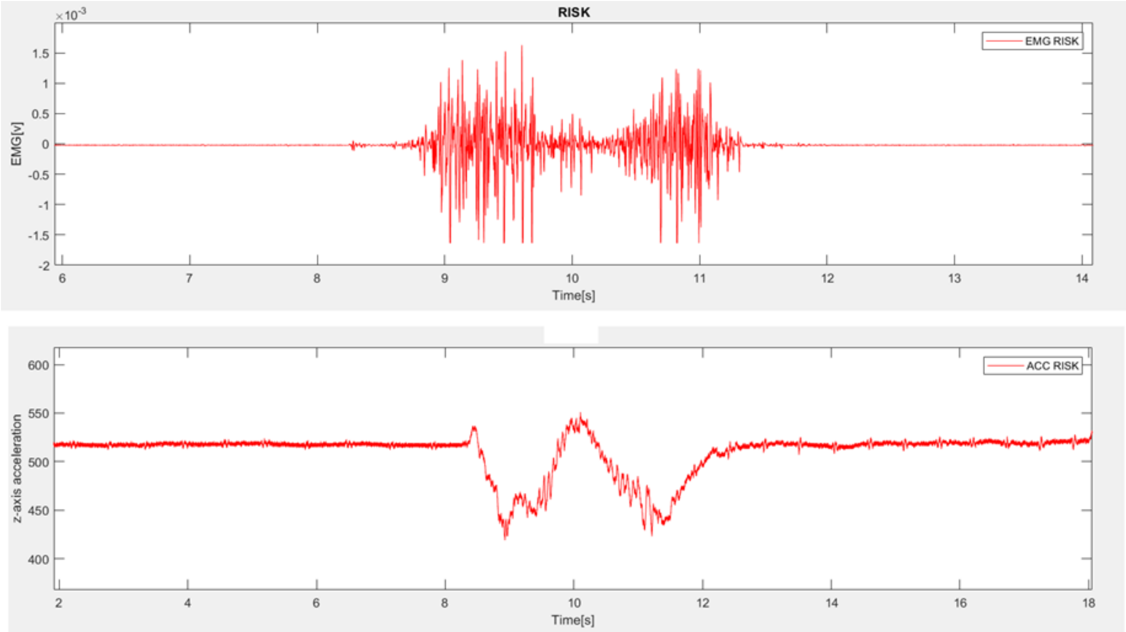

Figure 38. sEMG bicep and z-axis acceleration signals corresponding to a lifting action for the RISK trial

The EMG signal was filtered with a 8 order Butterworth band-pass filter with a band pass ranging from 5 Hz to 400 Hz. Therefore the signal was rectified and then filtered with a 4 order Butterworth low-pass filter with a cut-off frequency equal to 20 Hz. Finally a Savitzky-Golay filter was applied on the resulting signal. The filtering was implemented in Matlab using butter and sgolayfilt functions. Sgolayfilt (x, ORDER, FRAMELEN) smooths the signal x using a Savitzky-Golay (polynomial) smoothing filter. The polynomial order, ORDER, must be less than the frame length, FRAMELEN, and FRAMELEN must be odd. The length of the input x must be >= FRAMELEN. In our case ORDER and FRAMELEN was set to 3 and 3001 respectively. Successively, a threshold equal to the maximum of the signal divided for 12 was set to calculate the start and end points in order to segment the EMG signal and extract the related Region of Interest.

In Figure 39 is shown the EMG envelope and the EMG signal after having applied the Savitzky-Golay filter for the sEMG bicep signal corresponding to a single lifting action while in the Figure 40 is reported the whole acquisition.

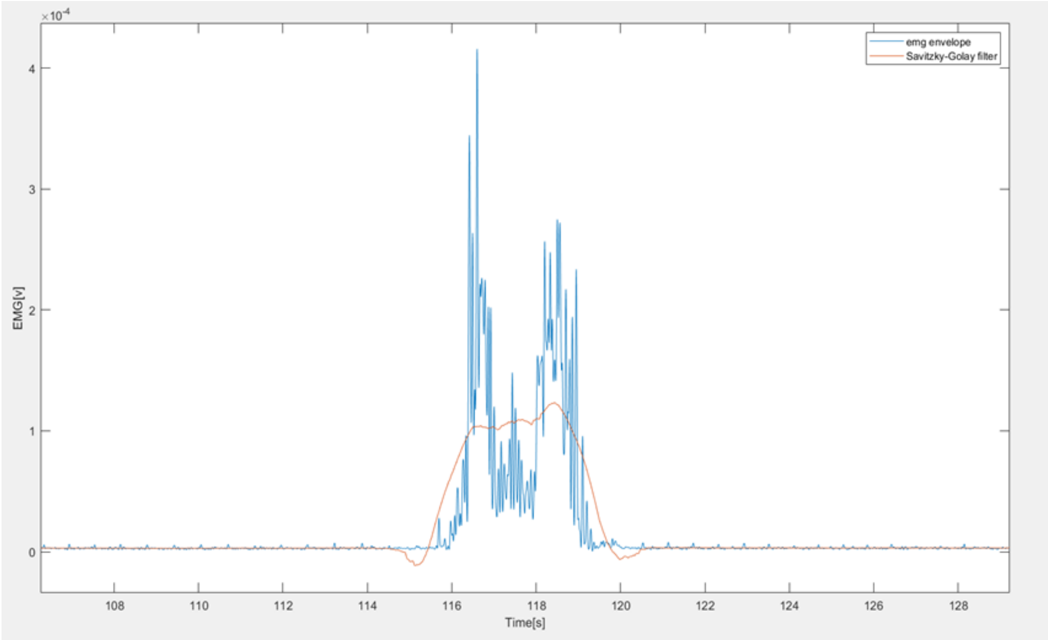

Figure 39. sEMG bicep envelope (blue) and sEMG bicep envelope filtered with a Savitzky-Golay filter (red) for a single contraction related to a single lifting

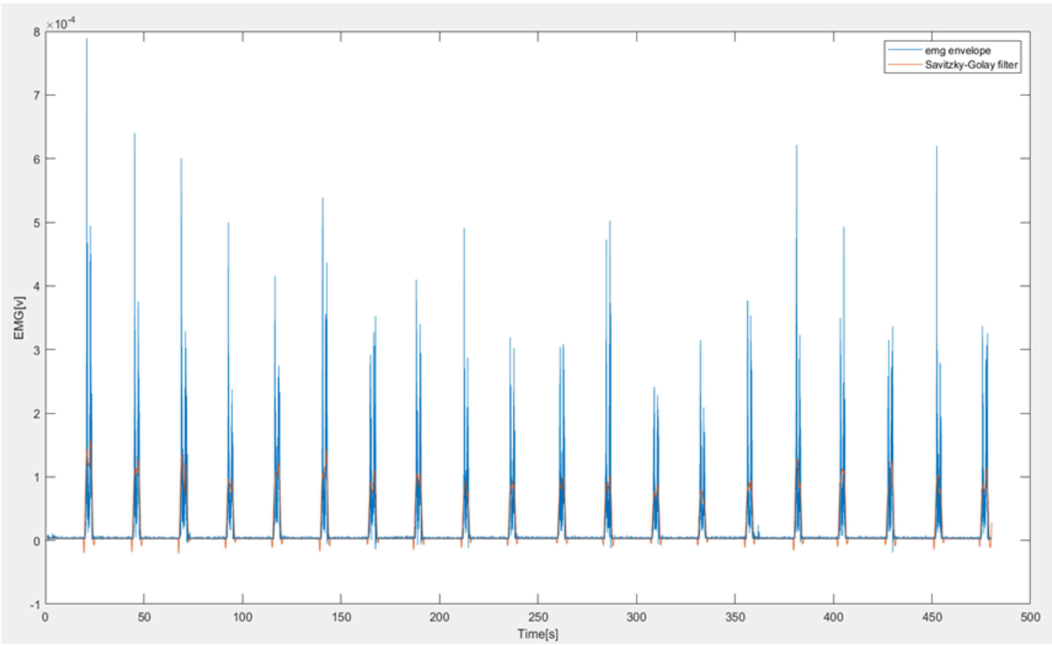

Figure 40. sEMG bicep envelope (blue) and sEMG bicep envelope filtered with a Savitzky-Golay filter (red) for the whole acquisition corresponding to 20 lifting

Successively, a threshold has been set in order to extract the vectors containing the start points and the end points in order to extract the ROI associated to each lifting and therefore to segment the signal.

In Figure 41 is reported the segmentation of the EMG signal with the extraction of the ROI. In Figure 42 it is showed a zoom on a single activity.

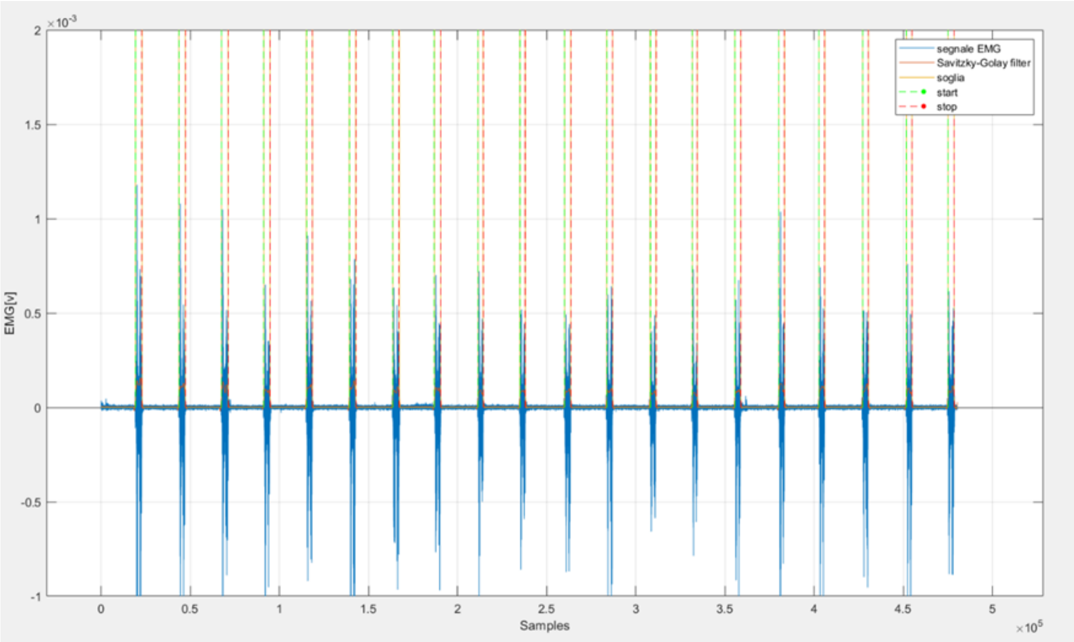

Figure 41. sEMG bicep segmentation

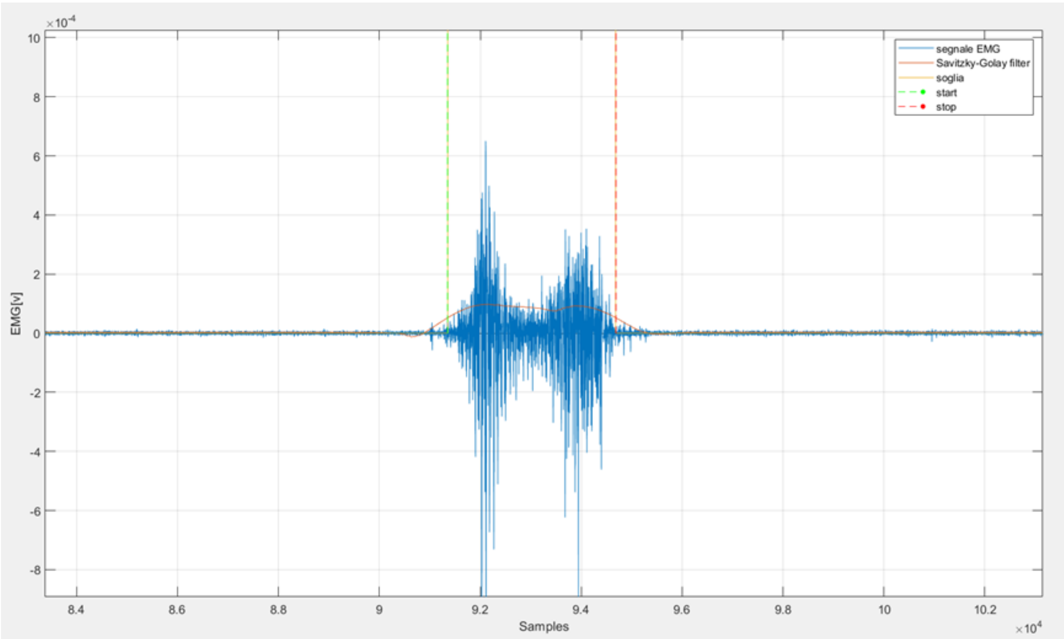

Figure 42. Zoom of a single sEMG bicep contraction

After having segmented the signal, for each ROI the mentioned features were extracted. These features were used to build a dataset containing the features extracted for each ROI and the risk class, namely NO RISK and RISK. The resulting datasets were used to study the potential discriminative power of the extracted features and the capability of several state-of-the-art ML algorithms do discriminate risk classes according to the RNLE.

A similar procedure was carried out for the z-axis acceleration signal, the details are not provided for the sake of brevity.

First, the machine learning analysis was carried out considering each single subject and each signal, namely EMG and z-axis acceleration.

In Tables 27, 28, 29, 30, 31, 32, 33, 34,35, 36 are reported the evaluation metrics score for each ML algorithm using as validation strategy the leave-one-out CV and repeating the leave-one-out CV ten time. The ML algorithms implemented were: DT, RF, Rotation Forest (Rot-F), GBT, ABT, kNN and NB.

Table 27. Evaluation metric scores reported as mean ± standard deviation for the subject id 1 using features extracted from sEMG bicep signal

	Recall	**Precison**	**Sensitivity**	**Specificity**	**F-measure**	**Accuracy**	**AucRoc**
DT	0.95 ± 0.00	1.00 ± 0.00	0.95 ± 0.00	1.00 ± 0.00	0.97 ± 0.00	0.98 ± 0.00	0.98 ± 0.00
RF	1.00 ± 0.00	0.95 ± 0.00	1.00 ± 0.00	0.95 ± 0.00	0.98 ± 0.00	0.98 ± 0.00	1.00 ± 0.00
Rot-F	1.00 ± 0.00	0.95 ± 0.00	1.00 ± 0.00	0.95 ± 0.00	0.98 ± 0.00	0.98 ± 0.00	0.99 ± 0.00
GBT	1.00 ± 0.00	0.95 ± 0.00	1.00 ± 0.00	0.95 ± 0.00	0.98 ± 0.00	0.98 ± 0.00	0.98 ± 0.00
ABT	1.00 ± 0.00	0.95 ± 0.00	1.00 ± 0.00	0.95 ± 0.00	0.98 ± 0.00	0.98 ± 0.00	0.98 ± 0.00
kNN	0.65 ± 0.00	0.68 ± 0.00	0.65 ± 0.00	0.70 ± 0.00	0.67 ± 0.00	0.68 ± 0.00	0.66 ± 0.00
NB	0.90 ± 0.00	1.00 ± 0.00	0.90 ± 0.00	1.00 ± 0.00	0.95 ± 0.00	0.95 ± 0.00	0.99 ± 0.00

Table 28. Evaluation metric scores reported as mean ± standard deviation for the subject id 1 using features extracted from z-axis acceleration signal

	Recall	**Precison**	**Sensitivity**	**Specificity**	**F-measure**	**Accuracy**	**AucRoc**
DT	0.95 ± 0.00	0.95 ± 0.00	0.95 ± 0.00	0.95 ± 0.00	0.95 ± 0.00	0.95 ± 0.00	0.95 ± 0.00
RF	0.95 ± 0.00	0.95 ± 0.00	0.95 ± 0.00	0.95 ± 0.00	0.95 ± 0.00	0.95 ± 0.00	0.99 ± 0.00
Rot-F	1.00 ± 0.00	0.95 ± 0.00	1.00 ± 0.00	0.95 ± 0.00	0.98 ± 0.00	0.98 ± 0.00	1.00 ± 0.00
GBT	0.95 ± 0.00	0.95 ± 0.00	0.95 ± 0.00	0.95 ± 0.00	0.95 ± 0.00	0.95 ± 0.00	0.95 ± 0.00
ABT	0.95 ± 0.00	0.95 ± 0.00	0.95 ± 0.00	0.95 ± 0.00	0.95 ± 0.00	0.95 ± 0.00	0.95 ± 0.00
kNN	1.00 ± 0.00	1.00 ± 0.00	1.00 ± 0.00	1.00 ± 0.00	1.00 ± 0.00	1.00 ± 0.00	1.00 ± 0.00
NB	1.00 ± 0.00	0.95 ± 0.00	1.00 ± 0.00	0.95 ± 0.00	0.98 ± 0.00	0.98 ± 0.00	0.99 ± 0.00

Table 29. Evaluation metric scores reported as mean ± standard deviation for the subject id 2 using features extracted from sEMG bicep signal

	Recall	**Precison**	**Sensitivity**	**Specificity**	**F-measure**	**Accuracy**	**AucRoc**
DT	1.00 ± 0.00	1.00 ± 0.00	1.00 ± 0.00	1.00 ± 0.00	1.00 ± 0.00	1.00 ± 0.00	1.00 ± 0.00
RF	1.00 ± 0.00	1.00 ± 0.00	1.00 ± 0.00	1.00 ± 0.00	1.00 ± 0.00	1.00 ± 0.00	1.00 ± 0.00
Rot-F	0.95 ± 0.00	1.00 ± 0.00	0.95 ± 0.00	1.00 ± 0.00	0.97 ± 0.00	0.98 ± 0.00	1.00 ± 0.00
GBT	1.00 ± 0.00	0.95 ± 0.00	1.00 ± 0.00	0.95 ± 0.00	0.98 ± 0.00	0.98 ± 0.00	0.98 ± 0.00
ABT	1.00 ± 0.00	0.95 ± 0.00	1.00 ± 0.00	0.95 ± 0.00	0.98 ± 0.00	0.98 ± 0.00	0.98 ± 0.00
kNN	0.85 ± 0.00	0.74 ± 0.00	0.85 ± 0.00	0.70 ± 0.00	0.79 ± 0.00	0.76 ± 0.00	0.80 ± 0.00
NB	1.00 ± 0.00	1.00 ± 0.00	1.00 ± 0.00	1.00 ± 0.00	1.00 ± 0.00	1.00 ± 0.00	1.00 ± 0.00

Table 30. Evaluation metric scores reported as mean ± standard deviation for the subject id 2 using features extracted from z-axis acceleration signal

	Recall	Precison	Sensitivity	Specificity	F-measure	Accuracy	AucRoc
DT	1.00 ± 0.00	1.00 ± 0.00	1.00 ± 0.00	1.00 ± 0.00	1.00 ± 0.00	1.00 ± 0.00	1.00 ± 0.00
RF	0.95 ± 0.00	1.00 ± 0.00	0.95 ± 0.00	1.00 ± 0.00	0.97 ± 0.00	0.98 ± 0.00	1.00 ± 0.00
Rot-F	1.00 ± 0.00	0.95 ± 0.00	1.00 ± 0.00	0.95 ± 0.00	0.98 ± 0.00	0.98 ± 0.00	1.00 ± 0.00
GBT	1.00 ± 0.00	1.00 ± 0.00	1.00 ± 0.00	1.00 ± 0.00	1.00 ± 0.00	1.00 ± 0.00	1.00 ± 0.00
ABT	1.00 ± 0.00	1.00 ± 0.00	1.00 ± 0.00	1.00 ± 0.00	1.00 ± 0.00	1.00 ± 0.00	1.00 ± 0.00
kNN	1.00 ± 0.00	1.00 ± 0.00	1.00 ± 0.00	1.00 ± 0.00	1.00 ± 0.00	1.00 ± 0.00	1.00 ± 0.00
NB	0.90 ± 0.00	0.82 ± 0.00	0.90 ± 0.00	0.80 ± 0.00	0.86 ± 0.00	0.85 ± 0.00	0.92 ± 0.00

Table 31. Evaluation metric scores reported as mean ± standard deviation for the subject id 3 using features extracted from sEMG bicep signal

	Recall	Precison	Sensitivity	Specificity	F-measure	Accuracy	AucRoc
DT	1.00 ± 0.00	0.91 ± 0.00	1.00 ± 0.00	0.90 ± 0.00	0.95 ± 0.00	0.95 ± 0.00	1.00 ± 0.00
RF	1.00 ± 0.00	0.87 ± 0.00	1.00 ± 0.00	0.85 ± 0.00	0.93 ± 0.00	0.93 ± 0.00	0.99 ± 0.00
Rot-F	1.00 ± 0.00	1.00 ± 0.00	1.00 ± 0.00	1.00 ± 0.00	1.00 ± 0.00	1.00 ± 0.00	1.00 ± 0.00
GBT	1.00 ± 0.00	1.00 ± 0.00	1.00 ± 0.00	1.00 ± 0.00	1.00 ± 0.00	1.00 ± 0.00	1.00 ± 0.00
ABT	0.95 ± 0.00	0.91 ± 0.00	0.95 ± 0.00	0.90 ± 0.00	0.93 ± 0.00	0.93 ± 0.00	0.99 ± 0.00
kNN	0.75 ± 0.00	0.68 ± 0.00	0.75 ± 0.00	0.65 ± 0.00	0.71 ± 0.00	0.70 ± 0.00	0.79 ± 0.00
NB	1.00 ± 0.00	0.83 ± 0.00	1.00 ± 0.00	0.80 ± 0.00	0.91 ± 0.00	0.90 ± 0.00	0.97 ± 0.00

Table 32. Evaluation metric scores reported as mean ± standard deviation for the subject id 3 using features extracted from z-axis acceleration signal

	Recall	Precison	Sensitivity	Specificity	F-measure	Accuracy	AucRoc
DT	1.00 ± 0.00	1.00 ± 0.00	1.00 ± 0.00	1.00 ± 0.00	1.00 ± 0.00	1.00 ± 0.00	1.00 ± 0.00
RF	1.00 ± 0.00	1.00 ± 0.00	1.00 ± 0.00	1.00 ± 0.00	1.00 ± 0.00	1.00 ± 0.00	1.00 ± 0.00
Rot-F	1.00 ± 0.00	0.95 ± 0.00	1.00 ± 0.00	0.95 ± 0.00	0.98 ± 0.00	0.98 ± 0.00	1.00 ± 0.00
GBT	1.00 ± 0.00	1.00 ± 0.00	1.00 ± 0.00	1.00 ± 0.00	1.00 ± 0.00	1.00 ± 0.00	1.00 ± 0.00
ABT	1.00 ± 0.00	1.00 ± 0.00	1.00 ± 0.00	1.00 ± 0.00	1.00 ± 0.00	1.00 ± 0.00	1.00 ± 0.00
kNN	1.00 ± 0.00	1.00 ± 0.00	1.00 ± 0.00	1.00 ± 0.00	1.00 ± 0.00	1.00 ± 0.00	1.00 ± 0.00
NB	0.70 ± 0.00	0.78 ± 0.00	0.70 ± 0.00	0.80 ± 0.00	0.74 ± 0.00	0.75 ± 0.00	0.86 ± 0.00

Table 33. Evaluation metric scores reported as mean ± standard deviation for the subject id 4 using features extracted from sEMG bicep signal

	Recall	Precison	Sensitivity	Specificity	F-measure	Accuracy	AucRoc
DT	1.00 ± 0.00	1.00 ± 0.00	1.00 ± 0.00	1.00 ± 0.00	1.00 ± 0.00	1.00 ± 0.00	1.00 ± 0.00
RF	1.00 ± 0.00	1.00 ± 0.00	1.00 ± 0.00	1.00 ± 0.00	1.00 ± 0.00	1.00 ± 0.00	1.00 ± 0.00
Rot-F	1.00 ± 0.00	1.00 ± 0.00	1.00 ± 0.00	1.00 ± 0.00	1.00 ± 0.00	1.00 ± 0.00	1.00 ± 0.00
GBT	1.00 ± 0.00	1.00 ± 0.00	1.00 ± 0.00	1.00 ± 0.00	1.00 ± 0.00	1.00 ± 0.00	1.00 ± 0.00
ABT	1.00 ± 0.00	1.00 ± 0.00	1.00 ± 0.00	1.00 ± 0.00	1.00 ± 0.00	1.00 ± 0.00	1.00 ± 0.00
kNN	0.70 ± 0.00	0.74 ± 0.00	0.70 ± 0.00	0.75 ± 0.00	0.72 ± 0.00	0.73 ± 0.00	0.73 ± 0.00
NB	1.00 ± 0.00	1.00 ± 0.00	1.00 ± 0.00	1.00 ± 0.00	1.00 ± 0.00	1.00 ± 0.00	1.00 ± 0.00

Table 34. Evaluation metric scores reported as mean ± standard deviation for the subject id 4 using features extracted from z-axis acceleration signal

	Recall	Precison	Sensitivity	Specificity	F-measure	Accuracy	AucRoc
DT	0.95 ± 0.00	1.00 ± 0.00	0.95 ± 0.00	1.00 ± 0.00	0.97 ± 0.00	0.98 ± 0.00	0.98 ± 0.00
RF	0.95 ± 0.00	1.00 ± 0.00	0.95 ± 0.00	1.00 ± 0.00	0.97 ± 0.00	0.98 ± 0.00	1.00 ± 0.00
Rot-F	1.00 ± 0.00	1.00 ± 0.00	1.00 ± 0.00	1.00 ± 0.00	1.00 ± 0.00	1.00 ± 0.00	1.00 ± 0.00
GBT	0.95 ± 0.00	1.00 ± 0.00	0.95 ± 0.00	1.00 ± 0.00	0.97 ± 0.00	0.98 ± 0.00	0.98 ± 0.00
ABT	0.95 ± 0.00	1.00 ± 0.00	0.95 ± 0.00	1.00 ± 0.00	0.97 ± 0.00	0.98 ± 0.00	0.98 ± 0.00
kNN	1.00 ± 0.00	0.99 ± 0.02	1.00 ± 0.00	0.99 ± 0.02	0.99 ± 0.01	0.99 ± 0.01	1.00 ± 0.00
NB	0.90 ± 0.00	1.00 ± 0.00	0.90 ± 0.00	1.00 ± 0.00	0.95 ± 0.00	0.95 ± 0.00	0.99 ± 0.00

Table 35. Evaluation metric scores reported as mean ± standard deviation for the subject id 5 using features extracted from sEMG bicep signal

	Recall	**Precison**	**Sensitivity**	**Specificity**	**F-measure**	**Accuracy**	**AucRoc**
DT	1.00 ± 0.00	1.00 ± 0.00	1.00 ± 0.00	1.00 ± 0.00	1.00 ± 0.00	1.00 ± 0.00	1.00 ± 0.00
RF	1.00 ± 0.00	1.00 ± 0.00	1.00 ± 0.00	1.00 ± 0.00	1.00 ± 0.00	1.00 ± 0.00	1.00 ± 0.00
Rot-F	0.95 ± 0.00	1.00 ± 0.00	0.95 ± 0.00	1.00 ± 0.00	0.97 ± 0.00	0.98 ± 0.00	1.00 ± 0.00
GBT	1.00 ± 0.00	1.00 ± 0.00	1.00 ± 0.00	1.00 ± 0.00	1.00 ± 0.00	1.00 ± 0.00	1.00 ± 0.00
ABT	1.00 ± 0.00	1.00 ± 0.00	1.00 ± 0.00	1.00 ± 0.00	1.00 ± 0.00	1.00 ± 0.00	1.00 ± 0.00
kNN	0.35 ± 0.00	0.41 ± 0.00	0.35 ± 0.00	0.50 ± 0.00	0.38 ± 0.00	0.43 ± 0.00	0.42 ± 0.00
NB	1.00 ± 0.00	1.00 ± 0.00	1.00 ± 0.00	1.00 ± 0.00	1.00 ± 0.00	1.00 ± 0.00	1.00 ± 0.00

Table 36. Evaluation metric scores reported as mean ± standard deviation for the subject id 5 using features extracted from z-axis acceleration signal

	Recall	**Precison**	**Sensitivity**	**Specificity**	**F-measure**	**Accuracy**	**AucRoc**
DT	1.00 ± 0.00	1.00 ± 0.00	1.00 ± 0.00	1.00 ± 0.00	1.00 ± 0.00	1.00 ± 0.00	1.00 ± 0.00
RF	1.00 ± 0.00	0.95 ± 0.00	1.00 ± 0.00	0.95 ± 0.00	0.98 ± 0.00	0.98 ± 0.00	1.00 ± 0.00
Rot-F	1.00 ± 0.00	1.00 ± 0.00	1.00 ± 0.00	1.00 ± 0.00	1.00 ± 0.00	1.00 ± 0.00	1.00 ± 0.00
GBT	1.00 ± 0.00	1.00 ± 0.00	1.00 ± 0.00	1.00 ± 0.00	1.00 ± 0.00	1.00 ± 0.00	1.00 ± 0.00
ABT	1.00 ± 0.00	1.00 ± 0.00	1.00 ± 0.00	1.00 ± 0.00	1.00 ± 0.00	1.00 ± 0.00	1.00 ± 0.00
kNN	1.00 ± 0.00	1.00 ± 0.00	1.00 ± 0.00	1.00 ± 0.00	1.00 ± 0.00	1.00 ± 0.00	1.00 ± 0.00
NB	0.40 ± 0.00	0.89 ± 0.00	0.40 ± 0.00	0.95 ± 0.00	0.56 ± 0.00	0.68 ± 0.00	0.74 ± 0.00

Second, a machine learning analysis was carried out considering the entire study population. In Tables 37 are reported the evaluation metrics score for each ML algorithm using the features extracted from sEMG bicep signal. The ten-fold cross-validation was implemented as validation strategy, moreover this validation was repeated ten times.

Table 37. Evaluation metric scores reported as mean ± standard deviation for the entire study population using features extracted from sEMG bicep signal

	Recall	**Precison**	**Sensitivity**	**Specificity**	**F-measure**	**Accuracy**	**AucRoc**
DT	0.95 ± 0.01	0.98 ± 0.01	0.95 ± 0.01	0.98 ± 0.01	0.96 ± 0.01	0.96 ± 0.01	0.98 ± 0.01
RF	0.99 ± 0.01	0.98 ± 0.01	0.99 ± 0.01	0.98 ± 0.01	0.98 ± 0.00	0.98 ± 0.00	0.99 ± 0.00
Rot-F	0.99 ± 0.01	0.99 ± 0.01	0.99 ± 0.01	0.99 ± 0.01	0.99 ± 0.01	0.99 ± 0.01	0.99 ± 0.00
GBT	0.97 ± 0.02	0.97 ± 0.01	0.97 ± 0.02	0.97 ± 0.01	0.97 ± 0.01	0.97 ± 0.01	0.99 ± 0.01
ABT	0.95 ± 0.01	0.96 ± 0.01	0.95 ± 0.01	0.96 ± 0.01	0.96 ± 0.00	0.96 ± 0.00	0.98 ± 0.00
kNN	0.62 ± 0.02	0.69 ± 0.01	0.62 ± 0.02	0.72 ± 0.01	0.66 ± 0.02	0.67 ± 0.01	0.69 ± 0.02
NB	0.93 ± 0.01	0.72 ± 0.00	0.93 ± 0.01	0.63 ± 0.01	0.81 ± 0.00	0.78 ± 0.00	0.92 ± 0.00

In Table 38 is reported the confusion matrix of the best ML algorithm in terms of evaluation metric scores, namely Rot-F for the sEMG bicep signal.

Tabella 38. Confusion Matrix of the best ML algorithm: Rot-F – sEMG bicep

	NO RISK	RISK
NO RISK	100	0
RISK	1	99

Moreover in Figure 43 is reported the feature importance based on the calculation of the IG for the features extracted from the sEMG bicep signal.

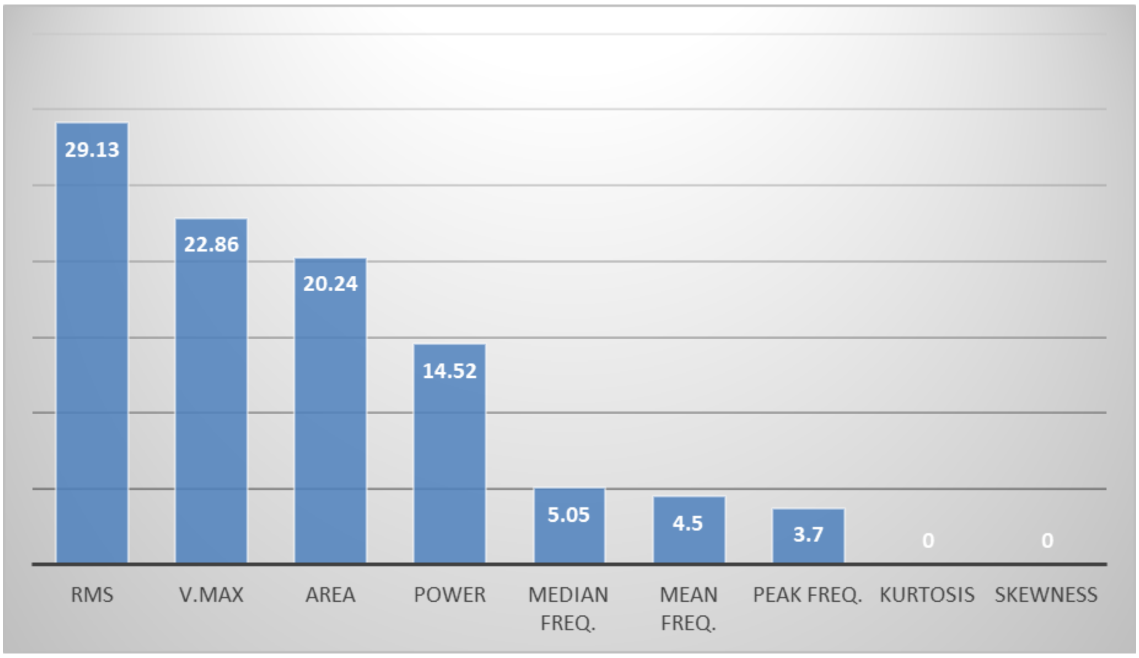

Figure 43. Feature Importance by means of IG (%) – sEMG bicep

In Tables 39 are reported the evaluation metrics score for each ML algorithm using the features extracted from the z-axis acceleration signal. The ten-fold CV was implemented as validation strategy, moreover this validation was repeated ten times.

Table 39. Evaluation metric scores reported as mean ± standard deviation for the entire study population using features extracted from z-axis acceleration signal

	Recall	Precison	Sensitivity	Specificity	F-measure	Accuracy	AucRoc
DT	1.00 ± 0.00	1.00 ± 0.00	1.00 ± 0.00	1.00 ± 0.00	1.00 ± 0.00	1.00 ± 0.00	1.00 ± 0.00
RF	1.00 ± 0.00	1.00 ± 0.00	1.00 ± 0.00	1.00 ± 0.00	1.00 ± 0.00	1.00 ± 0.00	1.00 ± 0.00
Rot-F	0.99 ± 0.01	1.00 ± 0.00	0.99 ± 0.01	1.00 ± 0.00	0.99 ± 0.00	0.99 ± 0.00	1.00 ± 0.00
GBT	1.00 ± 0.00	1.00 ± 0.00	1.00 ± 0.00	1.00 ± 0.00	1.00 ± 0.00	1.00 ± 0.00	1.00 ± 0.00
ABT	1.00 ± 0.00	1.00 ± 0.00	1.00 ± 0.00	1.00 ± 0.00	1.00 ± 0.00	1.00 ± 0.00	1.00 ± 0.00
kNN	1.00 ± 0.00	1.00 ± 0.00	1.00 ± 0.00	1.00 ± 0.00	1.00 ± 0.00	1.00 ± 0.00	1.00 ± 0.00
NB	0.60 ± 0.02	0.69 ± 0.02	0.60 ± 0.02	0.73 ± 0.02	0.64 ± 0.01	0.67 ± 0.01	0.67 ± 0.01

In Table 40 is reported the confusion matrix of the best ML algorithms in terms of evaluation metric scores, namely DT, RF, GBT, ABT, kNN for the z-axis acceleration signal.

Tabella 40. Confusion Matrix of the best ML algorithm: DT, RF, GBT, ABT, kNN – z-axis acceleration signal

	NO RISK	RISK
NO RISK	100	0
RISK	0	100

Moreover in Figure 44 is reported the feature importance based on the calculation of the IG for the features extracted from the z-axis acceleration signal.

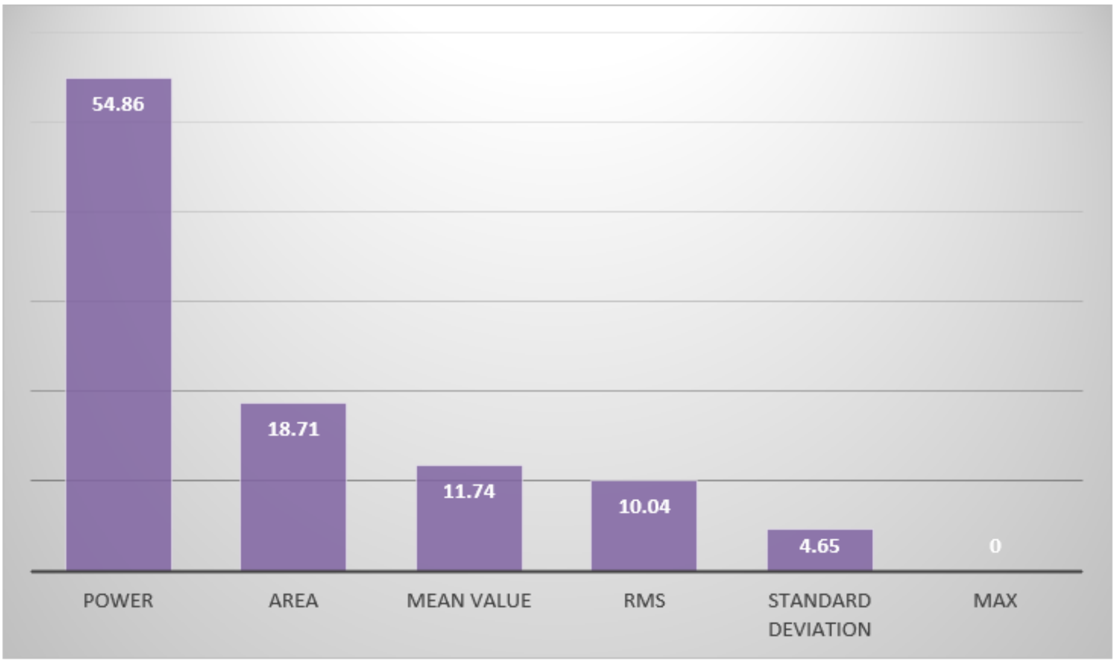

Figure 44. Feature Importance by means of IG (%) – z-axis acceleration

Finally, a leave-one-subject out validation strategy was performed using 4 subject to train the predictive models and 1 subject to validate the model, this procedure was performed in an iterative way 5 times in order to test the model on each subject using the remain 4 for the training phase. In the Table 41 are showed the results of this analysis considering the features extracted from the sEMG bicep signal while in Table 42 are showed the results of this analysis considering both the features extracted from the sEMG signal and z-axis acceleration signal.

Table 41. Evaluation metric scores reported as mean ± standard deviation for the entire study population using features extracted from sEMG bicep signal and the leave-one-subject-out as validation strategy

	Recall	**Precison**	**Sensitivity**	**Specificity**	**F-measure**	**Accuracy**	**AucRoc**
DT	0.81 ± 0.43	0.92 ± 0.13	0.81 ± 0.43	0.89± 0.19	0.77 ± 0.38	0.85 ± 0.20	0.85 ± 0.20
RF	0.81 ± 0.43	0.78 ± 0.25	0.81 ± 0.43	0.58 ± 0.51	0.68± 0.35	0.69 ± 0.25	0.91 ± 0.13
Rot-F	0.76 ± 0.41	0.97 ± 0.10	0.76 ± 0.41	0.96 ± 0.10	0.77 ± 0.38	0.86 ± 0.19	0.99 ± 0.01
GBT	1.00 ± 0.00	0.82 ± 0.22	1.00 ± 0.00	0.69 ± 0.43	0.89 ± 0.14	0.85 ± 0.21	0.81 ± 0.24
ABT	0.77 ± 0.41	0.74 ± 0.25	0.77 ± 0.41	0.51 ± 0.50	0.63 ± 0.31	0.64 ± 0.19	0.90 ± 0.21
kNN	0.45 ± 0.15	0.62 ± 0.22	0.45 ± 0.15	0.61 ± 0.25	0.48± 0.10	0.53 ± 0.10	0.54 ± 0.10
NB	0.81 ± 0.43	0.80 ± 0.25	0.81 ± 0.43	0.63 ± 0.49	0.69 ± 0.36	0.72 ± 0.25	0.99 ± 0.03

Table 42. Evaluation metric scores reported as mean ± standard deviation for the entire study population using features extracted from both sEMG bicep signal and z-axis acceleration signal, and the leave-one-subject-out as validation strategy

	Recall	Precison	Sensitivity	Specificity	F-measure	Accuracy	AucRoc
DT	1.00 ± 0.00	1.00 ± 0.00	1.00 ± 0.00	1.00 ± 0.00	1.00 ± 0.00	1.00 ± 0.00	1.00 ± 0.00
RF	0.81 ± 0.43	0.98 ± 0.04	0.81 ± 0.43	0.98 ± 0.10	0.81± 0.40	0.90 ± 0.21	1.00 ± 0.00
Rot-F	1.00 ± 0.00	1.00 ± 0.00	1.00 ± 0.00	1.00 ± 0.00	1.00 ± 0.00	1.00 ± 0.00	1.00 ± 0.00
GBT	1.00 ± 0.00	1.00 ± 0.00	1.00 ± 0.00	1.00 ± 0.00	1.00 ± 0.00	1.00 ± 0.00	1.00 ± 0.00
ABT	1.00 ± 0.00	1.00 ± 0.00	1.00 ± 0.00	1.00 ± 0.00	1.00 ± 0.00	1.00 ± 0.00	1.00 ± 0.00
kNN	1.00 ± 0.00	1.00 ± 0.00	1.00 ± 0.00	1.00 ± 0.00	1.00 ± 0.00	1.00 ± 0.00	1.00 ± 0.00
NB	0.75 ± 0.41	0.81 ± 0.26	0.75 ± 0.41	0.64 ± 0.49	0.66 ± 0.34	0.70 ± 0.22	0.99 ± 0.02

The results showed that the proposed combinations of features - extracted from sEMG bicep signal and z-axis acceleration related to the sternum- and state-of-the-art ML algorithms represents a potential valid approach to automatically classify the biomechanical risk to which subjects may be exposed during lifting activities, for example, at work. The presented methodology could represent a valid integration to the established protocols (e.g., NIOSH lifting equation) to evaluate the biomechanical risk more quickly and easily. Moreover, it could represent a valid alternative when the conditions required for the application of standardized evaluation methods do not exist. These results are of direct practical relevance for occupational ergonomics, as they present the opportunity for automatic, economic and non-invasive detection (wearing a shirt), to assess the musculoskeletal and biomechanical risk associated with lifting. Based on the promising results presented in this article, the next phase of thus research could consider an extension of the sample under consideration to further validate the methodology, new experiments that consider more than two LI values, and the integration of additional features from the time-domain and the frequency-domain.

Conclusion

In this dissertation, a new textile-sensor-based wearable device for the biomechanical risk assessment was developed and presented.

The innovative features of the system rely on the multi-parametric approach in health monitoring and on the wide ranging set of tools available for digital signal processing. In the development of the sensing unit, various sensors, electrodes, and bus structures were integrated within the textile garment, making it possible for the patient to perform normal daily activities without any discomfort. The system includes a custom-based app for real-time visualization of the acquired signals and a software desktop for off-line plotting and digital signal processing.

The presented e-textile prototype is able to noninvasively collect large amounts of body movement data during physical work and explore their association with occupational risk as assessed with standard methods. The portability and wearability of this technology represents an advantageous alternative to camera-based motion tracking systems.

Among the activities involving biomechanical overloading, material handling and lifting is one of the most studied in the scientific literature, including its association with the development of WMSDs. With a view to prevention, NIOSH established a methodology for assessing lifting actions by means of a quantitative method based on intensity, duration and frequency of the task, and other geometrical characteristics of lifting. The method determines RWL for the lifting tasks and calculates LI.

In the scientific literature, among the many applications of wearable technology to ergonomics, and in particular among those which use the NIOSH methodology, the association of features extracted directly from raw signals (acceleration and angular velocity) with NIOSH risk classes related to repeated load lifting activities has not yet been explored. Moreover, ML algorithms are gaining popularity in the ergonomic field for biomechanical risk assessment by means of data acquired by wearable systems.

The aim of this thesis was to prove the feasibility of a wearable e-textile technology coupled with a dedicated software developed based on algorithms of digital signal processing and ML to classify lifting tasks belonging to different risk classes according to the value of LI starting from features extracted from biosignals.

Based on the results presented, the experimented approach - which combines time-domain and frequency-domain features and machine learning algorithms - proved to be a valid indicator, although preliminary because of the low number of samples analyzed, of the risk of WMSDs for manual lifting (according to the NIOSH index) to which workers are potentially exposed during their working activity.

References

[1] Erdmier, C., Hatcher, J., & Lee, M. (2016). Wearable device implications in the healthcare industry. *Journal of medical engineering & technology*, *40*(4), 141-148.

[2] Lewy, H. (2015). Wearable technologies–future challenges for implementation in healthcare services. *Healthcare technology letters*, *2*(1), 2-5.

[3] DeRossi, D., & Lymberis, A. (2005). Guest editorial new generation of smart wearable health systems and applications. *IEEE transactions on information technology in biomedicine*, *9*(3), 293-294.

[4] Marschollek, M., Gietzelt, M., Schulze, M., Kohlmann, M., Song, B., & Wolf, K. H. (2012). Wearable sensors in healthcare and sensor-enhanced health information systems: all our tomorrows?. *Healthcare informatics research*, *18*(2), 97-104.

[5] Pani, D., Achilli, A., & Bonfiglio, A. (2018). Survey on textile electrode technologies for electrocardiographic (ECG) monitoring, from metal wires to polymers. *Advanced Materials Technologies*, *3*(10), 1800008.

[6] Di Rienzo, M., Rizzo, F., Parati, G., Brambilla, G., Ferratini, M., & Castiglioni, P. (2006, January). MagIC system: A new textile-based wearable device for biological signal monitoring. Applicability in daily life and clinical setting. In *2005 IEEE Engineering in Medicine and Biology 27th Annual Conference* (pp. 7167-7169). IEEE.

[7] Pandian, P. S., Mohanavelu, K., Safeer, K. P., Kotresh, T. M., Shakunthala, D. T., Gopal, P., & Padaki, V. C. (2008). Smart Vest: Wearable multi-parameter remote physiological monitoring system. *Medical engineering & physics*, *30*(4), 466-477.

[8] Paradiso, R., Loriga, G., & Taccini, N. (2005). A wearable health care system based on knitted integrated sensors. *IEEE transactions on Information Technology in biomedicine*, *9*(3), 337-344.

[9] Coyle, S., Lau, K. T., Moyna, N., O'Gorman, D., Diamond, D., Di Francesco, F., ... & Bini, C. (2010). BIOTEX—Biosensing textiles for personalised healthcare management. *IEEE transactions on information technology in biomedicine*, *14*(2), 364-370.

[10] Jeanne, M., Grillet, A., Weber, S., Chaud, P., Logier, R., & Weber, J. L. (2007, August). OFSETH: Optical fibre embedded into technical textile for healthcare, an efficient way to

monitor patient under magnetic resonance imaging. In *2007 29th Annual International Conference of the IEEE Engineering in Medicine and Biology Society* (pp. 3950-3953). IEEE.

[11] Cunha, J. P. S., Cunha, B., Pereira, A. S., Xavier, W., Ferreira, N., & Meireles, L. (2010, March). Vital-Jacket®: A wearable wireless vital signs monitor for patients' mobility in cardiology and sports. In *2010 4th International Conference on Pervasive Computing Technologies for Healthcare* (pp. 1-2). IEEE.

[12] Luprano, J., Solà, J., Dasen, S., Koller, J. M., & Chételat, O. (2006, April). Combination of body sensor networks and on-body signal processing algorithms: the practical case of MyHeart project. In *International Workshop on Wearable and Implantable Body Sensor Networks (BSN'06)* (pp. 4-pp). IEEE.

[13] Bernard, B. P., & Putz-Anderson, V. (1997). Musculoskeletal disorders and workplace factors; a critical review of epidemiologic evidence for work-related musculoskeletal disorders of the neck, upper extremity, and low back.

[14] Marras, W. S., Lavender, S. A., Leurgans, S. E., Fathallah, F. A., Ferguson, S. A., Gary Allread, W., & Rajulu, S. L. (1995). Biomechanical risk factors for occupationally related low back disorders. *Ergonomics*, *38*(2), 377-410.

[15] Punnett, L., Fine, L. J., Keyserling, W. M., Herrin, G. D., & Chaffin, D. B. (1991). Back disorders and nonneutral trunk postures of automobile assembly workers. *Scandinavian journal of work, environment & health*, 337-346.

[16] Keyserling, W. M., Brouwer, M., & Silverstein, B. A. (1992). A checklist for evaluating ergonomic risk factors resulting from awkward postures of the legs, trunk and neck. *International Journal of Industrial Ergonomics*, *9*(4), 283-301.

[17] RADwIN, R. G., Marras, W. S., & Lavender, S. A. (2001). Biomechanical aspects of work-related musculoskeletal disorders. *Theoretical Issues in Ergonomics Science*, *2*(2), 153-217.

[18] Smedley, J., Egger, P., Cooper, C., & Coggon, D. (1995). Manual handling activities and risk of low back pain in nurses. *Occupational and environmental medicine*, *52*(3), 160-163.

[19] Roffey, D. M., Wai, E. K., Bishop, P., Kwon, B. K., & Dagenais, S. (2010). Causal assessment of workplace manual handling or assisting patients and low back pain: results of a systematic review. *The Spine Journal*, *10*(7), 639-651.

[20] Hignett, S., & Griffiths, P. (2009). Risk factors for moving and handling bariatric patients. *Nursing standard*, *24*(11).

[21] Winkel, J., & Mathiassen, S. E. (1994). Assessment of physical work load in epidemiologic studies: concepts, issues and operational considerations. *Ergonomics*, *37*(6), 979-988.

[22] Valero, E., Sivanathan, A., Bosché, F., & Abdel-Wahab, M. (2016). Musculoskeletal disorders in construction: A review and a novel system for activity tracking with body area network. *Applied ergonomics*, *54*, 120-130.

[23] Nath, N. D., Chaspari, T., & Behzadan, A. H. (2018). Automated ergonomic risk monitoring using body-mounted sensors and machine learning. *Advanced Engineering Informatics*, *38*, 514-526.

[24] Waters, T. R., Putz-Anderson, V., Garg, A., & Fine, L. J. (1993). Revised NIOSH equation for the design and evaluation of manual lifting tasks. *Ergonomics*, *36*(7), 749-776.

[25] Karhu, O., Kansi, P., & Kuorinka, I. (1977). Correcting working postures in industry: a practical method for analysis. *Applied ergonomics*, *8*(4), 199-201.

[26] Buchholz, B., Paquet, V., Punnett, L., Lee, D., & Moir, S. (1996). PATH: A work sampling-based approach to ergonomic job analysis for construction and other non-repetitive work. *Applied ergonomics*, *27*(3), 177-187.

[27] McAtamney, L., & Corlett, E. N. (1993). RULA: a survey method for the investigation of work-related upper limb disorders. *Applied ergonomics*, *24*(2), 91-99.

[28] Hignett, S., & McAtamney, L. (2000). Rapid entire body assessment (REBA). *Applied ergonomics*, *31*(2), 201-205.

[29] Battevi, N., Menoni, O., Ricci, M. G., & Cairoli, S. (2006). MAPO index for risk assessment of patient manual handling in hospital wards: a validation study. *Ergonomics*, *49*(7), 671-687.

[30] Ranavolo, A., Draicchio, F., Varrecchia, T., Silvetti, A., & Iavicoli, S. (2018). Wearable monitoring devices for biomechanical risk assessment at work: Current status and future challenges—A systematic review. *International journal of environmental research and public health*, *15*(9), 2001.

[31] Lim, S., & D'Souza, C. (2020). A narrative review on contemporary and emerging uses of inertial sensing in occupational ergonomics. *International journal of industrial ergonomics*, *76*, 102937.

[32] David, G. C. (2005). Ergonomic methods for assessing exposure to risk factors for work-related musculoskeletal disorders. *Occupational medicine*, *55*(3), 190-199.

[33] Luinge, H.J. Inertial Sensing of Human Movement. Ph.D. Thesis, University of Twente, Twente, The Netherlands, 30 October 2002.

[34] Zheng, H., Black, N. D., & Harris, N. D. (2005). Position-sensing technologies for movement analysis in stroke rehabilitation. *Medical and biological engineering and computing*, *43*(4), 413-420.

[35] Faber, G. S., Koopman, A. S., Kingma, I., Chang, C. C., Dennerlein, J. T., & Van Dieën, J. H. (2018). Continuous ambulatory hand force monitoring during manual materials handling using instrumented force shoes and an inertial motion capture suit. *Journal of biomechanics*, *70*, 235-241.

[36] Yang, C. C., & Hsu, Y. L. (2010). A review of accelerometry-based wearable motion detectors for physical activity monitoring. *Sensors*, *10*(8), 7772-7788.

[37] Caputo, F., Greco, A., Egidio, D. A., Notaro, I., & Spada, S. (2018, July). Imu-based motion capture wearable system for ergonomic assessment in industrial environment. In *International Conference on Applied Human Factors and Ergonomics* (pp. 215-225). Springer, Cham.

[38] Scott, K. A., & Browning, R. C. (2016). Occupational physical activity assessment for chronic disease prevention and management: A review of methods for both occupational health practitioners and researchers. *Journal of occupational and environmental hygiene*, *13*(6), 451-463.

[39] Muro-De-La-Herran, A., Garcia-Zapirain, B., & Mendez-Zorrilla, A. (2014). Gait analysis methods: An overview of wearable and non-wearable systems, highlighting clinical applications. *Sensors*, *14*(2), 3362-3394.

[40] Hlucny, S. D., & Novak, D. (2020). Characterizing human box-lifting behavior using wearable inertial motion sensors. *Sensors*, *20*(8), 2323.

[41] Giannini, P., Bassani, G., Avizzano, C. A., & Filippeschi, A. (2020). Wearable sensor network for biomechanical overload assessment in manual material handling. *Sensors*, *20*(14), 3877.

[42] Xu, W., Li, Z., Huang, M. C., Amini, N., & Sarrafzadeh, M. (2011, May). ecushion: An etextile device for sitting posture monitoring. In *2011 International Conference on Body Sensor Networks* (pp. 194-199). IEEE.

[43] Pacelli, M., Loriga, G., Taccini, N., & Paradiso, R. (2006, September). Sensing fabrics for monitoring physiological and biomechanical variables: E-textile solutions. In *2006 3rd IEEE/EMBS International Summer School on Medical Devices and Biosensors* (pp. 1-4). IEEE.

[44] Pugo-Méndez, E., & Serpa-Andrade, L. (2020, March). WORK IN PROGRESS: Study of student ergonomics in classrooms based on posture monitoring. In *2020 IEEE World Conference on Engineering Education (EDUNINE)* (pp. 1-3). IEEE.

[45] Conforti, I., Mileti, I., Del Prete, Z., & Palermo, E. (2020). Measuring biomechanical risk in lifting load tasks through wearable system and machine-learning approach. *Sensors*, *20*(6), 1557.

[46] Lu, M. L., Barim, M. S., Feng, S., Hughes, G., Hayden, M., & Werren, D. (2020, July). Development of a wearable IMU system for automatically assessing lifting risk factors. In *International Conference on Human-Computer Interaction* (pp. 194-213). Springer, Cham.

[47] Lu, M. L., Feng, S., Hughes, G., Barim, M. S., Hayden, M., & Werren, D. (2019, November). Development of an algorithm for automatically assessing lifting risk factors using inertial measurement units. In *Proceedings of the human factors and ergonomics society annual meeting* (Vol. 63, No. 1, pp. 1334-1338). Sage CA: Los Angeles, CA: SAGE Publications.

[48] O'Reilly, M., Caulfield, B., Ward, T., Johnston, W., & Doherty, C. (2018). Wearable inertial sensor systems for lower limb exercise detection and evaluation: A systematic review. *Sports Medicine*, *48*(5), 1221-1246.

[49] Amitrano, F., Coccia, A., Ricciardi, C., Donisi, L., Cesarelli, G., Capodaglio, E. M., & D'Addio, G. (2020). Design and Validation of an E-Textile-Based Wearable Sock for Remote Gait and Postural Assessment. *Sensors*, *20*(22), 6691.

[50] D'Addio, G., Evangelista, S., Donisi, L., Biancardi, A., Andreozzi, E., Pagano, G., ... & Cesarelli, M. (2019, July). Development of a prototype e-textile sock. In *2019 41st Annual International Conference of the IEEE Engineering in Medicine and Biology Society (EMBC)* (pp. 17498-1752). IEEE.

[51] Holleczek, T., Rüegg, A., Harms, H., & Tröster, G. (2010, November). Textile pressure sensors for sports applications. In *SENSORS, 2010 IEEE* (pp. 732-737). IEEE.

[52] Morris, R., Stuart, S., McBarron, G., Fino, P. C., Mancini, M., & Curtze, C. (2019). Validity of Mobility Lab (version 2) for gait assessment in young adults, older adults and Parkinson's disease. *Physiological measurement*, *40*(9), 095003.

[53] Doheny, E. P., Foran, T. G., & Greene, B. R. (2010, August). A single gyroscope method for spatial gait analysis. In *2010 Annual International Conference of the IEEE Engineering in Medicine and Biology* (pp. 1300-1303). IEEE.

[54] Rampp, A., Barth, J., Schülein, S., Gaßmann, K. G., Klucken, J., & Eskofier, B. M. (2014). Inertial sensor-based stride parameter calculation from gait sequences in geriatric patients. *IEEE transactions on biomedical engineering*, *62*(4), 1089-1097.

[55] Salarian, A., Russmann, H., Vingerhoets, F. J., Dehollain, C., Blanc, Y., Burkhard, P. R., & Aminian, K. (2004). Gait assessment in Parkinson's disease: toward an ambulatory system for long-term monitoring. *IEEE transactions on biomedical engineering*, *51*(8), 1434-1443.

[56] Prieto, T. E., Myklebust, J. B., Hoffmann, R. G., Lovett, E. G., & Myklebust, B. M. (1996). Measures of postural steadiness: differences between healthy young and elderly adults. *IEEE Transactions on biomedical engineering*, *43*(9), 956-966.

[57] D'Addio, G., Iuppariello, L., Pagano, G., Biancardi, A., Lanzillo, B., Pappone, N., & Cesarelli, M. (2016, May). New posturographic assessment by means of novel e-textile and

wireless socks device. In *2016 IEEE International Symposium on Medical Measurements and Applications (MeMeA)* (pp. 1-5). IEEE.

[58] Reinfelder, S., Durlak, F., Barth, J., Klucken, J., & Eskofier, B. M. (2014, August). Wearable static posturography solution using a novel pressure sensor sole. In *2014 36th Annual International Conference of the IEEE Engineering in Medicine and Biology Society* (pp. 2973-2976). IEEE.

[59] Agostini, V., Aiello, E., Fortunato, D., Knaflitz, M., & Gastaldi, L. (2019, June). A wearable device to assess postural sway. In *2019 IEEE 23rd International Symposium on Consumer Technologies (ISCT)* (pp. 197-200). IEEE.

[60] Amitrano, F., Donisi, L., Coccia, A., Biancardi, A., Pagano, G., & D'Addio, G. (2020, June). Experimental development and validation of an e-textile sock prototype. In *2020 IEEE International Symposium on Medical Measurements and Applications (MeMeA)* (pp. 1-5). IEEE.

[61] Davis III, R. B., Ounpuu, S., Tyburski, D., & Gage, J. R. (1991). A gait analysis data collection and reduction technique. *Human movement science*, *10*(5), 575-587.

[62] Blair, R. C., & Cole, S. R. (2002). Two-sided equivalence testing of the difference between two means. *Journal of Modern Applied Statistical Methods*, *1*(1), 18.

[63] Passing, H., & Bablok, W. (1983). A new biometrical procedure for testing the equality of measurements from two different analytical methods. Application of linear regression procedures for method comparison studies in clinical chemistry, Part I.

[64] Zaki, R., Bulgiba, A., Ismail, R., & Ismail, N. A. (2012). Statistical methods used to test for agreement of medical instruments measuring continuous variables in method comparison studies: a systematic review. *PloS one*, *7*(5), e37908.

[65] Altman, D. G., & Bland, J. M. (1983). Measurement in medicine: the analysis of method comparison studies. *Journal of the Royal Statistical Society: Series D (The Statistician)*, *32*(3), 307-317.

[66] Bland, J. M., & Altman, D. G. (1999). Measuring agreement in method comparison studies. *Statistical methods in medical research*, *8*(2), 135-160.

[67] D'Addio, G., Donisi, L., Pagano, G., Improta, G., Biancardi, A., & Cesarelli, M. (2019, July). Agreement between opal and G-walk wearable inertial systems in gait analysis on

normal and pathological subjects. In *2019 41st Annual International Conference of the IEEE Engineering in Medicine and Biology Society (EMBC)* (pp. 3286-3289). IEEE.

[68] Donisi, L., Pagano, G., Cesarelli, G., Coccia, A., Amitrano, F., & D'Addio, G. (2021). Benchmarking between two wearable inertial systems for gait analysis based on a different sensor placement using several statistical approaches. *Measurement*, *173*, 108642.

[69] Doheny, E. P., Foran, T. G., & Greene, B. R. (2010, August). A single gyroscope method for spatial gait analysis. In *2010 Annual International Conference of the IEEE Engineering in Medicine and Biology* (pp. 1300-1303). IEEE.

[70] Tong, K., & Granat, M. H. (1999). A practical gait analysis system using gyroscopes. *Medical engineering & physics*, *21*(2), 87-94.

[71] Washabaugh, E. P., Kalyanaraman, T., Adamczyk, P. G., Claflin, E. S., & Krishnan, C. (2017). Validity and repeatability of inertial measurement units for measuring gait parameters. *Gait & posture*, *55*, 87-93.

[72] Patterson, M. R., Johnston, W., O'Mahony, N., O'Mahony, S., Nolan, E., & Caulfield, B. (2016, August). Validation of temporal gait metrics from three IMU locations to the gold standard force plate. In *2016 38th Annual International Conference of the IEEE Engineering in Medicine and Biology Society (EMBC)* (pp. 667-671). IEEE.

[73] Moore, S. A., Hickey, A., Lord, S., Del Din, S., Godfrey, A., & Rochester, L. (2017). Comprehensive measurement of stroke gait characteristics with a single accelerometer in the laboratory and community: a feasibility, validity and reliability study. *Journal of neuroengineering and rehabilitation*, *14*(1), 1-10.

[74] De Ridder, R., Lebleu, J., Willems, T., De Blaiser, C., Detrembleur, C., & Roosen, P. (2019). Concurrent validity of a commercial wireless trunk triaxial accelerometer system for gait analysis. *Journal of sport rehabilitation*, *28*(6).

[75] Knight, J. F., & Baber, C. (2005). A tool to assess the comfort of wearable computers. *Human factors*, *47*(1), 77-91.

[76] Knight, J. F., Deen-Williams, D., Arvanitis, T. N., Baber, C., Sotiriou, S., Anastopoulou, S., & Gargalakos, M. (2006, October). Assessing the wearability of wearable computers. In *2006 10th IEEE International Symposium on Wearable Computers* (pp. 75-82). IEEE.

[77] Coccia, A., Amitrano, F., Donisi, L., Cesarelli, G., Pagano, G., Cesarelli, M., & D'Addio, G. (2021). Design and validation of an e-textile-based wearable system for remote health monitoring. *ACTA IMEKO*, *10*(2), 220-229.

[78] Gomez, C., Oller, J., & Paradells, J. (2012). Overview and evaluation of bluetooth low energy: An emerging low-power wireless technology. *Sensors*, *12*(9), 11734-11753.

[79] Balestrieri, E., Daponte, P., De Vito, L., Picariello, F., Rapuano, S., & Tudosa, I. (2020). A Wi-Fi IoT prototype for ECG monitoring exploiting a novel Compressed Sensing method. *ACTA IMEKO*, *9*(2), 38-45.

[80] Picariello, F., Iadarola, G., Balestrieri, E., Tudosa, I., & De Vito, L. (2021). A novel compressive sampling method for ECG wearable measurement systems. *Measurement*, *167*, 108259.

[81] Mahdiani, S., Jeyhani, V., Peltokangas, M., & Vehkaoja, A. (2015, August). Is 50 Hz high enough ECG sampling frequency for accurate HRV analysis?. In *2015 37th Annual International Conference of the IEEE Engineering in Medicine and Biology Society (EMBC)* (pp. 5948-5951). IEEE.

[82] Okada, M. (1979). A digital filter for the QRS detection complex. *IEEE Trans. Biomed. Eng*, *26*, 700-703.

[83] CAMM, A., Malik, M., Bigger, J. T., Breithardt, G., Cerutti, S., Cohen, R. J., ... & SCHWARTZ, E. mad SINGER, DH (1996):'Heart rate variability--staaadards of measurement, physiological interpretation, mad clinical use'. *Circulation*, *93*, 1043-1065.

[84] Malliani, A., Pagani, M., Lombardi, F., & Cerutti, S. (1991). Cardiovascular neural regulation explored in the frequency domain. *Circulation*, *84*(2), 482-492.

[85] Welch, W. J., Smith, M. L., & Rea, R. F. (1967). Enhancement of sympathetic nerve activity by single premature ventricular beats in humans. J Am Co11 Cardiol 13: 1693, 1989 Welch PD: The use of fast Fourier transform for the estimation of power spectra: a method based on time averaging over short, modified periodograms. *IEEE Trans Audi Electroacoust*, *15*, 70.

[86] Burg, J. P. (1985). Absolute Power Density Spectra. In *Maximum-Entropy and Bayesian Methods in Inverse Problems* (pp. 273-286). Springer, Dordrecht.

[87] Lomb, N. R. (1976). Least-squares frequency analysis of unequally spaced data. *Astrophysics and space science*, *39*(2), 447-462.

[88] Cygankiewicz, I., & Zaręba, W. (2006). Heart rate turbulence-an overview of methods and applications. *Cardiology Journal*, *13*(5), 359-368.

[89] Schmidt, G., Malik, M., Barthel, P., Schneider, R., Ulm, K., Rolnitzky, L., ... & Schömig, A. (1999). Heart-rate turbulence after ventricular premature beats as a predictor of mortality after acute myocardial infarction. *The Lancet*, *353*(9162), 1390-1396.

[90] Al-Angari, H. M., & Sahakian, A. V. (2007). Use of sample entropy approach to study heart rate variability in obstructive sleep apnea syndrome. *IEEE Transactions on Biomedical Engineering*, *54*(10), 1900-1904.

[91] Huikuri, H. V., Mäkikallio, T. H., Peng, C. K., Goldberger, A. L., Hintze, U., & Møller, M. (2000). Fractal correlation properties of RR interval dynamics and mortality in patients with depressed left ventricular function after an acute myocardial infarction. *Circulation*, *101*(1), 47-53.

[92] Higuchi, T. (1988). Approach to an irregular time series on the basis of the fractal theory. *Physica D: Nonlinear Phenomena*, *31*(2), 277-283.

[93] Acharya, R., Bhat, P. S., Kannathal, N., Rao, A., & Lim, C. M. (2005). Analysis of cardiac health using fractal dimension and wavelet transformation. *Itbm-Rbm*, *26*(2), 133-139.

[94] A. Padoan (2020). Passing and Bablok regression, MATLAB Central File Exchange. Online [Accessed 24 June 2020] https://www.mathworks.com/matlabcentral/fileexchange/24894-passing-and-bablok-regression

[95] Bablok, W., & Passing, H. (1985). Application of statistical procedures in analytical instrument testing. *Journal of Automatic Chemistry*, *7*(2), 74-79.

[96] Akhmad, S., Arendra, A., Findiastuti, W., Lumintu, I., & Pramudita, Y. D. (2020, October). Wearable IMU Wireless Sensors Network for Smart Instrument of Ergonomic Risk Assessment. In *2020 6th Information Technology International Seminar (ITIS)* (pp. 213-218). IEEE.

[97] Donisi, L., Cesarelli, G., Coccia, A., Panigazzi, M., Capodaglio, E. M., & D'Addio, G. (2021). Work-Related Risk Assessment According to the Revised NIOSH Lifting Equation: A Preliminary Study Using a Wearable Inertial Sensor and Machine Learning. *Sensors*, *21*(8), 2593.

[98] Mancini, M., & Horak, F. B. (2016). Potential of APDM mobility lab for the monitoring of the progression of Parkinson's disease. *Expert review of medical devices*, *13*(5), 455-462.

[99] Schmitz-Hübsch, T., Brandt, A. U., Pfueller, C., Zange, L., Seidel, A., Kühn, A. A., ... & Doss, S. (2016). Accuracy and repeatability of two methods of gait analysis–GaitRite™ und Mobility Lab™–in subjects with cerebellar ataxia. *Gait & posture*, *48*, 194-201.

[100] Pagano, G., D'Addio, G., De Campi, M., Donisi, L., Biancardi, A., & Cesarelli, M. (2020, June). Rehabilitation outcome in patients undergone hip or knee replacement surgery using inertial technology for gait analysis. In *2020 IEEE International Symposium on Medical Measurements and Applications (MeMeA)* (pp. 1-5). IEEE.

[101] Coccia, A., Lanzillo, B., Donisi, L., Amitrano, F., Cesarelli, G., & D'Addio, G. (2020, June). Repeatability of spatio-temporal gait measurements in Parkinson's disease. In *2020 IEEE International Symposium on Medical Measurements and Applications (MeMeA)* (pp. 1-6). IEEE.

[102] Cleland, I., Kikhia, B., Nugent, C., Boytsov, A., Hallberg, J., Synnes, K., ... & Finlay, D. (2013). Optimal placement of accelerometers for the detection of everyday activities. *Sensors*, *13*(7), 9183-9200.

[103] Matijevich, E. S., Volgyesi, P., & Zelik, K. E. (2021). A Promising Wearable Solution for the Practical and Accurate Monitoring of Low Back Loading in Manual Material Handling. *Sensors*, *21*(2), 340.

[104] Waters, T. R., Lu, M. L., Piacitelli, L. A., Werren, D., & Deddens, J. A. (2011). Efficacy of the revised NIOSH lifting equation to predict risk of low back pain due to manual lifting: expanded cross-sectional analysis. *Journal of Occupational and Environmental Medicine*, *53*(9), 1061-1067.

[105] Spector, J. T., Lieblich, M., Bao, S., McQuade, K., & Hughes, M. (2014). Automation of workplace lifting hazard assessment for musculoskeletal injury prevention. *Annals of occupational and environmental medicine*, *26*(1), 1-8.

[106] Waters, T. R., Baron, S. L., Piacitelli, L. A., Anderson, V. P., Skov, T., Haring-Sweeney, M., ... & Fine, L. J. (1999). Evaluation of the revised NIOSH lifting equation: a cross-sectional epidemiologic study. *Spine*, *24*(4), 386-394.

[107] Brandt, M., Madeleine, P., Samani, A., Jakobsen, M. D., Skals, S., Vinstrup, J., & Andersen, L. L. (2018). Accuracy of identification of low or high risk lifting during standardised lifting situations. *Ergonomics*, *61*(5), 710-719.

[108] Long, X., Yin, B., & Aarts, R. M. (2009, September). Single-accelerometer-based daily physical activity classification. In *2009 Annual International Conference of the IEEE Engineering in Medicine and Biology Society* (pp. 6107-6110). IEEE.

[109] Arif, M., & Kattan, A. (2015). Physical activities monitoring using wearable acceleration sensors attached to the body. *PloS one*, *10*(7), e0130851.

[110] Breiman, L. (2001). Random forests. *Machine learning*, *45*(1), 5-32.

[111] Murthy, S. K. (1998). Automatic construction of decision trees from data: A multi-disciplinary survey. *Data mining and knowledge discovery*, *2*(4), 345-389.

[112] Sheng, P., Chen, L., & Tian, J. (2018, May). Learning-based road crack detection using gradient boost decision tree. In *2018 13th IEEE Conference on Industrial Electronics and Applications (ICIEA)* (pp. 1228-1232). IEEE.

[113] Freund, Y., & Schapire, R. E. (1997). A decision-theoretic generalization of on-line learning and an application to boosting. *Journal of computer and system sciences*, *55*(1), 119-139.

[114] Weinberger, K. Q., & Saul, L. K. (2009). Distance metric learning for large margin nearest neighbor classification. *Journal of machine learning research*, *10*(2).

[115] Sun, S., & Huang, R. (2010, August). An adaptive k-nearest neighbor algorithm. In *2010 seventh international conference on fuzzy systems and knowledge discovery* (Vol. 1, pp. 91-94). IEEE.

[116] Al-Aidaroos, K. M., Bakar, A. A., & Othman, Z. (2010, March). Naive Bayes variants in classification learning. In *2010 International Conference on Information Retrieval & Knowledge Management (CAMP)* (pp. 276-281). IEEE.

[117] Pal, S. K., & Mitra, S. (1992). Multilayer perceptron, fuzzy sets, classifiaction.

[118] Kotsiantis, S. B., Zaharakis, I., & Pintelas, P. (2007). Supervised machine learning: A review of classification techniques. *Emerging artificial intelligence applications in computer engineering*, *160*(1), 3-24.

[119] Schölkopf, B., Smola, A. J., & Bach, F. (2002). *Learning with kernels: support vector machines, regularization, optimization, and beyond*. MIT press.

[120] Stoltzfus, J. C. (2011). Logistic regression: a brief primer. *Academic Emergency Medicine*, *18*(10), 1099-1104.

[121] Anguita, D., Ghelardoni, L., Ghio, A., Oneto, L., & Ridella, S. (2012). The 'K'in K-fold cross validation. In *20th European Symposium on Artificial Neural Networks, Computational Intelligence and Machine Learning (ESANN)* (pp. 441-446). i6doc. com publ.

[122] Sechidis, K., Tsoumakas, G., & Vlahavas, I. (2011, September). On the stratification of multi-label data. In *Joint European Conference on Machine Learning and Knowledge Discovery in Databases* (pp. 145-158). Springer, Berlin, Heidelberg.

[123] Powers, D. M. (2020). Evaluation: from precision, recall and F-measure to ROC, informedness, markedness and correlation. *arXiv preprint arXiv:2010.16061*.

[124] Lei, S. (2012, March). A feature selection method based on information gain and genetic algorithm. In *2012 International Conference on Computer Science and Electronics Engineering* (Vol. 2, pp. 355-358). IEEE.

[125] Hall, M., Frank, E., Holmes, G., Pfahringer, B., Reutemann, P., & Witten, I. H. (2009). The WEKA data mining software: an update. *ACM SIGKDD explorations newsletter*, *11*(1), 10-18.

[126] Scrutinio, D., Ricciardi, C., Donisi, L., Losavio, E., Battista, P., Guida, P., ... & D'Addio, G. (2020). Machine learning to predict mortality after rehabilitation among patients with severe stroke. *Scientific reports*, *10*(1), 1-10.

[127] Tougui, I., Jilbab, A., & El Mhamdi, J. (2020). Heart disease classification using data mining tools and machine learning techniques. *Health and Technology*, *10*, 1137-1144.

[128] Mannini, A., & Sabatini, A. M. (2010). Machine learning methods for classifying human physical activity from on-body accelerometers. *Sensors*, *10*(2), 1154-1175.

[129] Stoltzfus, J. C. (2011). Logistic regression: a brief primer. *Academic Emergency Medicine*, *18*(10), 1099-1104.

[130] Varrecchia, T., De Marchis, C., Rinaldi, M., Draicchio, F., Serrao, M., Schmid, M., ... & Ranavolo, A. (2018). Lifting activity assessment using surface electromyographic features and neural networks. *International Journal of Industrial Ergonomics*, *66*, 1-9.

[131] Varrecchia, T., De Marchis, C., Draicchio, F., Schmid, M., Conforto, S., & Ranavolo, A. (2020). Lifting activity assessment using kinematic features and neural networks. *Applied Sciences*, *10*(6), 1989.

[132] Ranavolo, A., Varrecchia, T., Iavicoli, S., Marchesi, A., Rinaldi, M., Serrao, M., ... & Draicchio, F. (2018). Surface electromyography for risk assessment in work activities designed using the "revised NIOSH lifting equation". *International Journal of Industrial Ergonomics*, *68*, 34-45.

[133] Snyder, K., Thomas, B., Lu, M. L., Jha, R., Barim, M. S., Hayden, M., & Werren, D. (2021). A deep learning approach for lower back-pain risk prediction during manual lifting. *Plos one*, *16*(2), e0247162.

[134] Conforti, I., Mileti, I., Del Prete, Z., & Palermo, E. (2020). Measuring biomechanical risk in lifting load tasks through wearable system and machine-learning approach. *Sensors*, *20*(6), 1557.

[135] Veiga, J. J. D., O'reilly, M., Whelan, D., Caulfield, B., & Ward, T. E. (2017). Feature-free activity classification of inertial sensor data with machine vision techniques: method, development, and evaluation. *JMIR mHealth and uHealth*, *5*(8), e7521.

[136] Donisi, L., Capodaglio, E.M., Amitrano, F., Cesarelli, G., Pagano, G., & D'Addio, G. (2021). A multiple linear regression approach to extimate lifted load from features extracted from inertial data. *Giornale Italiano di Medicina del Lavoro ed Ergonomia*, *43*(4), 373-378.

[137] D'Addio, G., Donisi, L., Pagano, G., Mercogliano, L., Cesarelli, M., & Cesarelli, G. (2020). Effetti sulla cinematica del cammino dello zaino scolastico: Un sovraccarico meccanico potenzialmente causa di disturbi muscolo-scheletrici in età evolutiva?. *Giornale Italiano di Medicina del Lavoro ed Ergonomia*, *42*(3), 201-207.

[138] Ahmad, H. N., & Barbosa, T. M. (2019). The effects of backpack carriage on gait kinematics and kinetics of schoolchildren. *Scientific reports*, *9*(1), 1-6.

[139] Hong, Y., & Li, J. X. (2005). Influence of load and carrying methods on gait phase and ground reactions in children's stair walking. *Gait & posture*, *22*(1), 63-68.

List of Publications

Journal Papers

- D'Addio, G., **Donisi, L.**, Pagano, G., Mercogliano, L., Cesarelli, M., & Cesarelli, G. (2020). Effetti sulla cinematica del cammino dello zaino scolastico: Un sovraccarico meccanico potenzialmente causa di disturbi muscolo-scheletrici in età evolutiva?. *Giornale Italiano di Medicina del Lavoro ed Ergonomia*, *42*(3), 201-207.
- Amitrano, F., Coccia, A., Ricciardi, C., **Donisi, L.**, Cesarelli, G., Capodaglio, E. M., & D'Addio, G. (2020). Design and Validation of an E-Textile-Based Wearable Sock for Remote Gait and Postural Assessment. *Sensors*, *20*(22), 6691. https://doi.org/10.3390/s20226691
- Scrutinio, D., Ricciardi, C., **Donisi, L.**, Losavio, E., Battista, P., Guida, P., ... & D'Addio, G. (2020). Machine learning to predict mortality after rehabilitation among patients with se vere stroke. *Scientific reports*, *10*(1), 1-10. https://doi.org/10.1038/s41598-020-77243-3
- **Donisi, L.**, Cesarelli, G., Balbi, P., Provitera, V., Lanzillo, B., Coccia, A., & D'Addio, G. (2021). Positive impact of short-term gait rehabilitation in Parkinson patients: a combined approach based on statistics and machine learning. *Mathematical Biosciences and Engineering*, *18*(5), 6995-7009. https://doi.org/10.3934/MBE.2021348
- Cantoni, V., Green, R., Ricciardi, C., Assante, R., **Donisi, L.**, Zampella, E., ... & Cuocolo, A. (2021). Comparing the Prognostic Value of Stress Myocardial Perfusion Imaging by Conventional and Cadmium-Zinc Telluride Single-Photon Emission Computed Tomography through a Machine Learning Approach. *Computational and Mathematical Methods in Medicine*, *2021*. https://doi.org/10.1155/2021/5288844
- **Donisi, L.**, Pagano, G., Cesarelli, G., Coccia, A., Amitrano, F., & D'Addio, G. (2021). Benchmarking between two wearable inertial systems for gait analysis based on a different sensor placement using several statistical approaches. *Measurement*, *173*, 108642. https://doi.org/10.1016/j.measurement.2020.108642
- **Donisi, L.**, Cesarelli, G., Coccia, A., Panigazzi, M., Capodaglio, E. M., & D'Addio, G. (2021). Work-Related Risk Assessment According to the Revised NIOSH Lifting

Equation: A Preliminary Study Using a Wearable Inertial Sensor and Machine Learning. *Sensors*, *21*(8), 2593. https://doi.org/10.3390/s21082593

- Coccia, A., Amitrano, F., **Donisi, L.**, Cesarelli, G., Pagano, G., Cesarelli, M., & D'Addio, G. (2021). Design and validation of an e-textile-based wearable system for remote health monitoring. *ACTA IMEKO*, *10*(2), 220-229. http://dx.doi.org/10.21014/acta_imeko.v10i2.912
- D'Addio, G., **Donisi, L.**, Cesarelli, G., Amitrano, F., Coccia, A., La Rovere, M. T., & Ricciardi, C. (2021). Extracting Features from Poincaré Plots to Distinguish Congestive Heart Failure Patients According to NYHA Classes. *Bioengineering*, *8*(10), 138. https://doi.org/10.3390/bioengineering8100138
- **Donisi, L.**, Cesarelli, G., Castaldo, A., De Lucia, D. R., Nessuno, F., Spadarella, G., & Ricciardi, C. (2021). A Combined Radiomics and Machine Learning Approach to Distinguish Clinically Significant Prostate Lesions on a Publicly Available MRI Dataset. *Journal of Imaging*, *7*(10), 215. https://doi.org/10.3390/jimaging7100215
- Caruso, M., Ricciardi, C., Delli Paoli, G., Di Dato, F., **Donisi, L.**, Romeo, V., ... & Maurea, S. (2021). Machine Learning Evaluation of Biliary Atresia Patients to Predict Long-Term Outcome after the Kasai Procedure. *Bioengineering*, *8*(11), 152. https://doi.org/10.3390/bioengineering8110152
- **Donisi, L.**, Capodaglio, E.M., Amitrano, F., Cesarelli, G., Pagano, G., & D'Addio, G. A multiple linear regression approach to extimate lifted load from features extracted from intertial data. *Giornale Italiano di Medicina del Lavoro ed Ergonomia*, *43*(4), 373-378.
- Amboni, M., Ricciardi, C., Cuoco, S., **Donisi, L.**, Volzone, A., Ricciardelli, G., Pellecchia, M.T., Santangelo, G., Cesarelli, M., & Barone, P. Mild Cognitive Impairment subtypes are associated with peculiar gait patterns in Parkinson Disease. *Frontiers in Aging Neuroscience*. (Under consideration)

Conference Papers

- D'Addio, G., Evangelista, S., **Donisi, L.**, Biancardi, A., Andreozzi, E., Pagano, G., ... & Cesarelli, M. (2019, July). Development of a prototype e-textile sock. In *2019 41st Annual International Conference of the IEEE Engineering in Medicine and*

Biology Society (EMBC) (pp. 17498-1752). IEEE. https://doi.org/10.1109/EMBC.2019.8856739

- D'Addio, G., **Donisi, L.**, Pagano, G., Improta, G., Biancardi, A., & Cesarelli, M. (2019, July). Agreement between opal and G-walk wearable inertial systems in gait analysis on normal and pathological subjects. In *2019 41st Annual International Conference of the IEEE Engineering in Medicine and Biology Society (EMBC)* (pp. 3286-3289). IEEE. https://doi.org/10.1109/EMBC.2019.8857841
- D'Antò, M., Cosentino, C., Cuomo, A., Accardo, R., Bifulco, P., **Donisi, L.**, & Romano, M. (2019, September). Evaluation of a new endobronchial double lumen tube with integrated camera: a hospital based HTA experience. In *Mediterranean Conference on Medical and Biological Engineering and Computing* (pp. 1028-1037). Springer, Cham. https://doi.org/10.1007/978-3-030-31635-8_125
- D'Addio, G., **Donisi, L.**, Mercogliano, L., Cesarelli, G., Bifulco, P., & Cesarelli, M. (2019, September). Potential biomechanical overload on skeletal muscle structures in students during walk with backpack. In *Mediterranean Conference on Medical and Biological Engineering and Computing* (pp. 262-266). Springer, Cham. https://doi.org/10.1007/978-3-030-31635-8_31
- **Donisi, L.**, Coccia, A., Amitrano, F., Mercogliano, L., Cesarelli, G., & D'Addio, G. (2020, June). Backpack influence on kinematic parameters related to Timed Up and Go (TUG) test in school children. In *2020 IEEE International Symposium on Medical Measurements and Applications (MeMeA)* (pp. 1-5). IEEE. https://doi.org/10.1109/MeMeA49120.2020.9137198
- Coccia, A., Lanzillo, B., **Donisi, L.**, Amitrano, F., Cesarelli, G., & D'Addio, G. (2020, June). Repeatability of spatio-temporal gait measurements in Parkinson's disease. In *2020 IEEE International Symposium on Medical Measurements and Applications (MeMeA)* (pp. 1-6). IEEE. https://doi.org/10.1109/MeMeA49120.2020.9137357
- Pagano, G., D'Addio, G., De Campi, M., **Donisi, L.**, Biancardi, A., & Cesarelli, M. (2020, June). Rehabilitation outcome in patients undergone hip or knee replacement surgery using inertial technology for gait analysis. In 2020 IEEE International Symposium on Medical Measurements and Applications (MeMeA) (pp. 1-5). IEEE. https://doi.org/10.1109/MeMeA49120.2020.9137125

- Amitrano, F., **Donisi, L.**, Coccia, A., Biancardi, A., Pagano, G., & D'Addio, G. (2020, June). Experimental development and validation of an e-textile sock prototype. In *2020 IEEE International Symposium on Medical Measurements and Applications (MeMeA)* (pp. 1-5). IEEE. https://doi.org/10.1109/MeMeA49120.2020.9137302
- **Donisi, L.**, Coccia, A., Amitrano, F., Ricciardi, C., Cesarelli, G., & D'Addio, G. (2020, June). Benchmarking between a Sensorized E-textile Sock for Remote Monitoring and a Stereophotogrammetric System. In *VII Congress of the National Group of Bioengineering (GNB)*. (In press).
- Amitrano, F., Coccia, A., **Donisi, L.**, Biancardi, A., Pagano, G., & D'Addio, G. (2020, June). Experimental validation of an e-textile t-shirt for ECG monitoring. In *VII Congress of the National Group of Bioengineering (GNB)*. (In press).
- **Donisi, L.**, Ricciardi, C., Cesarelli, G., Pagano, G., Amitrano, F., & D'Addio, G. (2020, July). Machine Learning applied on Poincaré Analyisis to discriminate different cardiac issues. In *2020 11th Conference of the European Study Group on Cardiovascular Oscillations (ESGCO)* (pp. 1-2). IEEE. https://doi.org/10.1109/ESGCO49734.2020.9158144
- Ricciardi, C., **Donisi, L.**, Cesarelli, G., Pagano, G., Coccia, A., & D'Addio, G. (2020, July). Feasibility of machine learning applied to poincaré plot analysis on patients with CHF. *In 2020 11th Conference of the European Study Group on Cardiovascular Oscillations (ESGCO)* (pp. 1-2). IEEE. https://doi.org/10.1109/ESGCO49734.2020.9158152
- **Donisi, L.**, Cesarelli, G., Amitrano, F., Coccia, A., Gargiulo, P., & D'Addio, G. (2020, September). An overall agreement evaluation between two measuring systems for gait analysis through a machine learning approach. In *Nordic Baltic Conference on Biomedical Engineering and Medical Physics*. Springer, Cham. (In press).
- **Donisi, L.**, Moretta, P., Cesarelli, G., Pagano, G., Gargiulo, P., & D'Addio, G. (2020, September). Using lower limb gait parameters to distinguish stroke patients with and without neglect: a data mining approach. In *Nordic Baltic Conference on Biomedical Engineering and Medical Physics*. Springer, Cham. (In press)
- Trunfio, T. A., Baviello, D., Perrone, A., Formisano, R., & **Donisi, L.** (2020, November). Medical Technologies Procurement, Management and Maintenance in

Developing Countries: The Case of Health Challenges in Africa. In *European Medical and Biological Engineering Conference* (pp. 793-804). Springer, Cham. https://doi.org/10.1007/978-3-030-64610-3_89

- **Donisi, L.**, Amintrano, F., Coccia, A., Mercogliano, L., Cesarelli, G., & D'Addio, G. (2020, November). Influence of the Backpack on School Children's Gait: A Statistical and Machine Learning Approach. In *European Medical and Biological Engineering Conference* (pp. 682-688). Springer, Cham. https://doi.org/10.1007/978-3-030-64610-3_76
- Cesarelli, G., **Donisi, L.**, Di Caprio, G., Scioli, M., Biancardi, A., & D'Addio, G. (2021, June). Statistical correlation analysis between kinematic features and clinical indexes and scales for obese patients. In *2021 IEEE International Symposium on Medical Measurements and Applications (MeMeA)* (pp. 1-5). IEEE. https://doi.org/10.1109/MeMeA52024.2021.9478776
- Coccia, A., Amitrano, F., Balbi, P., **Donisi, L.**, Biancardi, A., & D'Addio, G. (2021, June). Analysis of Test-Retest Repeatability of Gait Analysis Parameters in Hereditary Spastic Paraplegia. In *2021 IEEE International Symposium on Medical Measurements and Applications (MeMeA)* (pp. 1-6). IEEE. https://doi.org/10.1109/MeMeA52024.2021.9478743
- **Donisi, L.**, Moretta, P., Coccia, A., Amitrano, F., Biancardi, A., & D'Addio, G. (2021, June). Distinguishing stroke patients with and without unilateral spatial neglect by means of clinical features: A tree-based machine learning approach. In 2021 IEEE International Symposium on Medical Measurements and Applications (MeMeA) (pp. 1-5). IEEE. https://doi.org/10.1109/MeMeA52024.2021.9478727
- Amitrano, F., Coccia, A., **Donisi, L.**, Pagano, G., Cesarelli, G., & D'Addio, G. (2021, June). Gait Analysis using Wearable E-Textile Sock: an Experimental Study of Test-Retest Reliability. In *2021 IEEE International Symposium on Medical Measurements and Applications (MeMeA)* (pp. 1-6). IEEE. https://doi.org/10.1109/MeMeA52024.2021.9478702
- Pagano, G., **Donisi, L.**, Marsico, V., Losavio, E., Cesarelli, M., & D'Addio, G. (2021, June). Reliability of kinematic parameters related to the Timed Up and Go Test in patients with gait impairments. In *2021 IEEE International Symposium on Medical Measurements and Applications (MeMeA)* (pp. 1-5). IEEE. https://doi.org/10.1109/MeMeA52024.2021.9478762

- Montella, E., Scala, A., Di Lillo, M., Lamberti, M., **Donisi, L.**, Triassi, M., Profeta, M. (2021, October). Impact of Hospital Infections in the Clinical Medicine Area of “Federico II” University Hospital of Naples Assessed by means of Statistical Analysis and Machine Learning. *In 10th International Conference on Bioinformatics and Biomedical Sciences*. (In press).

Letters

- D'Addio, G., De Felice, A., **Donisi, L.**, Braghiroli, A., & Maniscalco, M. (2021). Heart rate turbulence in obstructive sleep apnea syndrome: The effect of short-term CPAP therapy. *European Journal of Internal Medicine*, *86*, 111-114. https://doi.org/10.1016/j.ejim.2020.12.015

Reviews

- Landolfi, A., Ricciardi, C., **Donisi, L.**, Cesarelli, G., Troisi, J., Vitale, C., ... & Amboni, M. (2021). Machine Learning Approaches in Parkinson’s Disease. *Current Medicinal Chemistry*. doi.org/10.2174/0929867328999210111211420
- Cesarelli, G., **Donisi, L.**, Coccia, A., Amitrano, F., D’Addio, G., & Ricciardi, C. (2021). The E-Textile for Medical Applications: a Systematic Review of Literature. *Diagnostics.* (In press).

Acknowledgement

First of all, I want to thank my father to whom I dedicated this work for having always believed in me despite everything.

I am profoundly grateful to my family for having fostered my education as a scholar allowing me to achieve this goal.

I would like to express my sincere gratitude to my tutor Professor Mario Cesarelli for having transmitted his knowledge and experience helping me to grow as researcher.

I would like to say a big thank you to Professor Giovanni D'Addio for giving me the opportunity to collaborate with the Institute of Care and Scientific Research Maugeri expanding my education also on clinical aspects and for having dedicated his time to me.

I would like to express my heartfelt thanks to Professor Paolo Gargiulo for giving me the opportunity to collaborate with his group giving my research activity an international dimension and for having welcomed me at the Reykjavik University.

I would like to thank Dott.ssa Edda Maria Capodaglio and Dott.ssa Monica Panigazzi for transferring their knowledge of ergonomics and occupational medicine to me.

I would like to thank all the Biomedical engineering staff: Professor Francesco Amato, Professor Paolo Bifulco, Professor Maria Romano, Professor Mario Sansone. I would like also to thank my colleagues. The discussion with each of them was always motivating.

I would like to thank the staff of Adiramef Srl for giving me the opportunity to extend my education from an industrial point of view.

I would like to thank all my friends and relatives who were close to me.

La borsa di dottorato è stata cofinanziata con risorse del
Programma Operativo Nazionale Ricerca e Innovazione 2014-2020 (CCI 2014IT16M2OP005),
Fondo Sociale Europeo, Azione I.1 "Dottorati Innovativi con caratterizzazione Industriale"

UNIONE EUROPEA
Fondo Sociale Europeo

Ministero dell'Università
e della Ricerca

PON
RICERCA
E INNOVAZIONE
2014 - 2020